FINAL REPORT

NAS9-18175

INVESTIGATION OF LONG TERM STABILITY IN METAL HYDRIDES

NOVEMBER, 1991

SUBMITTED TO

NATIONAL AERONAUTICS & SPACE ADMINISTRATION
LYNDON B. JOHNSON SPACE CENTER
HOUSTON, TEXAS

SUBMITTED BY

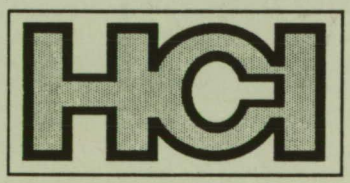

HYDROGEN CONSULTANTS, INC.
12420 NORTH DUMONT WAY, LITTLETON, CO 80125
(303) 791-7972 FAX (303) 791-7975

FINAL REPORT NAS9-18175

INVESTIGATION OF LONG TERM STABILITY IN METAL HYDRIDES

NOVEMBER, 1991

SUBMITTED TO

NATIONAL AERONAUTICS & SPACE ADMINISTRATION
LYNDON B. JOHNSON SPACE CENTER
HOUSTON, TEXAS

Prepared by:

Roger W. Marmaro, Research Engineer

Franklin E. Lynch, President

In Collaboration with:

University of Nevada, Reno

Dr. Dhanesh Chandra
Steve Lambert
Archana Sharma

Subcontract No. 80-0237

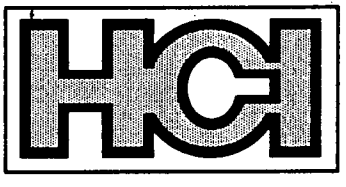

HYDROGEN CONSULTANTS, INC.
12420 NORTH DUMONT WAY, LITTLETON, CO 80125
(303) 791-7972 FAX (303) 791-7975

TABLE OF CONTENTS

LIST OF FIGURES

LIST OF TABLES

1.0 EXECUTIVE SUMMARY

This is the Final Report on Contract No. NAS 9-18175, "Investigation of Long Term Stability in Metal Hydrides". Hydrogen Consultants, Inc. (HCI), Littleton, CO and its subcontractor, the University of Nevada, Reno (UNR) conducted the study. Additional inputs came through parallel IRAD collaboration with Aerojet Electronic Systems Division, Azusa, CA, and from UNR graduate studies in metal hydrides. JSC's Technical Monitor for the contract was Ms. Tricia Petete.

This Executive Summary omits references to published studies and private communications with others in the interest of brevity. The body of the report contains much greater detail and all appropriate citations.

Advanced NASA applications for metal hydride reversible hydrogen sorbers fall into three general categories:

- Thermal Control:
  Heat pumps, refrigerators, thermal storage devices, heat pipes

- Hydrogen Storage:
  Long term H_2 propellant storage, LH_2 boiloff capture

- Hydrogen Compression:
  Joule-Thomson H_2 liquefaction, cryorefrigeration, fluid-mechanical actuators.

Many of these applications require stability of hydrogen capacity and pressure-temperature properties over large numbers of absorption/desorption cycles and many years.

Certain metal hydrides are degraded by time and cycling while other apparently similar hydrides are not. This study sought an understanding of the reasons for cyclic degradation. Special apparatuses for cycling and aging hydrides were constructed and analytical methods were devised to examine degraded hydride specimens. Hydrides were degraded in a Rapid Cycle Apparatus (RCA), a Slow Cycle Apparatus (SCA) and by a Thermal Aging (TA) process.

The study focused upon two families of metal hydrides that are especially important for future NASA applications; 1) AB_5-hydrides, typified by $LaNi_5H_6$, and 2) variants of vanadium dihydride, VH_2. Within each family, the effects of additives were evaluated, e.g., $La_{0.9}Gd_{0.1}Ni_5$ and $V_{0.995}C_{0.005}$.

All degraded hydrides exhibited broadened peaks in their X-ray diffraction patterns. This is an artifact of the strain that accompanies expansion and contraction during hydriding and dehydriding. Expansion and contraction is roughly 20-30% by

volume for the materials studied. A cause-effect relationship between strain accumulation and hydride degradation is inferred by the following observations; metals that are mechanically strained before hydriding yield degraded isotherms that resemble hydride isotherms after large numbers of cycles; annealing of mechanically strained specimens before hydriding results in normal undegraded metal hydride characteristics; cyclically degraded hydrides show X-ray evidence of severe strain; annealing of cyclically degraded hydrides also reverses the damage, although explanations other than strain relief are plausible in the latter case.

Further support for the cause-effect relationship between strain and hydride degradation comes from the observation that degradation resistant hydrides, such as $LaNi_{4.8}Sn_{0.2}H_{\sim 6}$, show relatively little strain via X-ray line broadening analysis. Hypotheses for explaining the effectiveness of additives in stabilizing the AB_5 crystal structure are offered in the literature. Some researchers propose that an additive interferes with detrimental rearrangement of atoms by strong attractions between the host metal atoms and the additive atoms.

Other studies (neutron diffraction) have identified specific sites within hydride crystals where hydrogen (actually deuterium) is most likely to be found. Cycling of hydrides results in localized atom arrangements that are different from the original structure, thereby decreasing the number of normal hydrogen sites and, therefore, the *reversible* hydrogen capacity. *Reversible*, in this context means hydrogen that can be absorbed and desorbed under the same pressure-temperature conditions as the original hydride phase. The original structure in some badly degraded AB_5-hydrides is either absent (amorphous) or so fragmented (nanocrystalline) that peaks are difficult to observe even with lengthy and intense Bragg X-ray exposure.

Clearly, hydrogen trapping is one mode of hydride degradation. An ideal solution of hydrogen in a metal obeys Sieverts' Law ($C=kP^{1/2}$). Positive deviation from Sieverts' Law is, by definition, hydrogen trapping. The mode of trapping however is controversial. Some evidence (Mössbauer spectroscopy) suggests the formation of stable hydride phases. Others claim that the hydrogen is trapped in crystal defects. X-ray line broadening analysis confirms the existence of crystal disorder. Peak broadening of the hexagonal structure is apparent, suggesting that crystal disorder accompanies hydride degradation. Crystal imperfections may place La atoms closer to one another than their normal spacing in the hexagonal AB_5 lattice. Hydrogen may be stably bound in La-rich sites within crystal defects. The controversy arises over whether trapping sites are randomly distributed throughout the material or organized into nanocrystals of stable hydride phases.

Annealing of cyclically degraded hydrides results in reversal of degradation. This may be interpreted from several points of view, including strain relief, reordering of defects when trapped hydrogen is removed, or decomposition of stable hydride phases upon heating. Some "annealing" reported in the literature occurred at

temperatures so far below the melting point of $LaNi_5$ that only short range reordering is possible. In the present study, strong AB_5 peaks developed in degraded materials at room temperature as hydrogen diffused out of them into room air. No additional hydride phases were found in AB_5-hydrides during this study. Others claim that such phases exist as small crystallites (<150 Å) that are below the detection limits of normal X-ray analysis. Several hydrides in the La-Ni-H system are amorphous and, therefore, void of X-ray diffraction peaks. X-ray diffraction alone cannot settle the controversy.

The present study identified nickel peaks in degraded ANi_5-hydrides. Free nickel in degraded hydrides was also observed by magnetic measurements reported in the literature. The existence of nickel clusters large enough to produce X-ray peaks (~150 Å) proves that the Ni/A ratio in the balance of the specimen is less than that of the original AB_5. Some researchers propose the decomposition $LaNi_5H_6 \rightarrow LaH_2 + 5Ni + 2H_2$, where the LaH_2 phase is nanocrystalline. This is refuted by other studies (quasi-elastic neutron scattering) that should have detected any significant quantity of LaH_2 regardless of crystallite size. Other possibilities include the formation of hydrides of ANi, A_2Ni_3, ANi_2, ANi_3, or A_2Ni_7, all of which are more stable than $LaNi_5$-hydride and some of which are reported to be amorphous.

An unexpected result of this study was that rapid cycling of AB_5-hydrides does not result in as much degradation over the same period of time as does slower cycling. Cycle periods of 60 minutes on the SCA seriously damaged $LaNi_{5.2}$ and $La_{0.9}Gd_{0.1}Ni_5$ during 1500 cycles in 2 months of testing. However, cycle periods of 6 minutes on the RCA had relatively little effect on these hydrides during ~6000 cycles in 1 month of testing. Lengthening the RCA's absorption period to simulate that of the SCA finally caused some damage (~10% loss of reversible H-capacity) after nearly 11000 cycles during 4 months of testing. However, the damage was not as severe as 1500 cycles in the SCA (~20% loss of reversible H-capacity) during 2 months of testing.

The literature suggests that time in the saturated condition, rather than number of cycles, may be responsible for hydride degradation. The less degraded RCA specimen was in saturated condition for a longer time at room temperature than the degraded specimen. This contradicts the notion that residence time in the hydrided condition is the primary mode of degradation.

Thermal Aging (TA) work in the present study confirms that holding hydrides at elevated pressures and temperatures causes degradation that resembles cyclic degradation. X-ray diffraction of a thermally degraded specimen during the present study showed significant broadening (disorder) but no additional peaks. If TA degradation were to occur by development of secondary hydride phases, that development should have occurred via normal nucleation and growth of macrocrystalline precipitates (e.g., precipitation hardening of aluminum). There is no reason to suppose that the growth of TA degradation products would be nanocrystalline, as some suspect in cyclically degraded specimens. The absence of

extra peaks suggests that the TA degradation product is amorphous. A post degradation bakeout of the TA specimen shows that hydrogen is released over a range of temperature at pressures that are several orders of magnitude above that of LaH_2. The degradation mechanism suggested in the literature, $LaNi_5H_6 \rightarrow LaH_2 + 5Ni + 2H_2$, is thereby disproven.

Just as in the AB_5-hydrides, cyclic degradation of vanadium dihydride is accompanied by X-ray line broadening. The reversible reaction of importance for practical applications of vanadium dihydride is:

$$VH + \tfrac{1}{2}H_2 \rightleftharpoons VH_2$$

where VH has the body-centered tetragonal (BCT) structure and VH_2 has the cubic fluorite structure (CaF_2). Line broadening analysis shows increases in strain in VH with the number of absorption/desorption cycles. Anisotropic broadening of the 002 and 220 Bragg peaks may suggest the presence of stacking faults in the VH phase.

A specimen of $V_{0.995}C_{0.005}$, milled into very fine shavings, confirmed the importance of strain in degradation of V-based dihydrides. The severely cold-worked specimen showed a large hysteresis band and reduced capacity, similar to a cyclically degraded hydride isotherm. Annealing the shavings reduced the hysteresis and recovered the original hydrogen capacity.

RCA data clearly show that hydrogen becomes trapped within degraded VH. After 6182 cycles in the RCA, VH_2 desorption yields hydrogen gas and a solid product whose composition is approximately $VH_{1.18}$. With pure vanadium, there is no concern, as with the AB_5-hydrides, that the trapping mechanism may involve stable hydride phases with different metal stoichiometry than the original material, e.g., A_2B_7. When the degraded VH_2 phase decomposes on heating in the RCA, it leaves VH with about 18% excess hydrogen trapped within its strained and disordered BCT structure.

A new form of cyclic degradation, peculiar to vanadium-based hydrides, was observed during this study. Over the course of 6182 absorption/desorption cycles in the RCA, time-lapse photography shows that the original shiny metallic-looking material undergoes a spontaneous physical change. A low density dark gray phase, graphically dubbed "dust bunnies" by HCI test personnel, gradually grows by transforming higher density metallic particles. The material appears to the eye, and to the highest resolutions of electron microscopy, as a fluffy, porous, sponge-like mass. This growth has strained and eventually fractured the sturdiest of hydride containers.

The low density material does not have a crystalline appearance, but X-ray diffraction patterns show BCT and cubic fluorite--just like the higher density material but with more strain. Hydride isotherms confirm that the normal and low density phases are chemically similar. The density decrease is of a physical nature, i.e., a

modified state of aggregation, rather than a chemical change. X-ray line broadening analysis indicates an increased domain size in the low density form of VH_2.

1.1 Acknowledgements

The authors gratefully acknowledge the collaboration of Dr. Robert C. Bowman and others at Aerojet Electronic Systems Division, Azusa, California.

2.0 BACKGROUND AND LITERATURE SURVEY

HCI's IRAD studies[1], confirmed by other studies[2, 3, 4, 5], have proven that certain hydrides will survive 10^3-10^4 cycles without significant changes in hydrogen capacity or thermodynamic properties. It is reasonable to expect, but not yet proven, that some of these hydrides will continue to perform well after 10^5 to 10^6 cycles. Other hydrides of very similar composition are severely degraded in 10^2 cycles or less. The purpose of the present study is to discover the reasons for this unpredictable behavior. Certain additives virtually eliminate the problem but the reason for their effectiveness is not known. Figure 2-1 shows absorption/desorption isotherms taken after 10,000 hydride/dehydride cycles for 3 alloys with nearly identical crystal structures.

About 15-25% volume expansion occurs as hydrogen enters the metal phase to form the hydride. An early hypothesis held that physical breakdown (external and internal fracturing) of the hydride powder particles might progress through thousands of cycles until the particles lost their crystalline identity, becoming nearly amorphous. Scanning electron microscope studies by HCI/University of Denver did not support this hypothesis. There was not much outward physical difference between 10-cycle material (nearly new) and the same material after 2483 cycles. Average particle size had decreased only slightly during cycling, from 13 microns down to 11 microns. Internal fracturing in the hydride particles after 10 cycles and 2483 cycles was similar. Each particle contains internal microfractures that separate it into subparticles on the order of 1 micron in size. Detachment, or spalling, of these subparticles is thought to be responsible for the reduced average particle size of the 2483-cycle material. There was no evidence in the micrographs that severe internal particle fracturing was responsible for the degraded performance of the hydrides.

Repeated incoherent phase changes may be the cause of degradation in hydrides, but not by the types of physical damage that are observable with scanning electron microscopy. Strain and crystal disorder that accompany incoherent phase transformations are the suspected causes of crystallite size reduction in degraded hydrides.

The literature suggests that chemical decomposition, such as:

[I] $LaNi_5H_6 \rightarrow LaH_2 + 5Ni + 2H_2$ gas,

[1] D. Chandra and F.E. Lynch, "Cyclic Stability of Rare Earth Pentanickel Hydrides", Proc. AIME Rare Earth Symposium, ed. R. G. Bautista and M. M. Wong, TMS Publications, p. 83 (1989).

[2] P.D. Goodell, "Stability of Rechargeable Hydriding Alloys During Extended Cycling" *J. Less Common Metals*, Vol. 99, pp. 1-14, Elsevier Sequoia S. A., Lausanne, Netherlands, 1984.

[3] G.H. Kim and Jai-Young Lee, *J. Less-Common Metals*, 132, pp. 123-132 (1987).

[4] J. M. Park and Jai-Young Lee, *Mater. Res. Bull.* 22, (187) pp. 455-462.

[5] Y. Josephy, E. Bershadsky and M. Ron, "Investigation of $LaNi_5$ upon Prolonged Cycling" Proc. International Symposium on Metal Hydrogen Systems, Banff, Alberta, Canada (1990).

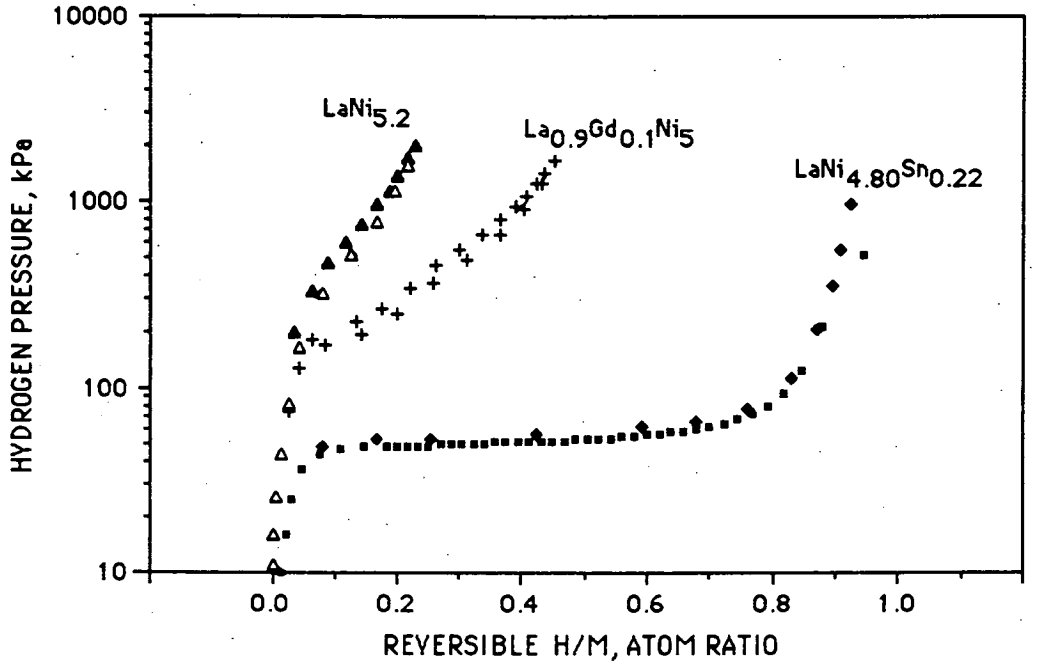

Figure 2-1. Absorption (upper) and desorption (lower) isotherms for three AB_5-type hydride alloys show significant differences in long- term performance. All three hydrides originally had flat plateaux and hydrogen capacities near H/M = 1. After 10,000 cycles only $LaNi_{4.80}Sn_{0.22}$ retained its original plateau pressure and most of its original *reversible*[6] hydrogen capacity.

may be the cause of cyclic degradation. Cohen and co-workers[7, 8] support this explanation, but were unable to find X-ray diffraction peaks of LaH_2 or Ni in samples that were 76% degraded. They claim that the LaH_2 and Ni precipitates "must occur on a scale of about 200Å or less" and are therefore unobservable by X-ray diffraction[9] . Their Mössbauer spectroscopy indicates the presence of Ni in clusters of less than 100Å.

It may be true that the crystal domains are very small in hydrides after large numbers of hydride/dehydride cycles, but there is no direct evidence indicating the presence of LaH_2. Temperature, composition data for degraded samples were

[6] Absolute calibration is lost during cyclic testing. Figure 2-1 is drawn assuming that H/M = 0 at the minimum pressure of each isotherm. This ignores dissolved and trapped hydrogen that is known to be present but unquantifiable.

[7] "Degradation Of $LaNi_5$ Hydrogen-absorbing Material by Cycling", *Journal of the Less Common Metals*, Vol. 70, pp. 229-241, Elsevier Sequoia S. A., Lausanne, Netherlands, 1979.

[8] "Intrinsic Cycling Degradation in $LaNi_5$ and Annealing Procedures for Re-forming the Material", *Journal of the Less Common Metals*, Vol. 95, pp. 17-23, Elsevier Sequoia S. A., Lausanne, Netherlands, 1983.

[9] *Applied Physics Letters*, Vol. 40. p. 999, 1982

obtained by Cohen et al by slowly raising the temperature of the sample from room temperature to 500°C while pumping. The rate of temperature rise was manually controlled to maintain $2x10^{-4}$ Torr dynamic vacuum pressure (certainly not an equilibrium pressure). Most of the hydrogen seems to have evolved over a temperature range from 250-300°C and they claim this indicates that "a relatively well-defined phase was being decomposed". On the contrary, a hydride phase with the stability they suggest (ΔH = -33.6 kcal/mol of hydrogen) would yield 17 times as much hydrogen pressure at 300°C (572°F) as it would at 250°C (482°F). The relatively constant desorption rate they observed would be impossible with a 17-fold increase in equilibrium pressure so the results do not indicate a "well-defined phase". The hydrogen was observed to evolve over a significant range of temperature. This behavior is typical of dissolved hydrogen whose stability is dependent on concentration. To extract dissolved hydrogen at a constant rate, the temperature of a metal must be steadily increased. A hydride phase, such as LaH_2, forms and decomposes with a characteristic pressure at any given temperature[10].

A recent study by inelastic neutron scattering[11] concludes that there is no LaH_2 present in degraded $LaNi_5$-hydride. Several distinct hydrogen occupation sites were observed in the degraded material but, at the time of publication, the sites had not been characterized.

Jeong In Han and Jai-Young Lee[12] performed a study by cycling hydrides in UHP hydrogen and vacuum at room temperature, then quenching in LN_2. Subsequent constant rate heating to 600 K was performed while monitoring hydrogen flow into the vacuum system. Fresh material showed one desorption rate peak at 265 K. Degraded material showed two peaks, one sharp peak at 256 K (just slightly less than fresh material) and a second broader rate peak centered around 520 K. The authors attribute the second peak in the degraded samples to trapping at sites where small amounts of various stoichiometric compounds in the La-Ni system (e.g., La_7Ni_3, LaNi, $LaNi_2$, $LaNi_3$, La_2Ni_7) have been formed by the disordering of $LaNi_5$ during cycling.

Their X-ray data showed no indication of phases other than $LaNi_5$. The $LaNi_5$ pattern showed broadened peaks that were attributed to disordering and strain. The authors suggest that the phases formed by disordering could be in clusters too fine to be observed by X-ray diffraction. The fact that the hydrides of some phases are amorphous was also mentioned. They observed a small increase in saturation magnetization in fresh samples and a large increase in degraded samples. They attribute this to the formation of Ni-clusters.

[10] W.L. Korst and J.C. Warf, "Rare Earth-Hydrogen Systems. I. Structural Thermodynamic Properties, Inorg. Chem., Vol. 5, No. 10, pp. 1719-1726 (1966).

[11] Benham, M.J. et al, "Inelastic Neutron Scattering Studies of Multiply Cycled La-Ni-Hydride", *Zeitschrift für Physikalische Chemie Neue Folge*, R. Oldenbourg Verlag, Munich, West Germany, Vol. 147, pp. 219-229 (1986).

[12] Jeong In Han and Jai-Young Lee, "An Investigation of the Intrinsic Degradation Mechanism of $LaNi_5$ by Thermal Desorption Technique," Int. J. Hydrogen Energy, Vol. 13, pp. 577-581, 1988.

The X-ray results of Jeong In Han and Jai-Young Lee largely confirm the UNR study, i.e., no phases other than $LaNi_5$ were found and the existence of broadened peaks was interpreted as evidence for strain-induced disorder. UNR X-ray data, with a larger number of cycles on samples that were much more severely degraded, support the magnetic measurements of Jeong In Han and Jai-Young Lee--peaks with the d-spacing of nickel were observed.

HCI/UNR studies[13], have found X-ray evidence that crystal disorder in hydriding alloys may be the cause of cyclic degradation. Badly degraded specimens had none of the original peaks strong enough to observe with the methods applied while the hydrogen was still in the sample, but the peaks of the original hexagonal lattice reappeared when hydrogen was removed. One possible explanation is that the saturated cyclic degradation are amorphous. X-ray diffraction patterns of desorbed 10-cycle and 10,000-cycle samples show peak broadening in the hexagonal structure. As a working hypothesis, it is suspected that crystal imperfections, resulting from strain that occurs during absorption/desorption cycles, produce sites that are favorable for hydrogen trapping.

Mordkovich et al[14] report the formation of a new phase with the stoichiometry $LaNi_5H_4$ after "thermobaric" cycling (similar to HCI's "SCA" tests). This supports an earlier observation by Matsumoto and Matsushita[15] that a phase with the composition $LaNi_5H_4$ forms at temperatures above 40°C (104°F). The mechanism is apparently a eutectoid decomposition. Just 60 cycles was enough to greatly intensify the γ-phase peaks. The authors observed that the γ-phase becomes more stable after a large number of cycles, retaining its hydrogen at room temperature and atmospheric pressure. The latter observation implies that the eutectoid temperature falls during cycling. Formation of the γ-phase could account for a loss of reversible hydrogen capacity, e.g. $LaNi_5H_6 \rightarrow LaNi_5H_4+H_2$, with a reduction in hydrogen equilibrium pressure[16]. This mechanism could not account for hydrogen capacities less than H_4/H_6=67% of the original hydrogen capacity. Others place the hydrogen (deuterium) concentration nearer to $LaNi_5H_3$[17] and the crystal structure of the new phase is variously reported as hexagonal or orthorombic.

[13] D. Chandra and F.E. Lynch, Op. cit.

[14] V. Z, Mordkovich et al, "Degradation of LaNi5 by Thermobaric Cycling in Hydrogen and Hydrogen-Nitrogen Mixture", Int. J. Hydrogen Energy, Vol. 15, No. 10 (1990).

[15] T. Matsumoto and A. Matsushita, "A New Intermediate Hydride in the $LaNi_5$-H_2 System Studied by In Situ X-ray Diffractometry", *Journal of the Less Common Metals*, Vol. 123, pp. 135-144, Elsevier Sequoia S. A., Lausanne, Netherlands, 1986.

[16] A. L. Shilov, M. E. Kost and N.T. Kuznetsov, "The System $LaNi_5$- H_2", *Journal of the Less Common Metals*, Vol. 144, pp. 23-30, Elsevier Sequoia S. A., Lausanne, Netherlands, 1988.

[17] H. Hayakawa et al, "Time of Flight Neutron Powder Diffraction Study of the $LaNi_5D_3$ Structure", *Journal of the Less Common Metals*, Vol. 143, pp. 315-324, Elsevier Sequoia S. A., Lausanne, Netherlands, 1988.

Investigations of hydride degradation usually involve cycling, either by temperature swing or by pressure swing, suggesting a general belief that the number of cycles accumulated over time is the important test parameter rather than *time* per se. Aging tests at elevated temperatures by Sandrock et al[18] showed that degradation may occur without cycling. Samples aged at 180°C (356°F) showed degradation if they were held at temperature with enough hydrogen pressure to maintain the saturated hydride phase. Samples held at 180°C (356°F) temperature with hydrogen pressure just below the plateau pressure (i.e., desorbed) did not show significant degradation. This shows that degradation of this type mainly occurs in the saturated condition and does not require cycling--just time.

The experimental study, reported in the following sections of this report, confirms the findings of Sandrock et al regarding rapid degradation of $LaNi_5$-type hydrides at elevated temperatures and pressures. It is not clear whether this is the same mechanism as cyclic degradation. It is clear from the results presented in Section 7.3 that LaH_2 is not a primary product of $LaNi_5$-hydride degradation.

[18] G. D. Sandrock et al. "On the Disproportionation of Intermetallic Hydrides", *Zeitschrift für Physikalische Chemie Neue Folge*, R. Oldenbourg Verlag, Munich, West Germany, Vol. 164, pp. 1285-1290 (1989).

3.0 EXPERIMENTAL EQUIPMENT AND PROCEDURE

The experimental work was carried out by HCI and UNR at their facilities in Littleton, CO and Reno, NV respectively. Melting, heat treatment, metallography, rapid cycling and Sieverts analyses were carried out at HCI. X-ray diffraction and electron microscopy, were performed at UNR.

3.1 Alloy Preparation

Alloys were prepared by arc-melting on a water-cooled copper hearth in an argon atmosphere. Lanthanum and gadolinium (99%) were obtained from Union Molycorp. Electrolytic grade (99.92%) nickel was obtained from Inco. Vanadium from two sources was used in the study, 1) USBM Lot #11, 99.999% purity and 2) Teledyne Wah Chang 99.7% purity plate. High purity tin (99.999%) from Atlantic Metals and 99.8% VC from Alfa Products were used as additives in certain alloys.

Heat treatment of alloys, where required, was conducted by wrapping the specimens in tantalum foil, encapsulation in a stainless steel envelope sealed with a reduced pressure of argon and heating in a resistance furnace flooded with argon. Times for solution anneals of rare earth-nickel-tin alloys were established previously by metallography and by Sieverts analysis.

Brittle rare earth-nickel based alloys break readily into pieces sized to fit into the various reactors used in the study. There was no attempt to crush these alloys because they naturally become powders upon the first hydride cycle. Vanadium alloy buttons from the arc-furnace are too tough to crush. They were reduced to ca. 2 mm particles on a milling machine prior to hydriding.

3.2 Sieverts Apparatus

Pressure-temperature-composition (PTC) data were obtained with a conventional Sieverts apparatus, illustrated in Figure 3-1. HCI's Sieverts apparatus is located in a temperature-controlled room where the air temperature is maintained at 23°C by electric heaters with a proportional controller. The room air is stirred by a ceiling fan placed directly over the Sieverts apparatus. Hydride isotherms were obtained by adding or withdrawing small aliquots of hydrogen gas and noting the resulting hydrogen pressure after equilibrium was attained. The mass of hydrogen added or removed from the hydride samples was measured by noting the pressure changes in the precisely known volumes of the Sieverts apparatus. Pressure is measured by a variety of pressure gages and transducers, typically with 0.1% precision and recent calibration via a dead weight tester. Lower pressure instruments are calibrated against a mercury manometer. Hydrogen mass changes were calculated from an empirical equation of state based on National Bureau of Standards Technical Note 617.

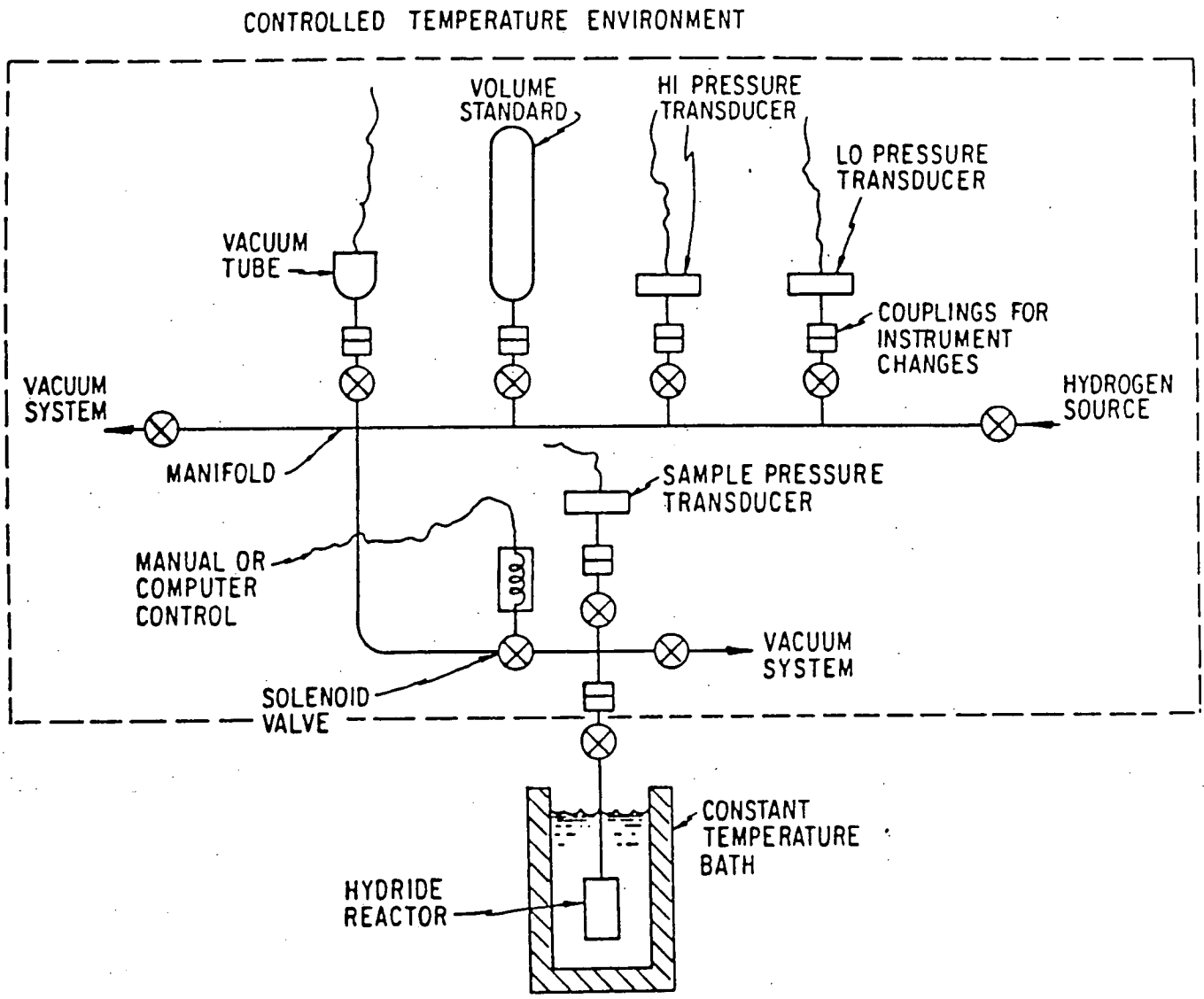

Figure 3-1. Schematic of a Sieverts Apparatus for measuring H_2 capacities and thermodynamic properties of metal hydrides.

The hydride specimens were sealed in stainless steel reactors containing a 2 micron sintered stainless steel (frit-type) filter to prevent the powdered material from escaping when hydrogen flows out of the reactor. Figure 3-2 is a photo of a disassembled hydride reactor showing the reaction chamber, the gland, connecting tube and valve that comprise the upper half of the reactor and the filter/gasket assembly that seals the two halves of the reactor together. Also shown in the photo are chunks of hydride alloy prior to activation, and the powdered hydride (in the metal pan) that results from reacting the alloy with hydrogen.

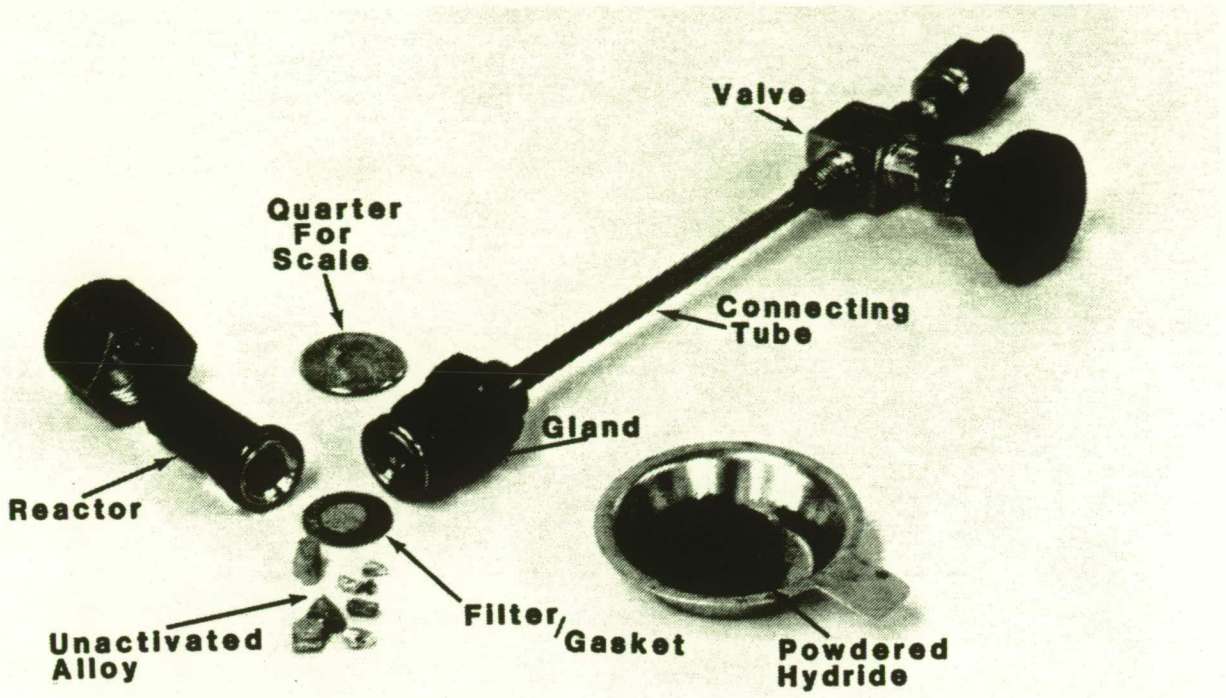

Figure 3-2. Disassembled hydride reactor showing the reaction chamber, the gland, valve and stem that form the upper half of the reactor, and the filter/gasket assembly that seals the two halves together. The metal pan holds the powder that results from reacting large granules of alloy with hydrogen.

3.3 Rapid Cycle Apparatus

In order to accumulate a large number of hydride/dehydride cycles in a reasonable period of time, a special apparatus was designed and fabricated. The rapid cycle apparatus (RCA) uses jets of superheated steam and cold water to heat and cool hydride alloy, contained in a shallow cup. Figure 3-3 is a schematic cross section of the RCA. Figure 3-4 is a photo of the RCA. The apparatus was proof-tested in a flack shield with argon gas at 10.3 MPa (1500 psig). The volume (1133cc) in the upper portion of the RCA serves as a hydrogen accumulator, receiving hydrogen as the sample desorbs and supplying hydrogen as the sample absorbs. The RCA is loaded with hydride alloy in a glove box filled with UHP hydrogen. The RCA is equipped with two sight glasses; one is used for viewing the sample, the other transmits light. The sight glasses were recommended by JSC's Mike Rouen at the project kick-off meeting. Some of the most intriguing and valuable information gained during this study was obtained by viewing and photographing hydrides through these sight glasses.

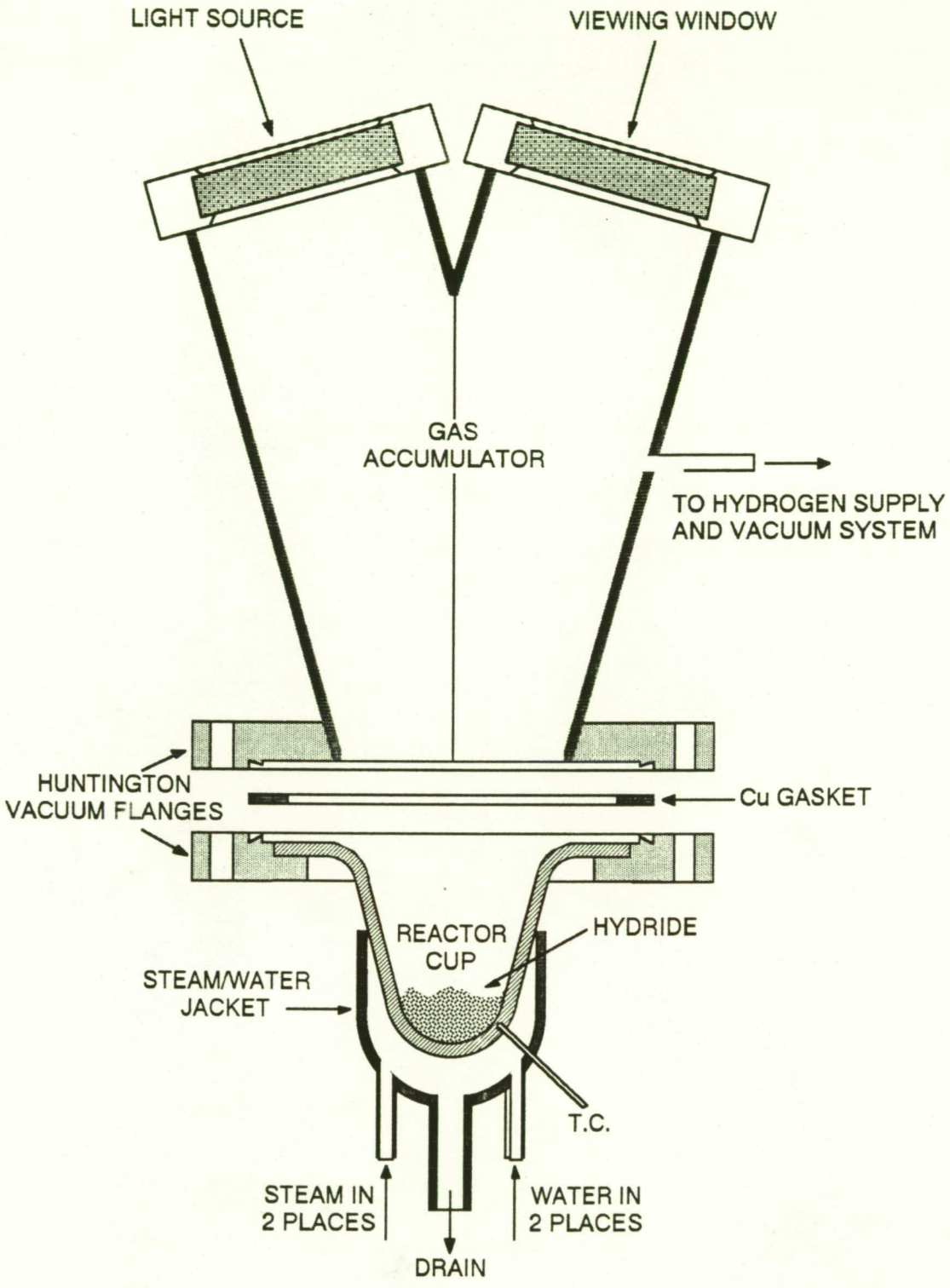

Figure 3-3. Schematic of the RCA. The hydride specimen is heated by steam jets and cooled by water jets in typical cycle periods of a few minutes.

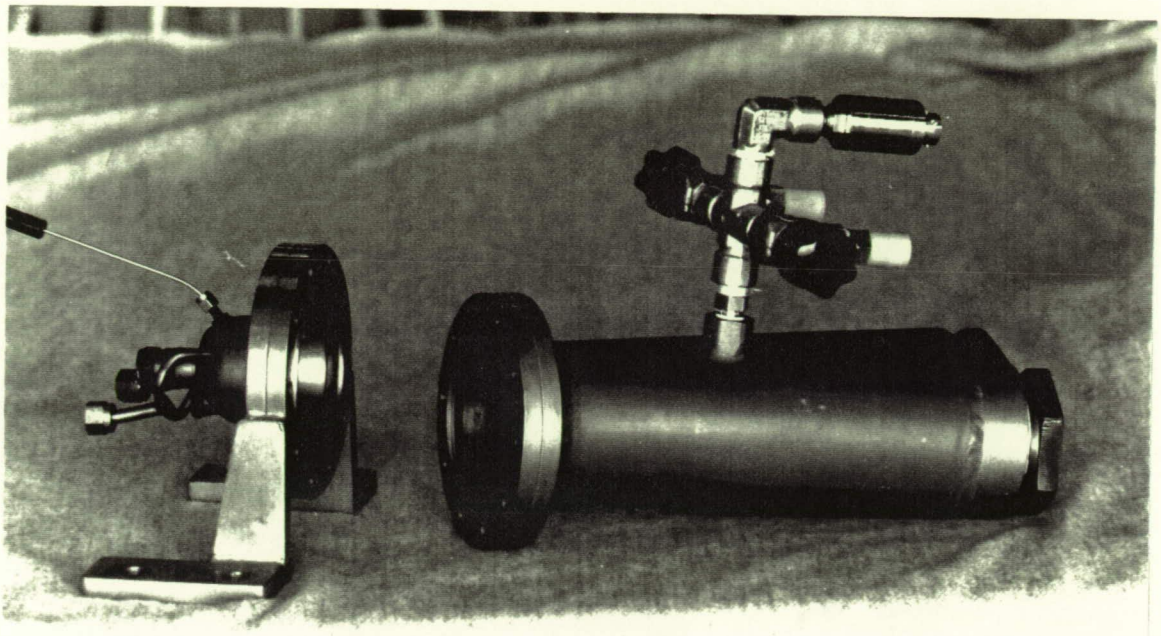

Figure 3-4. Photograph of the two halves of the RCA. The upper half (on the right here) is fitted with a pressure transducer, a hydrogen valve and a vacuum valve. The lower half (on the left here) if fitted with a thermocouple and the manifolding for cold water and steam.

A deionized water supply is alternately fed to the cooling water jets or a steam generator by the water control valves. A throttle valve adjusts the flow of water to the steam generator to achieve the desired heating rate. The heating and cooling rates vary according to the sample size and are generally in the neighborhood of 3 to 5 minutes. The temperature of the reactor cup is monitored by a type J thermocouple embedded in the wall of the cup. It is recognized that there are temperature gradients in the powdered sample and that only the portion nearest the wall reaches the temperature of the cup. HCI has designed hydride reactors in the past that minimize sample temperature gradients, but those designs are not amenable to rapid cycling or viewing. The powdered sample stirs itself during cycling as it expands and contracts so, on the average, all particles accrue the same cyclic history (see Section 7.1, Fig.s 7-3a, b, c, d). In a self-stirring RCA specimen, the material closest to the surface of the reactor cup transforms in seconds. At increasing distances inward from the wall, transformation takes place over periods of a few minutes, depending on the cooling cycle period. The material at the center of the cup does not transform at all until stirring transports it to the edge.

The rise and fall of hydrogen pressure during the heating/cooling cycles is monitored on a Sensometrics 6895 kPa (1000 psia) pressure transducer whose stated accuracy is 0.1% of full scale (1 psia). Observation of the cyclic pressure swing on this transducer provides a great deal of information about the status of the hydride. The initial pressure loading in the apparatus is set by centering the dynamic pressure swing around the log mean equilibrium pressure as shown in Figure 3-5, i.e.;

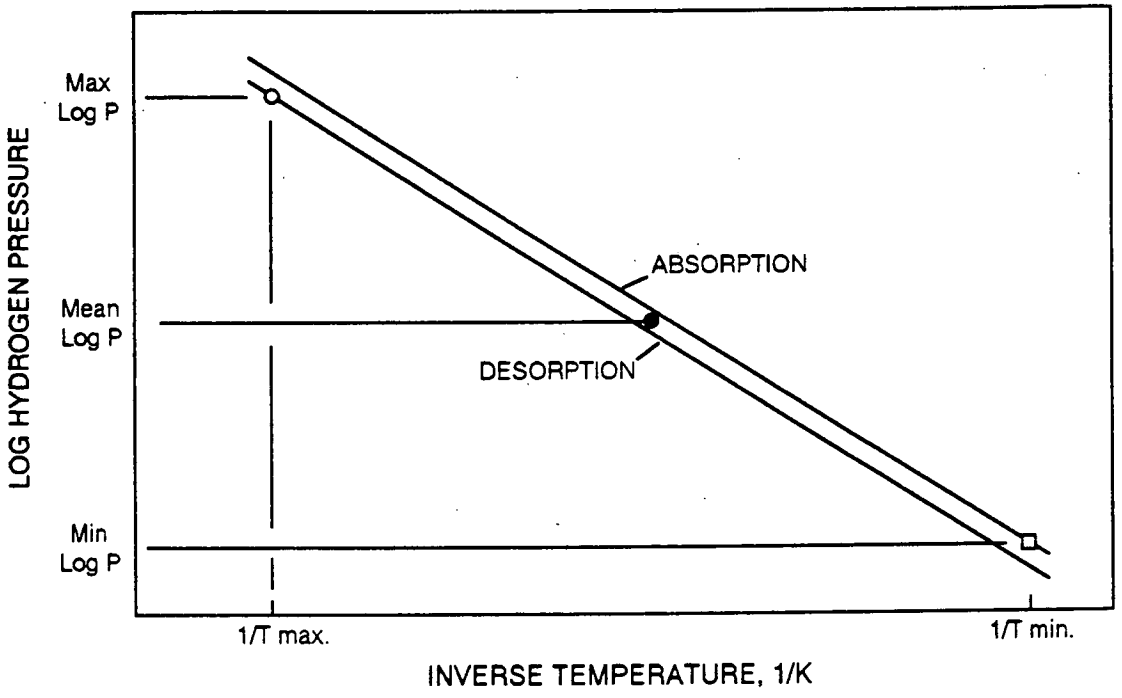

Figure 3-5. Initial pressure loading in the RCA is P = exp (log mean P).

[II] $$\text{Mean Log P} = [\text{Log}(P_{des} @ \text{Max T}) + \text{Log}(P_{abs} @ \text{Min. T})] \div 2$$

The minimum and maximum cycle pressures and temperatures are noted throughout the cyclic testing. The minimum pressure, observed toward the end of a cooling period indicates any changes in hydrogen capacity. The RCA is a closed system so there are only two places for hydrogen to be; 1) as a gas in the accumulator volume or 2) as a solid, adsorbed or absorbed by the metal. The gas accumulator undergoes a small temperature swing as the warm hydrogen comes and goes from the sample but this is the same on each cycle, and the room temperature is held constant in HCI's hydride laboratory. Therefore, if the minimum cycle pressure in the accumulator is constant, the hydrogen content of the hydride must be constant. If the minimum hydrogen pressure increases with cycling the only explanation is that the metal has lost some of its *total* hydrogen capacity. This type of degradation is illustrated in Figure 3-6.

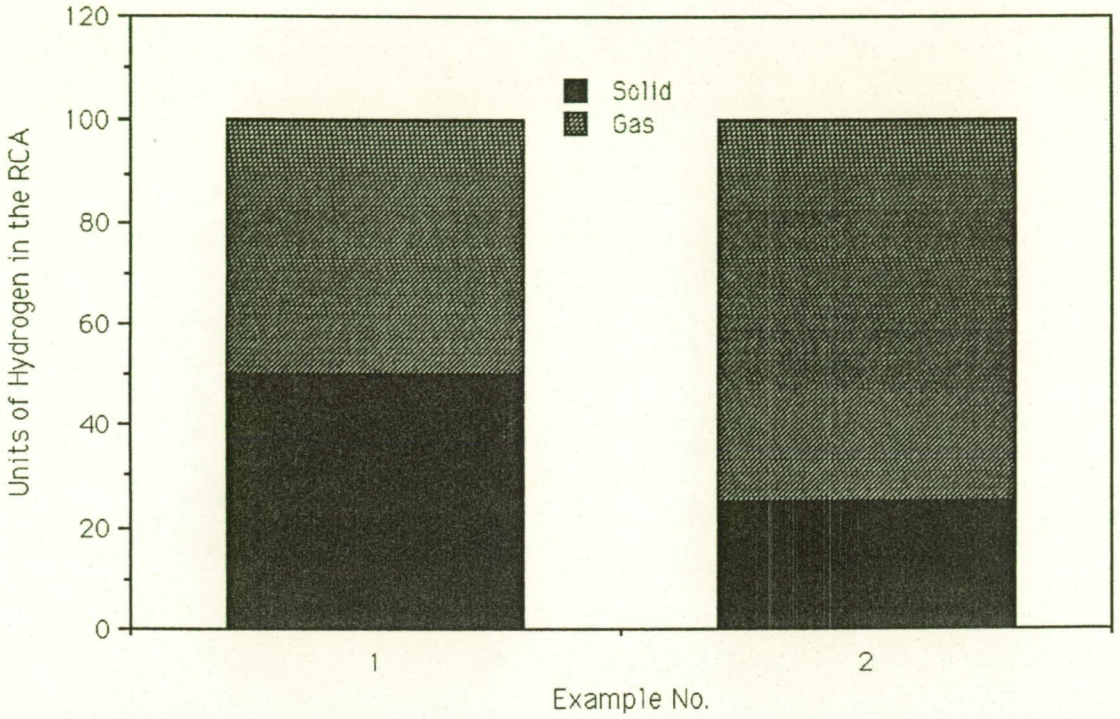

Figure 3-6. Hypothetical examples of hydrogen inventory in the RCA at the end of a cooling period;

Example 1 shows 100 units of hydrogen in the RCA at the end of a cooling period -- 50 units in the gaseous state and 50 units in the solid state in an undegraded hydride.

Example 2 shows that if the hydride retains less in the solid state, say 25 units, the difference will be observed as an increase in the amount of gas, i.e., a pressure increase in the RCA's gas volume.

If the minimum cycle pressure is constant and the maximum cycle pressure falls during cycling, the *reversible* hydrogen capacity decreases while the *total* hydrogen capacity remains constant. This type of degradation is illustrated in Figure 3-7.

By combining the information gained from the hot and cold hydrogen inventories the degradation status of the hydride is defined. The cold data show any changes in the *total* hydrogen content of the solid. The hot data show any change in the *reversible* hydrogen content. The difference between *total* and *reversible* hydrogen capacity is *irreversible* (at least under the these test conditions) hydrogen retained in the solid.

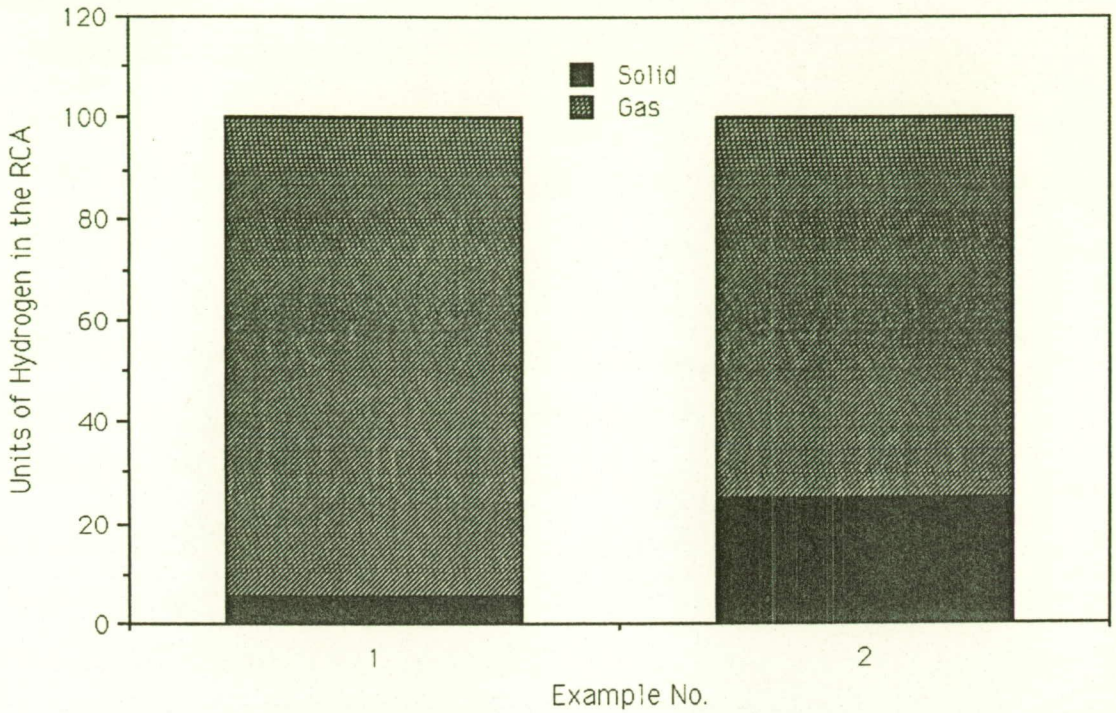

Figure 3-7. Hypothetical examples of hydrogen inventory in the RCA at the end of a heating period;

Example 1 shows 100 units of hydrogen in the RCA at the end of a heating period -- 95 units in the gaseous state (the original 50 plus 45 desorbed) and 5 units dissolved in an undegraded metal.

Example 2 shows that if the hydride releases less gas during desorption, say only 25 units, the difference is observed as a decrease in the amount of gas (the maximum cycle pressure is decreased) because 25 units of hydrogen are retained in the solid.

Thus the two types of degradation that can be observed with the RCA are changes in reversible and irreversible hydrogen capacities. The amount of each may be assessed by observing the maximum and minimum cycle pressures as described by Figures 3-6 and 3-7. Figure 3-8 compares an undegraded hydride with three degraded hydrides based on information gained from the high and low pressures in the cycle.

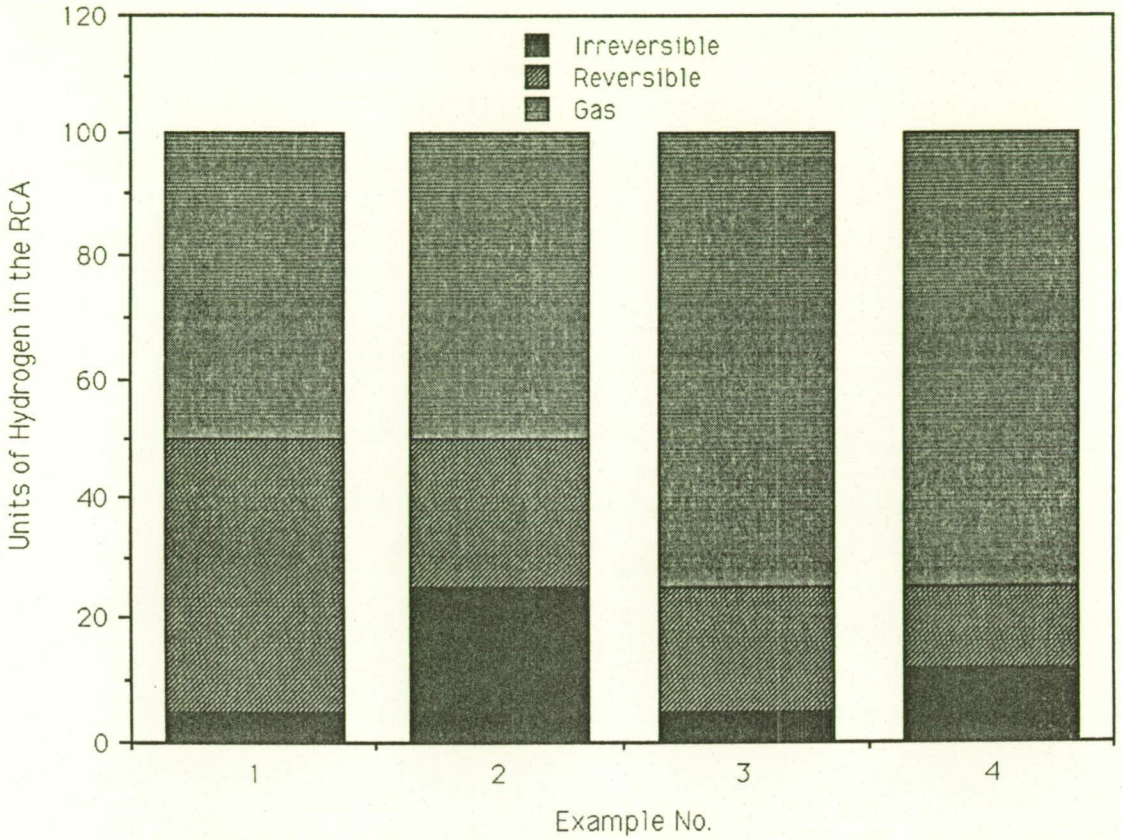

Figure 3-8. Hypothetical examples of hydrogen inventory in the RCA.

Example 1 shows 100 units of hydrogen in the RCA at the end of a cooling period -- 50 units in the gaseous state, 50 units in the solid state. On heating 45 of the solid units are found to be *reversible* and 5 units are retained in an undegraded metal.

Example 2 also shows 50 units of solid hydrogen but on heating only 25 units are found to be reversible. 25 units of hydrogen are therefore irreversibly retained in the solid.

Example 3 also shows a loss of *reversible* hydrogen capacity. A loss in *total* hydrogen capacity is responsible for the change and this is noted by an increased minimum cycle pressure corresponding to 75 units of gas at the end of the cooling period.

Example 4 shows both types of degradation. 75 units of gas in the cooled condition show a 25 unit loss of *total* hydrogen capacity. Upon heating only 13 units of gas are evolved, indicating that 12 units are retained in the solid.

The sensitivity of the digital pressure transducer and its readout is ± 7 kPa (±1 psia). Sample sizes are set to produce between 69 and 345 kPa (10 to 50 psia) of pressure swing thus yielding a sensitivity of between 10% and 2% to changes in maximum or minimum pressures. This rather low sensitivity is sufficient for qualitative observations of degradation. More precise measurements are made by transferring a portion of a degraded sample to the Sieverts apparatus.

3.4 Slow Cycling Apparatus

The SCA is shown schematically in Figure 3-9. The purpose of the apparatus is to cause hydrides to transform from hydride to metal and back again each time the reactors are heated to 125°C and cooled to room temperature. The pressure vessels are of two sizes. The larger (500 cc) pressure vessels have enough volume to receive the hydrogen discharged from lower pressure hydrides, e.g., $LaNi_{4.8}Sn_{0.22}$, at a pressure significantly less than the desorption plateau pressure at 125°C. The smaller (75 cc) pressure vessels accomplish the same thing for higher pressure hydrides, e.g., $La_{0.9}Gd_{0.1}Ni_5$.

The heating/cooling process is controlled by a clock timer that switches the heating element on and off during a one-hour cycle. The maximum air temperature is set at 125°C by adjusting the heater power with a variac transformer and by throttling the inlet air to the blower. Thermocouples in the reactors verify that the hydride at the center of the reactor reaches 125±5°C on each cycle.

Hydrides in this closed system (free of contamination from outside sources) are caused to charge and discharge as they are thermally cycled. The pressure gauges and thermocouples provide a simple way to check on the performance of the alloys during several months of charging and discharging, once per hour. Figure 3-10 shows the progress of a typical cycle. Starting from 24°C at 170 kPa, the sample pressure increased slowly to 250 kPa as the temperature at the core of the reactor rose to 60°C. From 60°C to 85°C most of the hydrogen was discharged to the pressure vessel as the pressure climbed from 250 kPa to 450 kPa. Further heating from 85°C to 125°C raised the pressure over the discharged hydride from 450 kPa to 510 kPa. As expected, most of the pressure change occurred when the hydride transformed to metal in the range of pressures and temperatures corresponding to the van't Hoff equilibrium lines.

During cooling, Figure 3-10 shows a similar pressure-temperature relationship. From 125°C to 85°C there was very little change in pressure. As the data crossed the equilibrium lines a large pressure drop occurred corresponding to the phase change from metal to hydride. Subsequent cooling resulted in a minor pressure drop as the hydride became saturated at room temperature.

Interpretation of changes in maximum and minimum cycle pressures are the same as with the RCA, discussed in Section 3.3 above. It is apparent from changes in maximum and minimum cycle pressures whether degradation has occurred via hydrogen trapping or by a decrease in total hydrogen capacity.

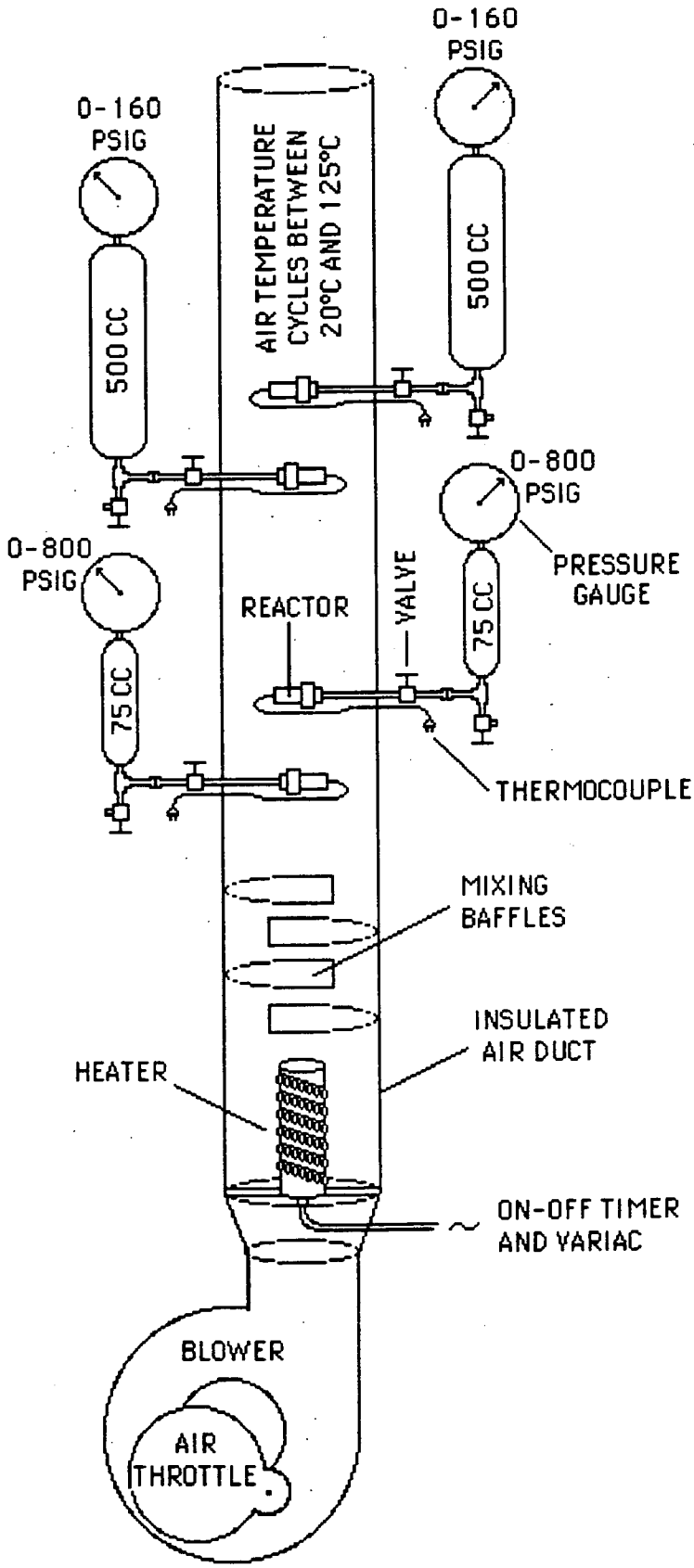

Figure 3-9. Slow Cycle Apparatus (SCA) heats and cools hydrides once per hour.

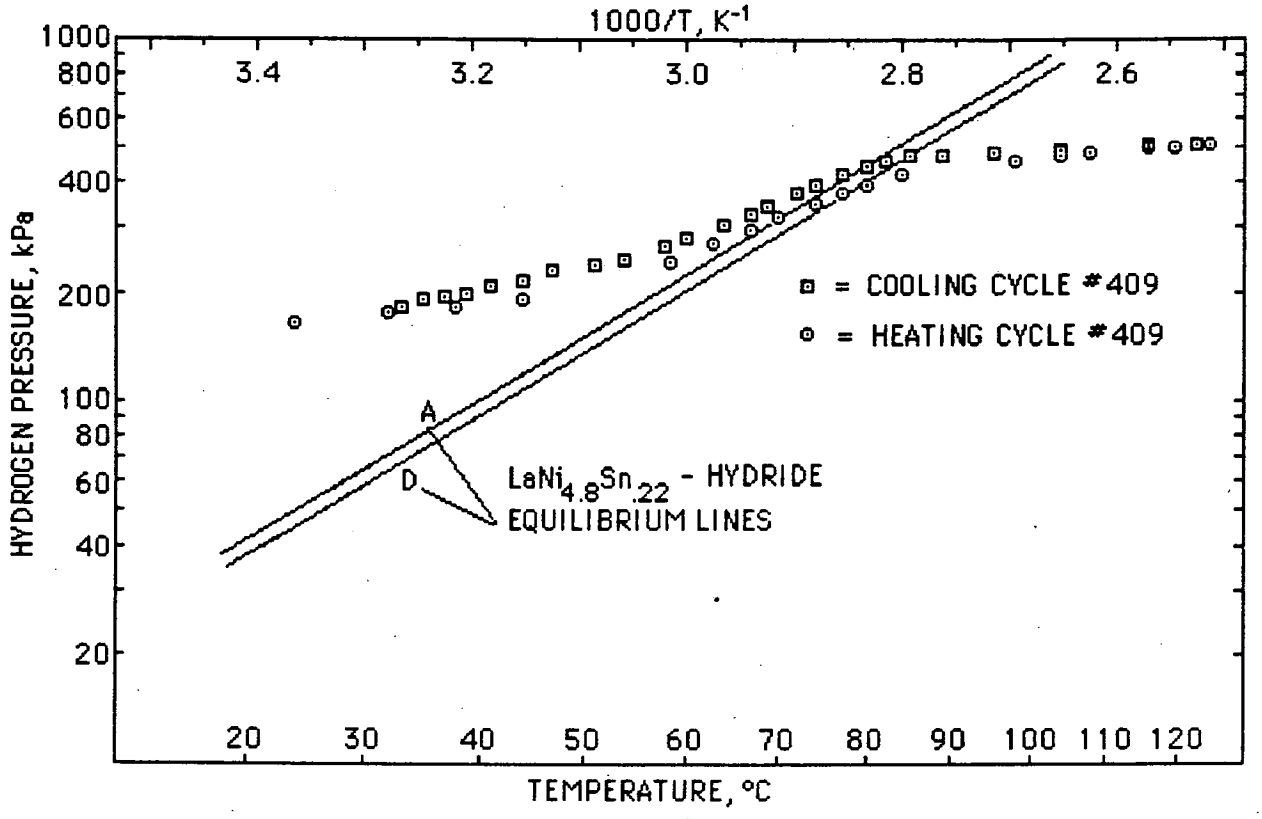

Figure 3-10. Heating in the SCA causes desorption as hydrogen pressure to falls below the van't Hoff equilibrium desorption pressure line (80-125°C). Cooling causes absorption as the pressure to exceeds the van't Hoff equilibrium pressure line (70-25°C).

3.5 Thermal Aging

Another method of aging applied to hydrides in this study consists of soaking the hydrides at elevated temperatures in a conventional Sieverts apparatus reactor. Earlier work by Ergenics[19] found that holding saturated hydrides well above room temperature with large hydrogen pressures accelerated the degradation process.

The tests consist of activating a hydride alloy, absorbing and desorbing 10 times to break-in the material, applying enough hydrogen pressure to hold the desired composition at elevated temperature, then heating the samples and holding them at high temperature for a specified period. Upon subsequent cooling and Sieverts analysis, any changes in the absorption or desorption isotherms are noted. By carefully observing hydrogen pressures in the closed system throughout the aging process it is possible to determine, by reasoning similar to the RCA studies (e.g.,

[19] G. D. Sandrock et al. "On the Disproportionation of Intermetallic Hydrides", *Zeitschrift für Physikalische Chemie Neue Folge*, R. Oldenbourg Verlag, Munich, West Germany, Vol. 164, pp. 1285-1290 (1989).

Figures 3-6, 3-7, 3-8), whether reversible capacity degradation has occurred by retention of stable hydrogen in the solid or by decreased total hydrogen capacity.

Figure 3-11 is a photograph of the TA apparatus. The large pressure gauge is a 3000 psia Heise (± 0.1% of full scale). The smaller pressure gage is attached to a metal hydride compressor/ultrapure hydrogen source used to attain up to 3000 psia. The electric cord powers the sheath heater for the hydride compressor. The Sieverts reactor at the bottom of Figure 3-11 is inserted in a tubular resistance furnace during the thermal aging process.

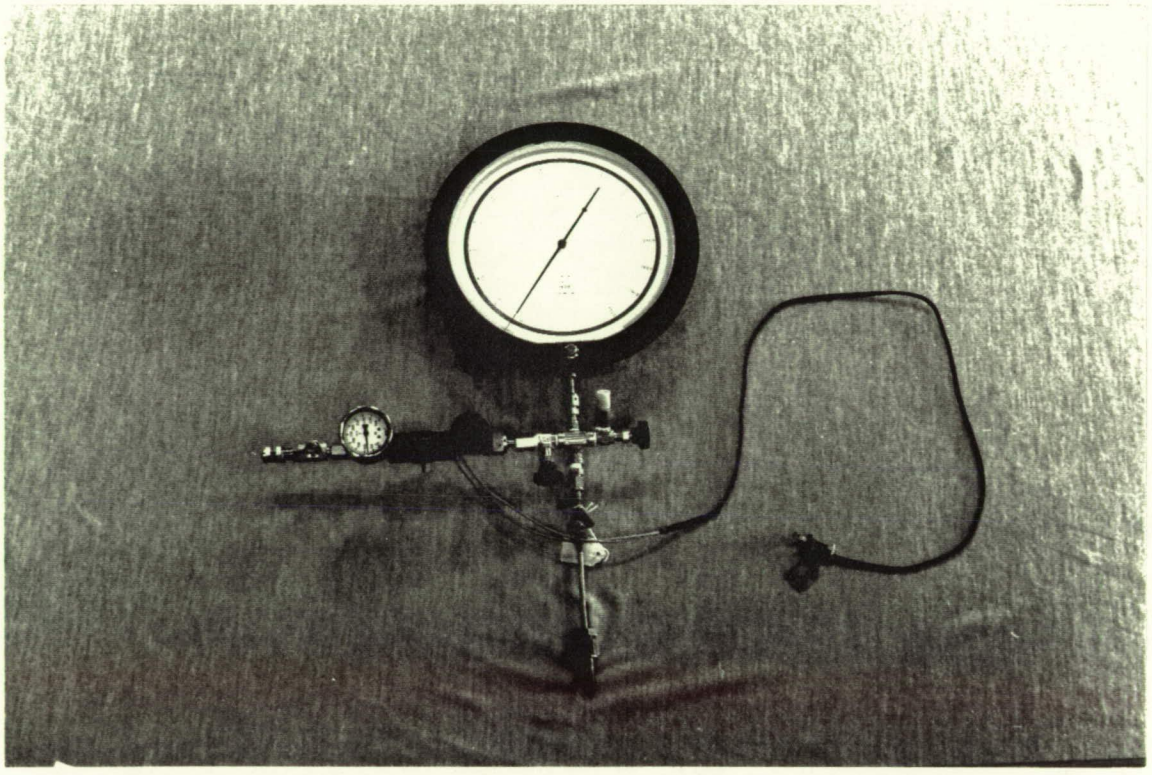

Figure 3-11. Photograph of the Thermal Aging Apparatus.

3.6 Hydrogen Glove Box

A pumpable glove box was equipped with an ultra high purity (UHP) hydrogen supply system. Just prior to each use of the glove box the system was pumped to ~10^{-3} Torr and back-filled with UHP hydrogen 3 times Figure 3-12 is a photograph of the hydrogen glove box.

A refrigerated aluminum block was built into the glove box to allow hydride specimens to be ground in a chilled mortar and pestle, mixed with silicon X-ray standard powder and sealed into chilled quartz capillaries for X-ray diffraction analysis (see Figure 3-13) The chilled aluminum block was refrigerated to 255 K (0°F). At this

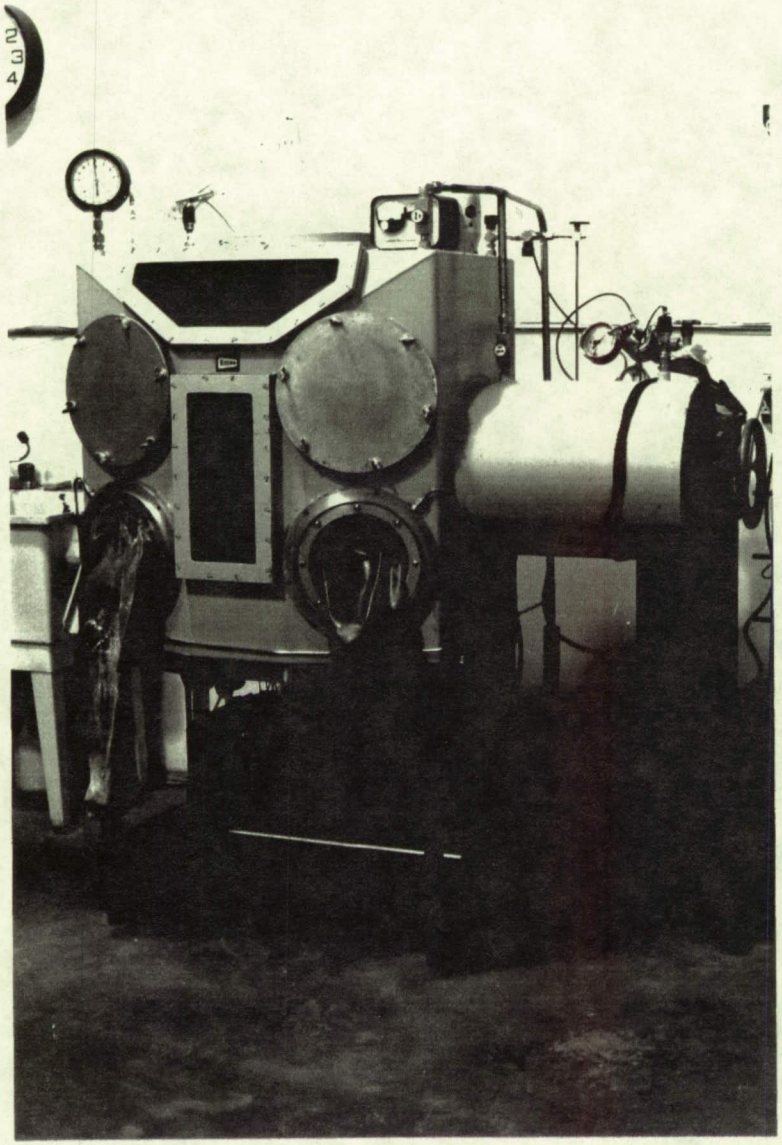

Figure 3-12. Photograph of the pumpable H_2 glove box.

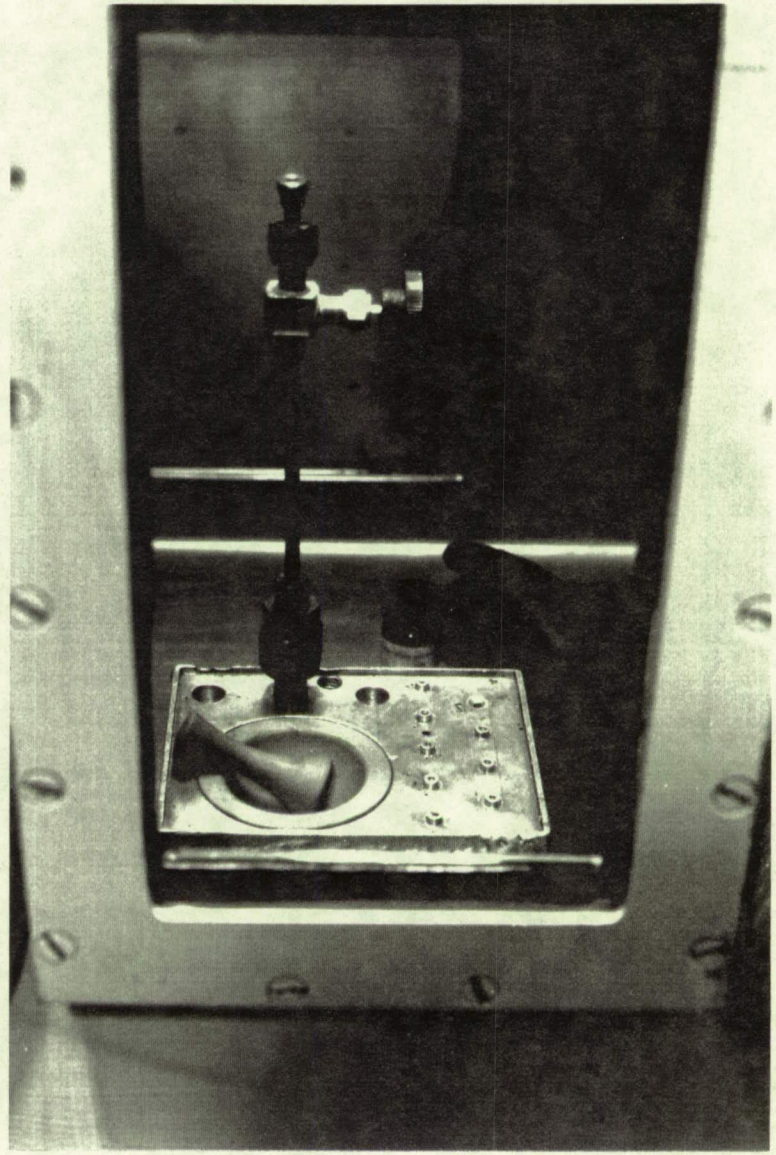

Figure 3-13. Photograph of the chilled aluminum block for preparation of X-ray specimens.

temperature, most hydrides of interest have equilibrium desorption pressures that are less than atmospheric (83 kPa or 12 psia in Littleton, CO). Therefore, when chilled hydrides are exposed to the glove box atmosphere, they remain fully charged with hydrogen. Recesses machined into the block fit tightly around Sieverts reactors to chill them prior to opening. A mortar also fits snugly into a recess in the block to chill it and a pestle so that X-ray samples do not warm up during grinding and mixing with silicon powder. The quartz capillaries also fit into holes in the aluminum block to pre-chill them. The capillaries are sealed with quick-setting epoxy.

3.7 X-ray Diffraction Analyses

Most of the X-ray diffraction analyses were performed on Philips APD 1740 and APD 3720 systems, equipped with graphite crystal monochromators. Copper K_α radiation was used. In the special case of highly degraded $La_{0.9}Gd_{0.1}Ni_5$, a Rigaku system with a high power rotating anode X-ray tube (Cu) was applied. An NBS silicon standard was added to all hydrided samples in sealed capillaries. Philips software was used to obtain the d-spacings, however indexing of the Bragg peaks was performed manually. The lattice parameters were obtained by using a least square method.

The line profile analyses were performed using the Philips line profile program. A Line B program was obtained from Prof. J.B. Cohen at a "Line Profile Analyses Workshop" held at Northwestern University in 1984. This has recently been installed on UNR's PDP 11 computer. A third program was obtained from Prof. De Angelis at the University of Kentucky, which also has a single line analysis program. Measurements of strain and domain size in the lattice were performed by first selecting appropriate sets of two peaks, such as (110), (220), and collecting over a 2θ range. The reference peaks for Stokes corrections from the standard were obtained by appropriate pattern treatment, i.e., background subtraction and correction of peak position errors via internal NBS Si standard. Then the line profile analyses were performed by obtaining cosine coefficients for both reflections. Applying Stokes correction[20], the true broadening of the peak and the sine and cosine coefficients of the true broadened function were obtained. The strain (E_n) was calculated by Fourier Analysis methods[21]. The particle sizes ($D_{eff.}$) were determined by the Warren-Averbach method[22]

[20] A.R. Stokes, Proc. Phys. Soc., 61, p. 382 (1942)

[21] L.H. Schwartz and J.B. Cohen, *Diffraction from Metals*, Academic Press (1977).

[22] B.E. Warren and B.L. Averbach, J. Appl. Phys., 21, p. 174 (1950)

4.0 CONTAINMENT PROBLEMS

A unique hydride containment problem recently surfaced to the detriment of two NASA development/demonstration projects. Metal hydrides are the basis of a hydrogen compressor in a hydrogen liquefaction system that HCI recently built and demonstrated for Kennedy Space Center (NAS 10-11401). HCI is currently developing an EMU metal hydride heat pump for Johnson Space Center (NAS 9-17819). Both of these programs were baselined with vanadium dihydride because of its large hydrogen capacity and large heat of reaction. HCI's Quality Control testing identified a problem that was subsequently traced to a phenomenon not mentioned in the literature. The problem only surfaced when hundreds of cycles of absorption/desorption were applied to qualify vanadium-based hydrides for use in NASA applications. Long term cycling causes the material to take on a sponge-like form whose volume increases until it fractures the strongest of containers.

The following is a discussion of hydride container design that serves as a backdrop for further explanation of the vanadium dihydride expansion problem in Section 5.

4.1 Overview of Hydride Containers

Metal hydrides require specialized containers. Many NASA applications involve significant hydrogen pressures in normal operation or in off-nominal conditions (e.g., hot environments). In addition to gas pressures, hydride containers must withstand expansion forces generated by hydrides--typically powders that grow 20-30% in volume as they absorb hydrogen. These expansion forces are, for all practical purposes, irresistible. Therefore, hydride containers must be designed to prevent the migration of the contracted metal powder into spaces that are too small to contain the expanded hydride phase. Otherwise enormous forces are generated, resulting in container strain and rupture. Even in well-designed containers, if there is any settling of the metal phase as the hydrogen is depleted, expansion during subsequent hydriding exerts moderate forces on the container walls as the settled powder grows to fill the available volume. For these reasons, hydride containers are usually configured as pressure vessels (PVs) with internal features that limit redistribution of the powder.

NASA applications are usually mass-sensitive. Lightweight PVs are inevitably cylindrical or spherical. Spherical PVs are the lightest alternative, but spheres are seldom used for hydride containment because of heat transfer considerations. A single spherical PV seldom has enough surface area to meet the charge/discharge rate requirements of practical hydride applications. Putting additional surface area inside the sphere (coils, plates, etc.) dilutes the PV mass advantage of a sphere, relative to a cylinder. Internal surfaces also complicate the design and are vulnerable to the expansion forces mentioned above. The alternative of employing many small spheres to improve heat transfer leads to complex plumbing networks and inefficient use of space (spheres pack poorly). For these reasons, HCI usually designs its hydride containers around thin cylindrical tubes. If a single tube will not suffice, tubes

are grouped into hexagonal bundles, as in Figure 4-1. The external jacket has inlet and outlet fittings to route heat transfer fluids through the tube bundle.

4.2 Typical Intermetallic Hydride Containment

Intermetallic compounds, such as $LaNi_5$ or FeTi, are very brittle. They crumble into fine powders when they are first exposed to hydrogen (i.e., "activated"). Aside from a gradual decrease in average particle size that eventually levels off on the order of 10μ, these materials retain their physical appearance through thousands of cycles, regardless of degradation in other hydride properties. The expansion and contraction can be accommodated in a hydride container by simply allowing enough room for the larger hydride phase, taking into account the void spaces in the powder. If the container is too small, the expanding hydride will damage it on the very first cycle. If the container is large enough to hold the hydride phase and some means, such as the filter support spiders in Figure 4-1, prevents uneven powder distribution inside the tubes, the hydride container may be cycled indefinitely without encountering hydride expansion problems. These hard brittle hydride powders may become compacted into loose clods but they will not fuse into a solid mass.

4.3 Vanadium Dihydride Sponges

The recently discovered vanadium dihydride expansion problem is entirely different from the intermetallic hydride expansion discussed above. At the beginning of a cyclic test, stainless steel containers that are capable of withstanding several 10s of MPas (thousands of psi) are loaded with metal chips generated by milling of solid metal samples. The containers are large enough to accommodate the expansion that accompanies the formation of the VH_2 phase with room to spare. Hundreds of absorption/desorption cycles pass with no outward indication of a problem. Eventually, however, swelling, distortion and rupture occur.

Examination of the contents of failed cyclic test reactors show that the crystalline mill chips loaded at the beginning of the test fuse themselves into a cohesive solid. Micrographs show that regions within the solid are riddled with holes, like a sponge (see Figure 4-2). This type of particle adhesion is not observed with the brittle intermetallic hydrides so HCI attempted to solve the problem by forming vanadium alloys with embrittling additives[23]. Minor amounts of carbon (e.g. 0.5 atom percent) had a beneficial effect on the cyclic reactor swelling problem. Whereas pure vanadium dihydride usually broke reactors in less than 200 cycles, a reactor filled with $V_{0.995}C_{0.005}$ showed no strain through ~1000 cycles of absorption/desorption.

Based on this apparent resolution to the problem, $V_{0.995}C_{0.005}$ was baselined as one of the two hydrides in the EMU's Metal Hydride Heat Pump (MHHP). A model of a MHHP heat exchanger tube was fabricated and filled with $V_{0.995}C_{0.005}$. Thermal cycling was applied via a high intensity quartz lamp and an air blower so that the

[23] W. Rostoker, *The Metallurgy of Vanadium*, Wiley N.Y. (1958).

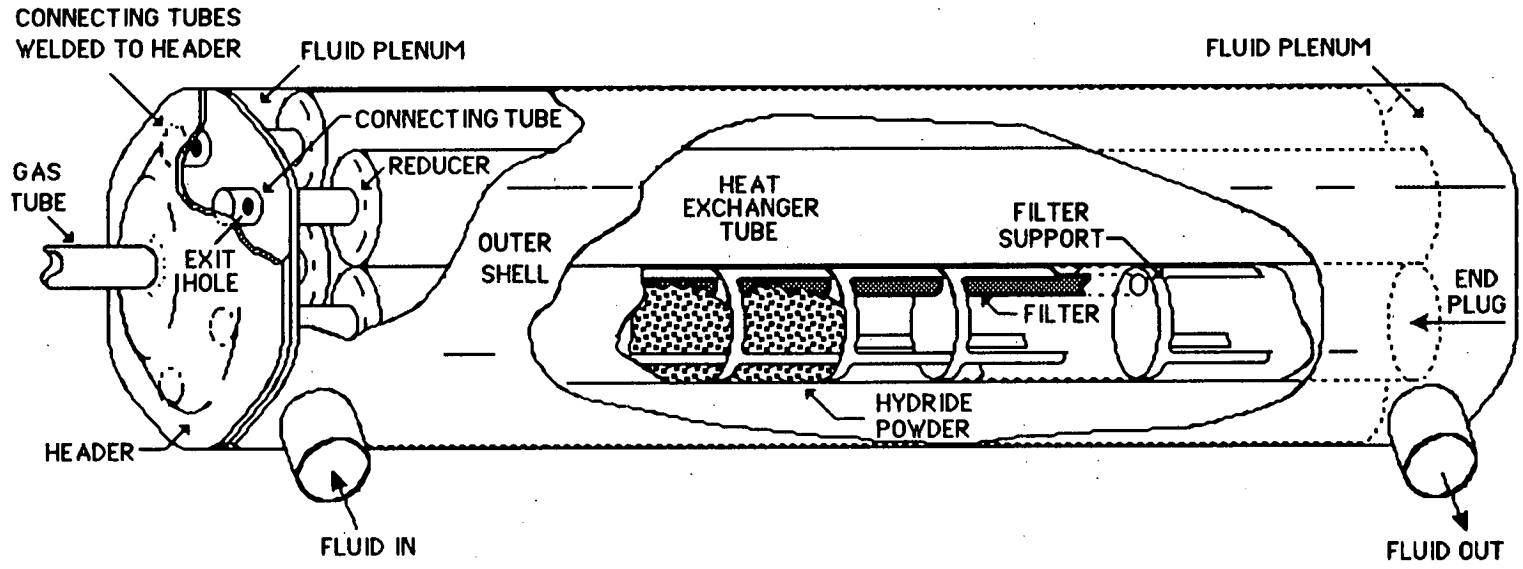

Figure 4-1. A typical metal hydride container/heat exchanger is a hexagonal bundle of thin-walled tubes surrounded by a shell that is filled with heat transfer fluids. Filters screen powder particles out of the hydrogen flow. The filter supports maintain even distribution of the powdered material along the length of the tube. Without the filter supports the powder could shift to one end of the tubes and strain them as the metal powder expands (typically 25%) to form the hydride.

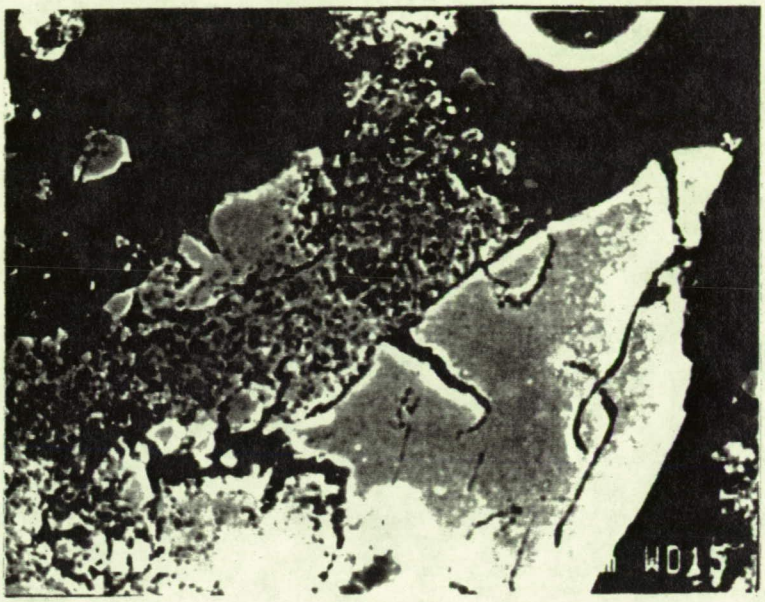

Figure 4-2. UNR Scanning electron micrograph of 778-cycle $V_{0.995}C_{0.005}$-hydride specimen at 3850x. A portion of the material has transformed into a porous sponge.

model tube heated to 125°C and cooled to room temperature (˜20°C) on a 2-hour schedule. After the tube had accumulated 336 cycles of thermally induced absorption/desorption, physical examination showed no change in external tube dimensions. A rough isotherm taken with the model heat exchanger tube showed a slight decrease in desorption pressure but the original hydrogen capacity was retained and no other problems were apparent.

The next periodic examination was conducted after 778 cycles of absorption/desorption had accumulated. At that time, the model tube showed significant bulges from expansion of its contents. The original tube diameter was 1.590-1.595 cm (0.626-0.628 in.). After 778 cycles, bulges were visually apparent between each filter support and the next. The largest bulge measured 1.694 cm (0.667 in.). Figure 4-3 is an X-ray photograph of the model tube.

Since it had taken so long for the expansion problem to develop in the thin-walled MHHP heat exchanger model, it was of interest to learn whether the much sturdier Sieverts-type reactor would resist it indefinitely. Cycling was resumed with the same reactor that had shown no swelling after ˜1000 cycles. Examination after 1345 cycles showed that the sturdy Sieverts reactor was also beginning to swell. The carbon additive delays the swelling, relative to pure vanadium dihydride, but eventually very strong containers will be strained by the expanding hydride sponge.

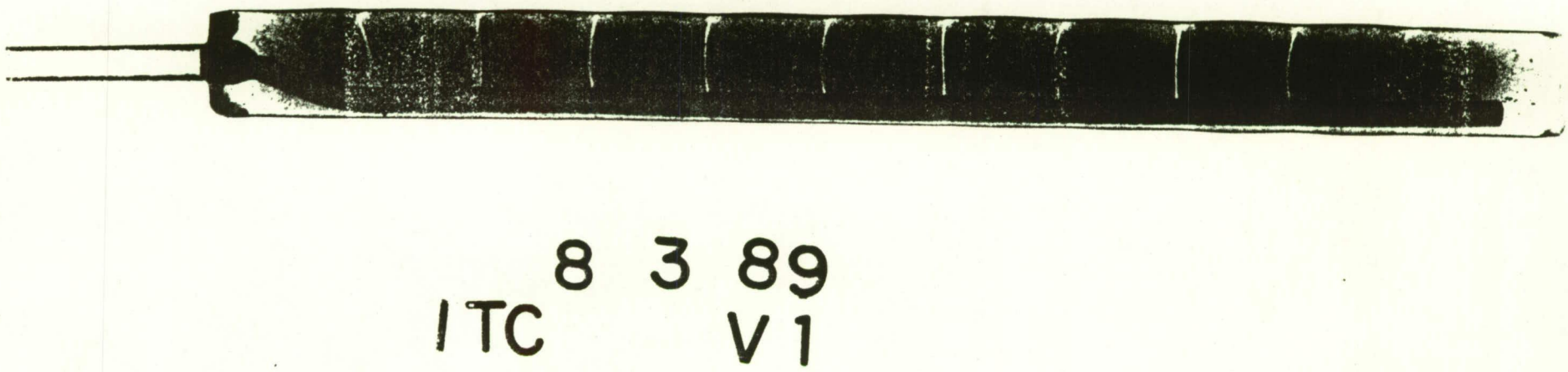

Figure 4-3. X-ray photograph of a model hydride heat exchanger tube that has developed bulges during 778 cycles of absorption/desorption.

Compared to the dramatic physical changes that occur as VH/VH_2 fuses into a growing sponge, there was relatively little variation in thermodynamic properties during the cyclic tests. The badly strained 778 cycle MHHP model tube produced a 25°C desorption isotherm that was not significantly different from the freshly activated material. Higher precision absorption and desorption isotherms, taken with a standard Sieverts reactor after 1345 cycles, are compared in Figure 4-4 to isotherms of fresh material. The hysteresis band grew (i.e., the absorption pressure increased) but the hydrogen capacity and desorption pressure are not seriously degraded after the equivalent of nearly four years of simulated daily MHHP use.

The reasons for the container damage and the increase in absorption/desorption hysteresis are discussed at length in Section 5.

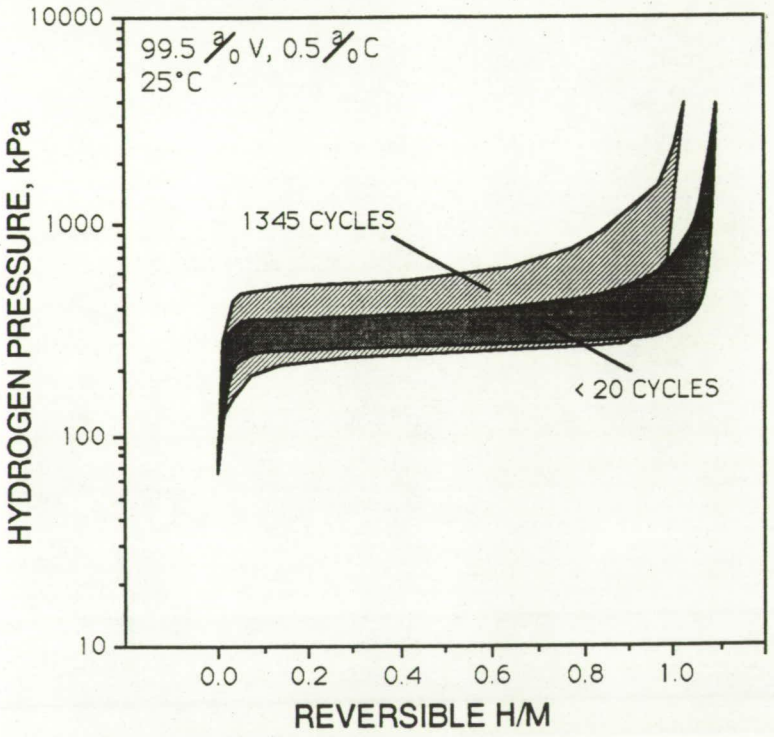

Figure 4-4. Comparison of 25°C isotherms of V-C hydrides before and after 1345 cycles of absorption/ desorption cycling in the Slow Cycle Apparatus.

5.0 CYCLIC DEGRADATION OF V-ALLOY DIHYDRIDE

One of the most intriguing observations of this project was the identification of a low density form of VH_2 not described in the literature. Time-lapse photography shows that the original shiny metallic-looking material undergoes a spontaneous physical change upon cycling. A low density dark gray material, nick-named "dust bunnies" by HCI test personnel, gradually grows by eroding higher density metallic particles. The material appears to the eye, and to the highest magnitude of scanning electron microscopy, as a formless fluffy mass. As discussed in Section 4.3, the growth is capable of straining and eventually fracturing the sturdiest of hydride containers.

Pure vanadium and its hydrides (VH, VH_2) formed a baseline for PTC and X-ray analyses. Vanadium with 0.5 atom-percent carbon was studied because it had shown improvements (see Section 4.3), relative to pure vanadium, in previous cyclic tests. A third alloy, $V_{0.975}Zr_{0.020}C_{0.005}$, was subjected to RCA tests because difficulties were experienced in activating pure V within the pressure/temperature range of the RCA. The zirconium additive is beneficial for ease of activation[24].

5.1 Baseline Hydride Isotherms

The "Reversible" H/M is defined as the concentration change, expressed in units of hydrogen atoms per metal atom, that is observed during measurement of a hydride isotherm. Absolute calibration (relative to H/M = 0) is lost due to the accumulation of instrumental errors and other uncertainties during activation, cycling and handling of samples in the hydrogen glove box. On a typical vanadium dihydride isotherm, Reversible H/M = 0 corresponds to an actual composition of $\tilde{}VH_1$ and Reversible H/M = 1 corresponds to an actual composition of $\tilde{}VH_2$.

Before beginning the RCA tests, baseline isotherms for $V_{0.975}Zr_{0.020}C_{0.005}$-H were taken at 25°C. In Figure 5-1 absorption and desorption pressures are plotted vs. Reversible H/M. The results are typical for low cycle vanadium dihydride isotherms.

5.2 Rapid Cycling

A specimen of $V_{0.975}Zr_{0.020}C_{0.005}$ was loaded into the RCA (see Section 3.3 for a description of the RCA). UHP hydrogen was then admitted at 4137 kPa (607 psia) to activate the alloy while running cold water under the reactor cup to remove the heat of reaction. When activation was complete, the pressure was decreased to 1034 kPa (150 psia). Figure 5-1 shows that this is sufficient pressure to nearly saturate the hydride phase when the material is cold (< 25°C). Heating to 94°C (201°F) was then commenced by switching from the cold water supply to the steam generator. The pressure rise was recorded as the material heated toward thermal equilibrium with the dry steam. The results are plotted in Figure 5-2.

[24] G.G. Libowitz, et al., "Advanced Hydrogen Storage; Modified Vanadium Alloys", Final Report BNL-37866, Brookhaven National Laboratory (1985).

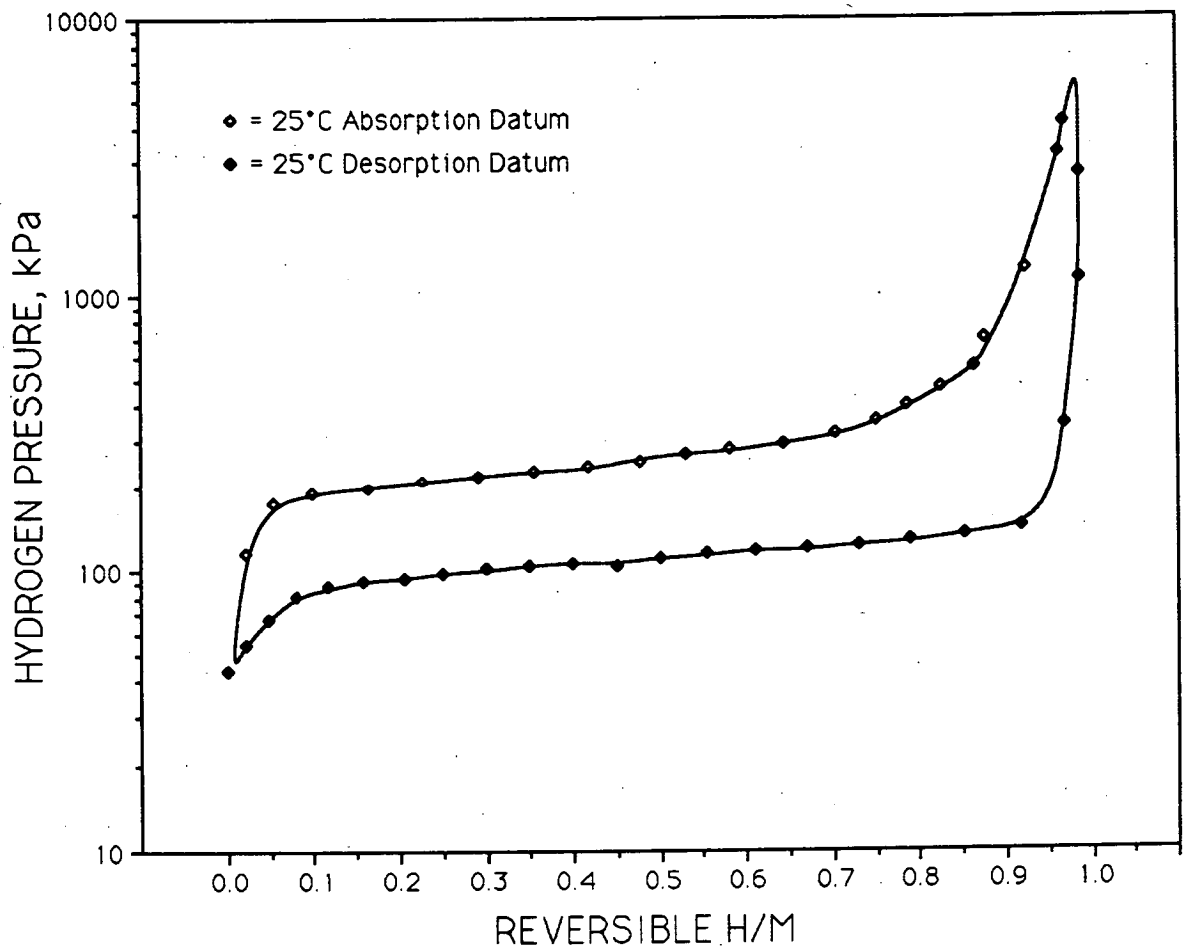

Figure 5-1. Baseline absorption/desorption isotherms for (97.5 atom-percent V, 2.0 atom-percent Zr, 0.5 atom-percent C)-dihydride at 298 K after 11 cycles.

The pressure rise tapers off after about 7 minutes because the desorption is virtually complete. The continued upward drift of pressure is mainly due to heating of the gas in the upper portion of the RCA by conduction from the heated reaction cup in the lower portion of the RCA (see Figure 3-3).

Subsequently the steam was switched off and cold water quenched the reactor cup downward to 18°C (64°F). The pressure decreased as hydrogen was reabsorbed by the metal as indicated in Figure 5-2. As in the heating curve, most of the pressure change occurs within the first 7 minutes. The gradual pressure fall thereafter is largely due to cooling of the warm gas in the upper portion of the RCA by conduction to the chilled reactor cup.

Figure 5-2 forms the basis of planning the RCA's heating/cooling schedule. It is apparent that most of the desorption/absorption occurs within 5 minutes. The heating/cooling schedule was therefore set at 5 minutes of steam heating and 5

minutes of water cooling. The pressure transducer swing was 21 psia during the early cycling indicating (via ΔP-V-T calculations) that 70% of the material transformed from dihydride to monohydride (i.e., VH_2 to VH_1) on heating and from monohydride to dihydride (i.e., VH_1 to VH_2) on cooling. Section 5.3 explains that the sample stirred itself during cycling so that the entire sample accrued about the same average number of cycles over the course of RCA testing.

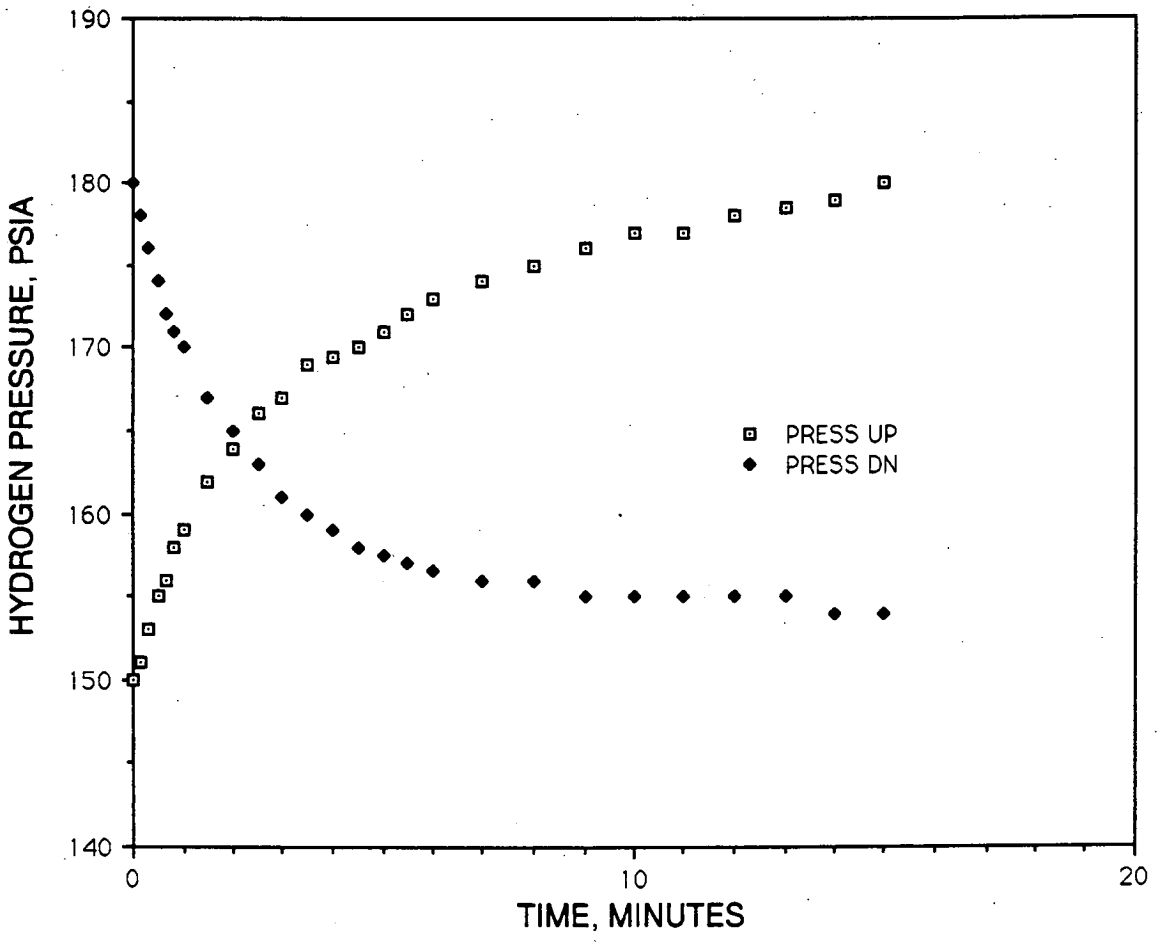

Figure 5-2. Pressure rise due to H_2 desorption from $V_{0.975}Zr_{0.020}C_{0.005}$-dihydride during heating in the RCA and pressure fall due to H_2 absorption by $V_{0.975}Zr_{0.020}C_{0.005}$-monohydride during cooling in the RCA.

Automatic cycling under control of the cycle timer proceeded for 6182 cycles. The maximum and minimum cycle pressures and temperatures were periodically recorded over the course of the test as a check on changes in sorption capacity (see discussion in Section 3.3. The data are plotted in Figure 5-3. The only significant change in the thermal cycle was a gradual decrease in minimum cup temperature. This was due to a decrease in tap water temperature during the month of December that, in turn decreased the temperature of the RCA's deionized water supply. The minimum cycle

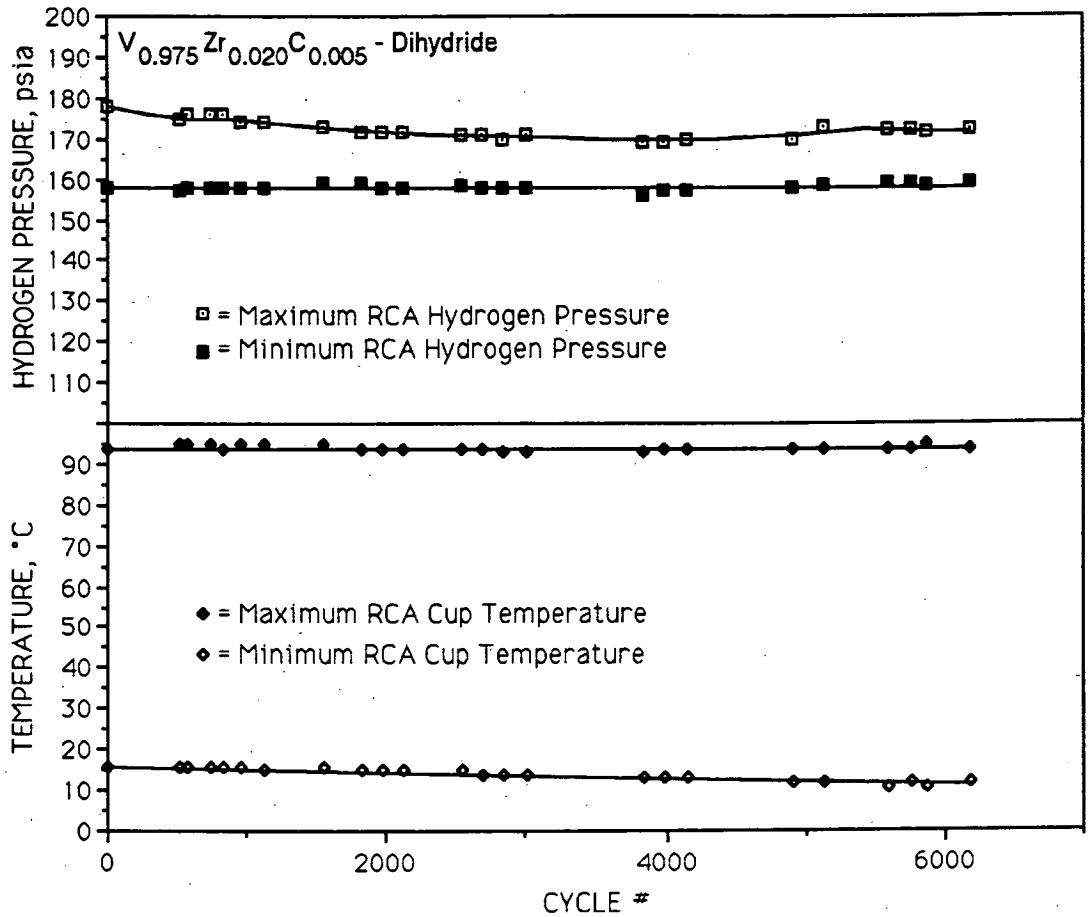

Figure 5-3. Variation of maximum and minimum cycle pressures and temperatures over the course of 6182 absorption/desorption cycles in the RCA. The decrease in maximum cycle pressure is an indication of hydrogen trapping within the solid phase.

pressure was steady at 158 ± 1 psia over the course of the test so the decline in minimum temperature had little influence on cycle ΔP. As explained in detail in Section 3.3, the constancy of minimum cycle pressure indicates that the *total* hydrogen capacity of the metal is constant. Any decrease in *total* hydrogen capacity of the solid phase would have led to an increase in gas phase hydrogen in the closed RCA. The minimum cycle pressure would have risen accordingly.

The maximum cycle temperature was steady at 94° ± 1°C over the course of the test. The most significant feature of Figure 5-3 is the decrease in maximum cycle pressure. This signals a decrease in *reversible* hydrogen content (see Section 3.3). Hydrogen trapping is indicated when *total* hydrogen content remains constant while *reversible* hydrogen content decreases.

Figure 5-4 amplifies the changes in cycle ΔP that occurred over the course of the RCA test. The ΔP data of Figure 5-3 are converted to "PERCENT REVERSIBLE

HYDROGEN CONTENT" by defining the ΔP on cycle #9 as 100% and expressing all subsequent cycle ΔPs as a percentage relative to cycle #9. It is apparent that most of the change in reversible hydrogen capacity occurred in the first 2000 cycles. The change was approximately linear over that period. The final ~4000 cycles caused no additional damage. There may have been a small recovery during the final 2000 cycles but the change is within limits of error of the RCA.

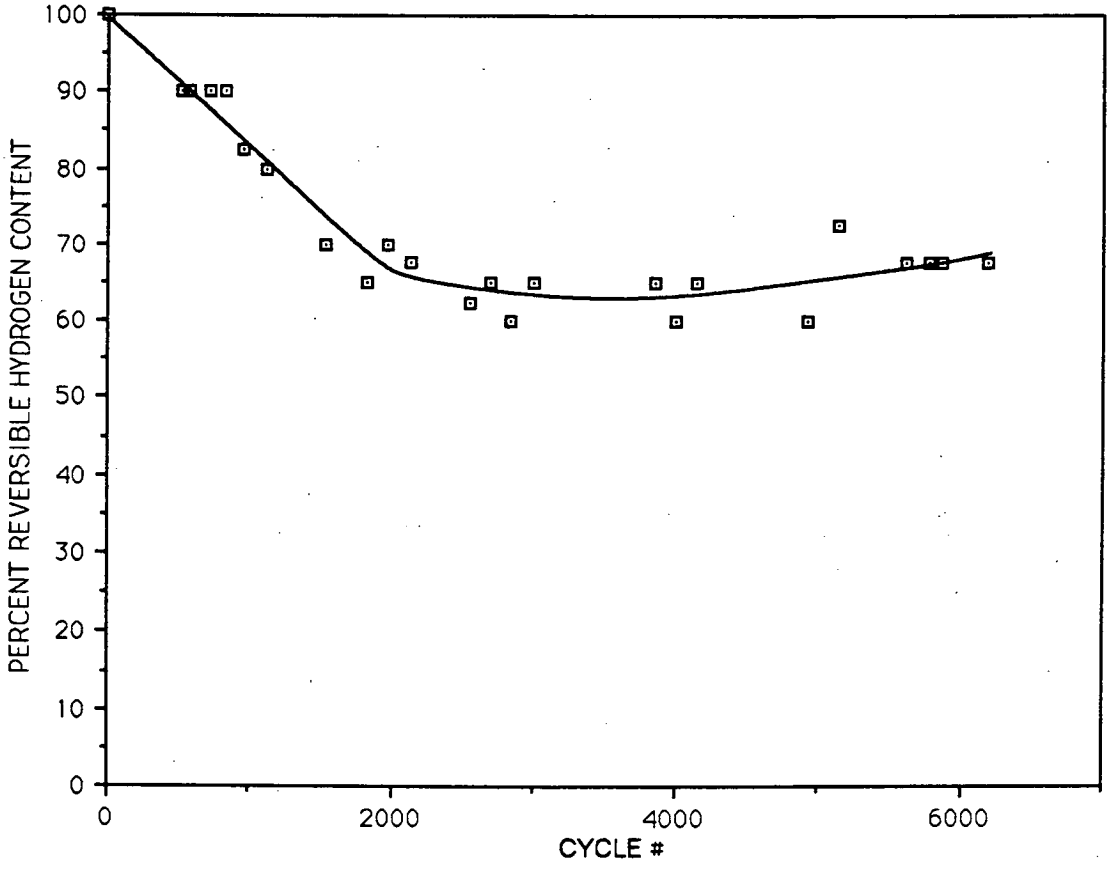

Figure 5-4. Changes in reversible hydrogen capacity of $V_{0.975}Zr_{0.020}C_{0.005}$-dihydride over the course of 6182 cycles of absorption/desorption in the RCA. The loss in reversibility is due to hydrogen trapping in the solid phase.

Figure 5-4 indicates a loss of about 33% of the reversible hydrogen capacity. More precise measurements, described in Section 5.4, indicate that the actual loss was about 18%. The disagreement may be partly due to a decrease in thermal conduction within the specimen caused by the physical changes discussed in Section 5.3. The fluffy product that accumulated during cycling may not have transformed as completely on each cycle as the original metallic chips.

5.3 Visual and Macrophotographic Observations

After a few hundred cycles in the RCA, the formation of a low density sponge-like material was observed through the viewing port of the RCA. The original $V_{0.975}Zr_{0.020}C_{0.005}$ material loaded into the RCA was in the form of bright shiny mill chips a few mm in size. Figure 5-5 is a photograph of the sample after 825 cycles. A dark gray (almost black) material is growing at discrete locations among the metallic chips.

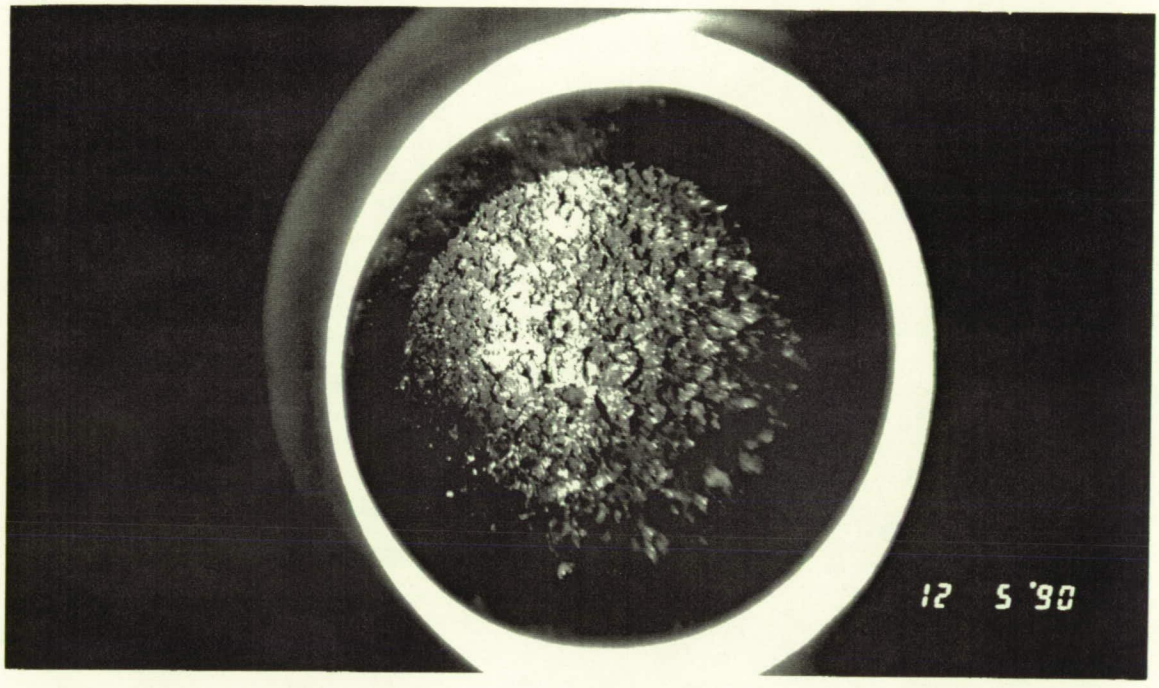

Figure 5-5. Photograph of $V_{0.975}Zr_{0.020}C_{0.005}$-dihydride after 825 cycles of absorption/ desorption in the RCA. 'Note the development of dark clusters of a new material developing among the bright metallic chips.

As the number of cycles grew so did the volume of the dark fluffy material. Figure 5-6 is a photo taken after 1826 cycles. Comparing Figures 5-5 and 5-6 shows that the overall volume of the sample increased over time. The edge of the sample is clearly higher on the wall at the upper left of the reactor cup in Figure 5-6. The low density material is developing into clusters. Time-lapse photography shows that the clusters are growing in irregular patterns that effectively stir the sample. Vertical scratches on the inside of the reactor cup attest to the passage of abrasive hydride particles as the sample stirred itself.

The test was terminated after 6182 cycles because the bright metallic material was becoming scarce. A few grams of the surviving mill chips were needed for comparison to the dark fluffy material in post cycling analyses. The final appearance of the sample after 6182 cycles is shown in Figure 5-7. It is apparent that the overall volume is much greater than Figure 5-5.

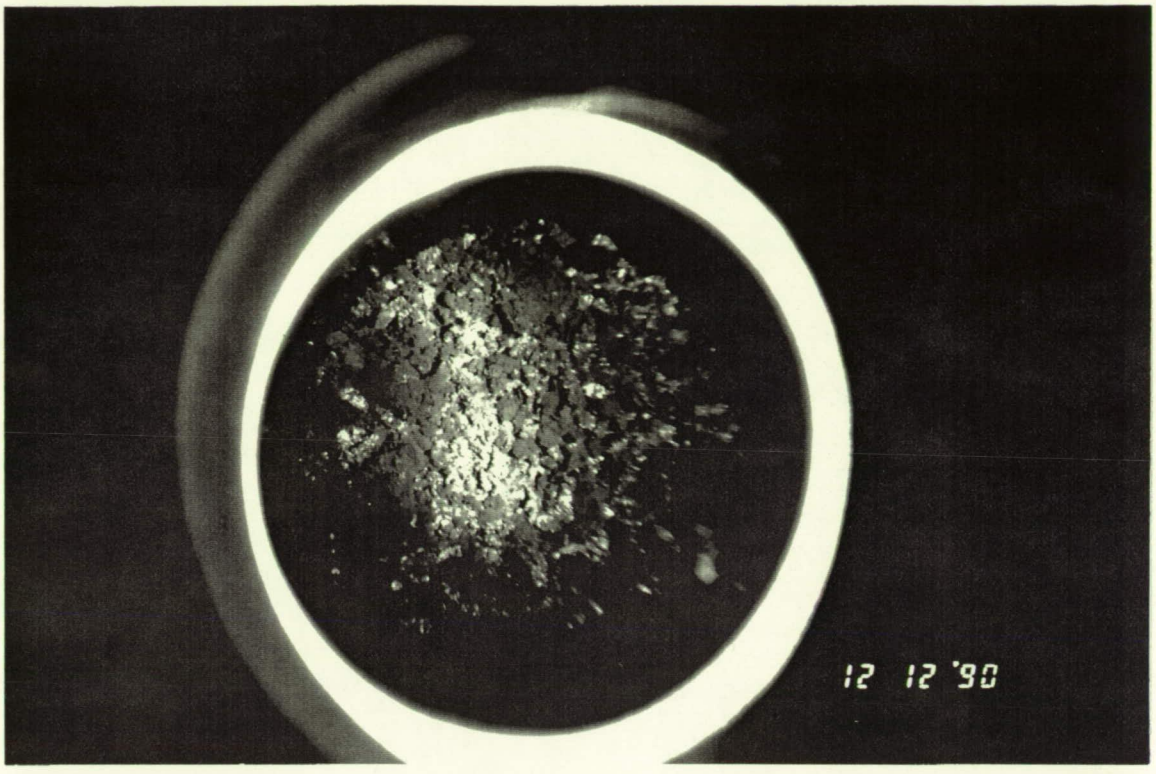

Figure 5-6. Photograph of $V_{0.975}Zr_{0.020}C_{0.005}$-dihydride after 1826 cycles of absorption/desorption in the RCA. 'Note the increased height of the sample on the wall of the reactor cup relative to Figure 5-5.

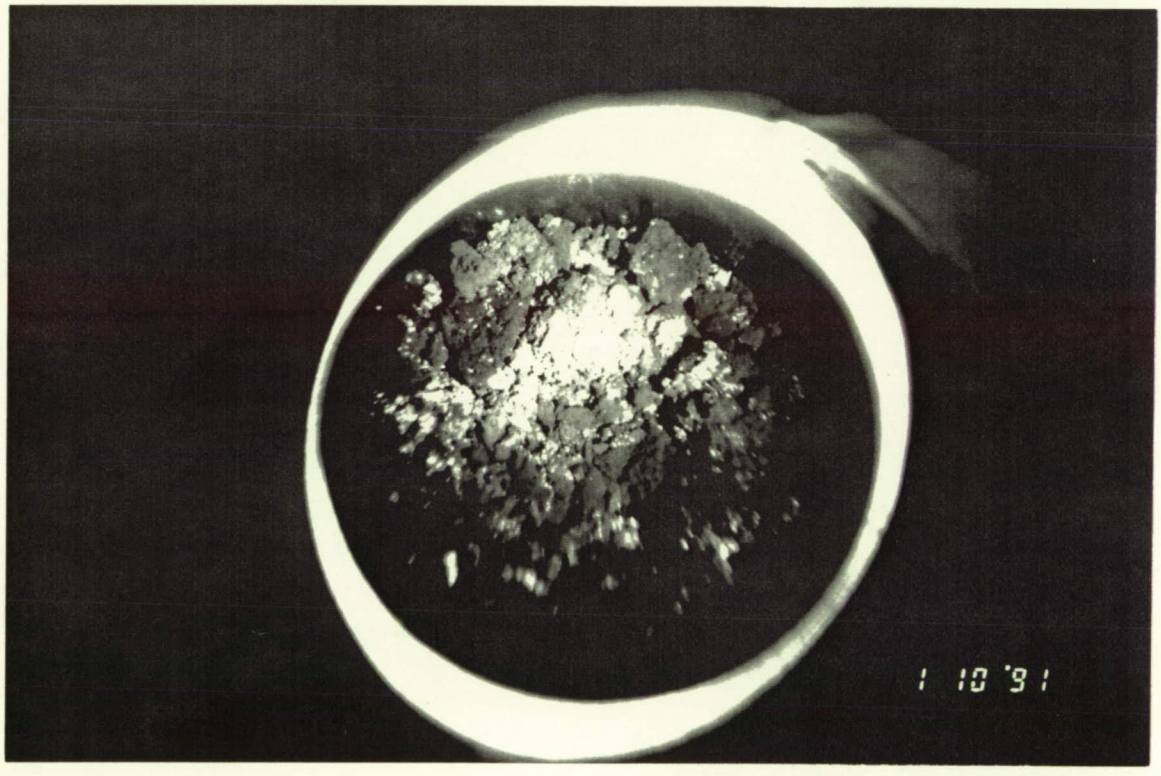

Figure 5-7. Photograph of $V_{0.975}Zr_{0.020}C_{0.005}$-dihydride after 6182 cycles of absorption/desorption in the RCA. The test was terminated at this point so that the few remaining metallic chips could be collected for Sieverts and X-ray analysis.

Before going on to discuss post cycling analyses, the photographs in Figures 5-5, 5-6 and 5-7 give evidence as to why containers of VH_2 do not show strain until hundreds of cycles have accumulated. The original mill chips, like all granular materials, have a sizable fraction of void volume between particles. The low density material is a very delicate friable material. It is difficult to handle, during preparation of X-ray specimens, without crushing it. Such a material is easily deflected into void spaces as it expands from within the original mill chips. As the void space is progressively filled, the forces generated by the expanding material must increase to press more and more of the low density material into the remaining space. These forces are exerted throughout the bulk of the hydride, wherever the low density material happens to grow.

These distributed forces exert pressure on the walls of the container, as is evident from the gradual swelling and eventual rupture. Unconstrained growth in the RCA produces the fragile fluffy material of Figures 5-5, 5-6 and 5-7. In heat exchanger tubes or Sieverts reactors, the surrounding walls apply compressive stress to the bulk of the expanding material. This leads to sintering (see Figure 4-2). Failed Sieverts reactors contain a cohesive solid with a shiny metallic luster. These sintered masses do not look like the original mill chips or like the fluffy gray material.

As discussed in Section 4.3, a lightweight thin-walled heat exchanger tube began to strain after a few hundred cycles when the expansion pressure builds to a few thousand psi (~10 MPa); stronger Sieverts reactors do not expand until the solid expansion pressure builds to tens of thousands of psi (~100 MPa). The expansion forces may not be *absolutely* irresistible, but for many NASA purposes they are. Full scale heat exchangers built to withstand thousands of psi of solid expansion pressure are extremely heavy.

Rough density measurements of the fluffy material were made by placing a weighed specimen in a graduated cylinder. The specimen was left in the hydrogen glove box at room temperature for several days prior to the density measurements so it is thought to consist mainly of VH, as opposed to VH_2. The density of solid $V_{0.975}Zr_{0.020}C_{0.005}H^{-}{}_{1}$, calculated from the lattice parameters in Section 5.7, is 5.56 grams/cc. The density of the fluffy sponge material was found to be 0.55 grams/cc--an order of magnitude below the solid density of the material that X-ray diffraction confirms is present. By tapping the graduated cylinder to allow the contents to settle, the density increased to 0.71 grams/cc.

Acetone was poured into the graduated cylinder and stirred into the fluffy mass in an attempt to determine its solid density by Archimedes' principle. This indicated a density of 3.5 grams/cc--only 63% of the solid density--implying that there is sealed porosity within the sponge that cannot be wetted by acetone. Hydrogen may be able to permeate into these holes better than acetone but sorption rates may be slowed in the process.

The fluffy material was subsequently dried in room air and hydraulically

compressed into a circular disk. A compressive stress of 77 ksi was applied via a titanium piston in a circular titanium die. The resulting disk had a density of 3.3 grams/cc. This is close to the Archimedes density (3.5 grams/cc). The compression caused cold-sintering of the fluffy material into a sturdy solid disk but with an amount of porosity similar to the uncompacted sponge.

The point of these rough density measurements, for containment purposes, is that the density depends upon the applied compressive stress. The sturdier the container, the greater is the number of cycles before strain occurs. As discussed in Section 4 however, even the sturdiest of hydride containers will eventually yield.

The following discussion of hydride isotherms confirms that the fluffy sponge material is not vastly different from the original $V_{0.975}Zr_{0.020}C_{0.005}$ in terms of hydriding characteristics. X-ray diffraction also confirms that the crystal structure of the sponge is virtually the same as the original crystalline mill chips. The fluffy growth involves a physical, rather than chemical, change.

5.4 Isotherms after 6182 RCA Cycles

Practice isotherms were run with a 10-cycle specimen to assure that handling in the glove box did not affect the features of the isotherm. Exposure for 30 minutes in the glove box did not affect the practice isotherms.

The RCA was disassembled in the hydrogen glove box. The specimen was separated into two types of material; the dark gray fluffy substance and the surviving shiny metallic particles. A portion of each type of material was transferred into Sieverts reactors. The sealed reactors were removed from the glove box and attached to the Sieverts apparatus. Figures 5-8 and 5-9 are the 298 K (77°F) isotherms for the shiny and dark gray materials respectively.

The 6182-cycle isotherms for the shiny and gray materials are compared to the 11-cycle isotherms in Figure 5-10. The similarity of these isotherms confirms the X-ray diffraction findings; all three specimens are undergoing the same monohydride/dihydride phase transformation. The fluffy sponge-like gray material has a different state of physical aggregation but the same crystalline identity as the 11-cycle specimen.

The differences in reversible hydrogen capacity and hysteresis that are apparent in Figure 5-10 are significant for engineering purposes and in terms of the physical implications. The X-ray diffraction patterns, discussed in Section 5.7, show broadened peaks in the 6182-cycle material relative to the 11-cycle material. This broadening is associated with strain.

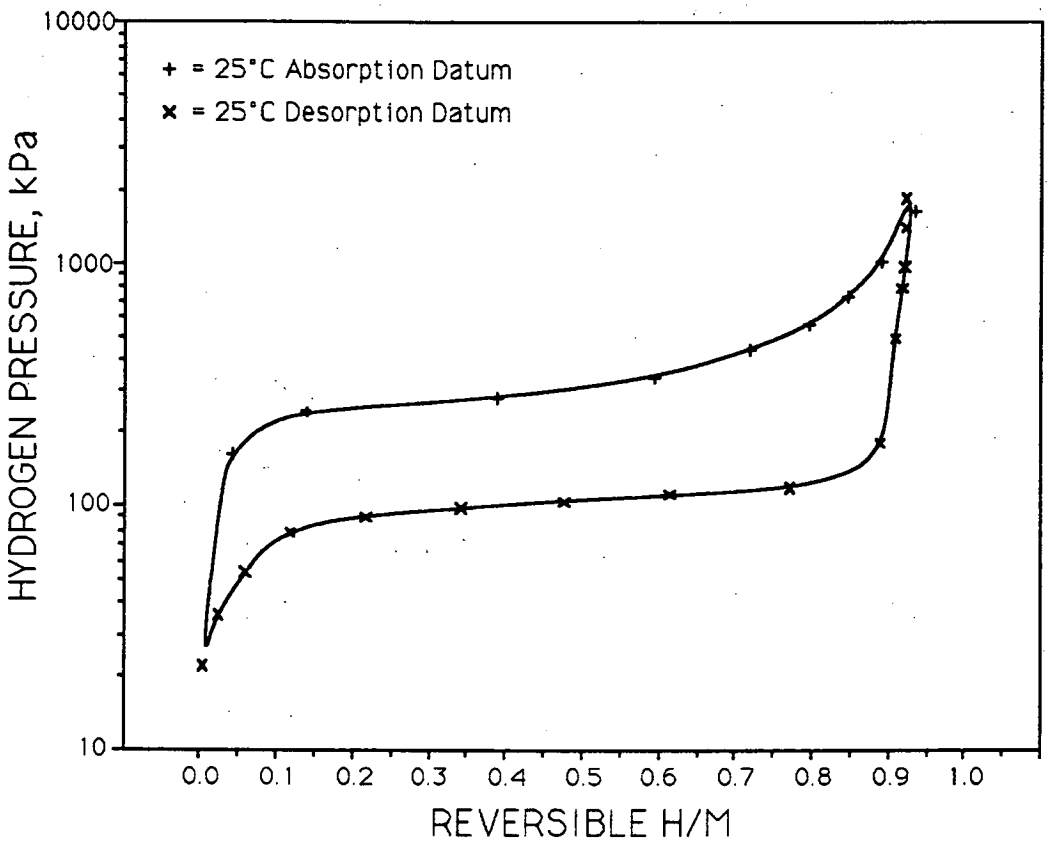

Figure 5-8. Absorption/desorption isotherms of the shiny metallic material at 298 K after 6182 cycles. This material appears to be the original (97.5 atom-percent V, 2.0 atom-percent Zr, 0.5 atom-percent C)-dihydride.

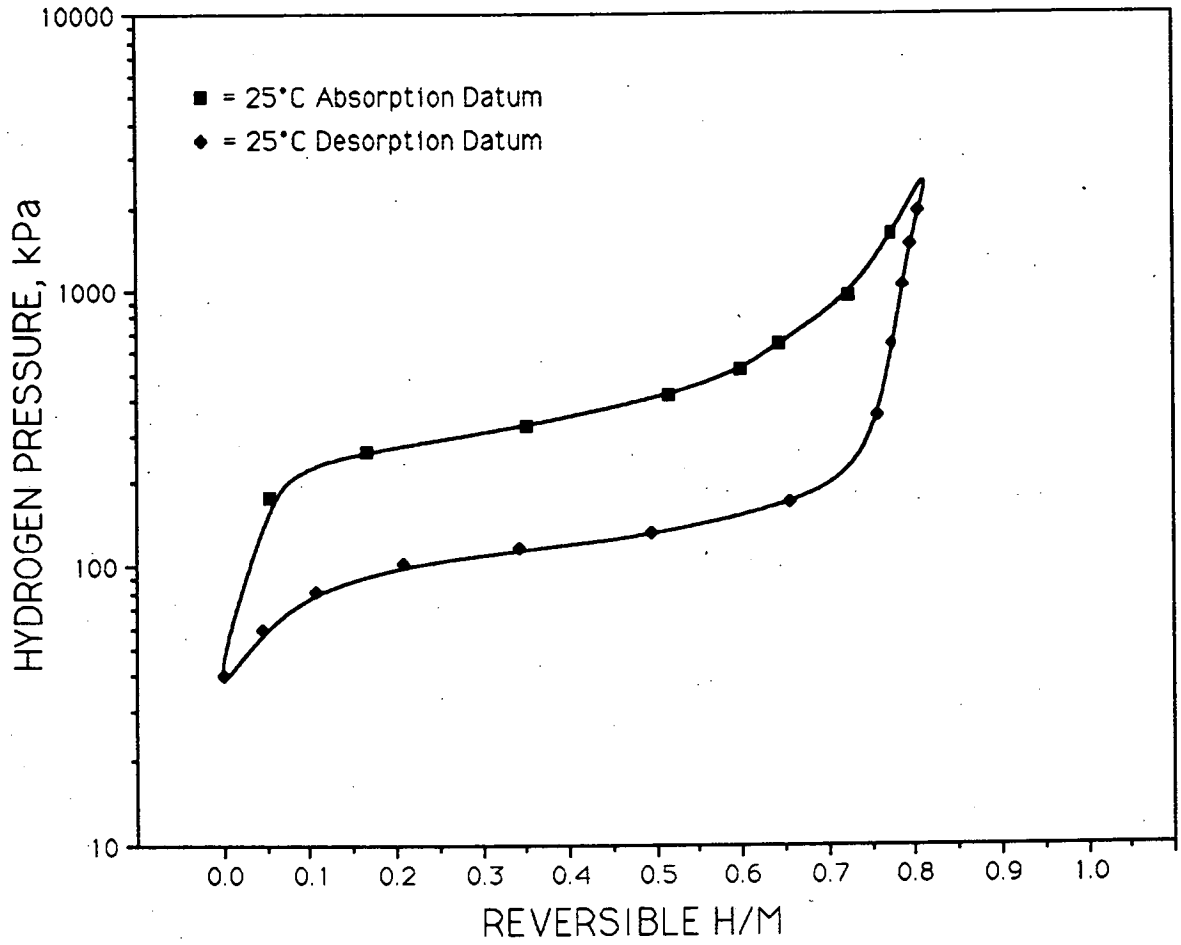

Figure 5-9. 298 K absorption/desorption isotherms of a low density material that accumulated during 6182 cycles. This material is a fluffy black sponge--very different from the original shiny metallic mill chips.

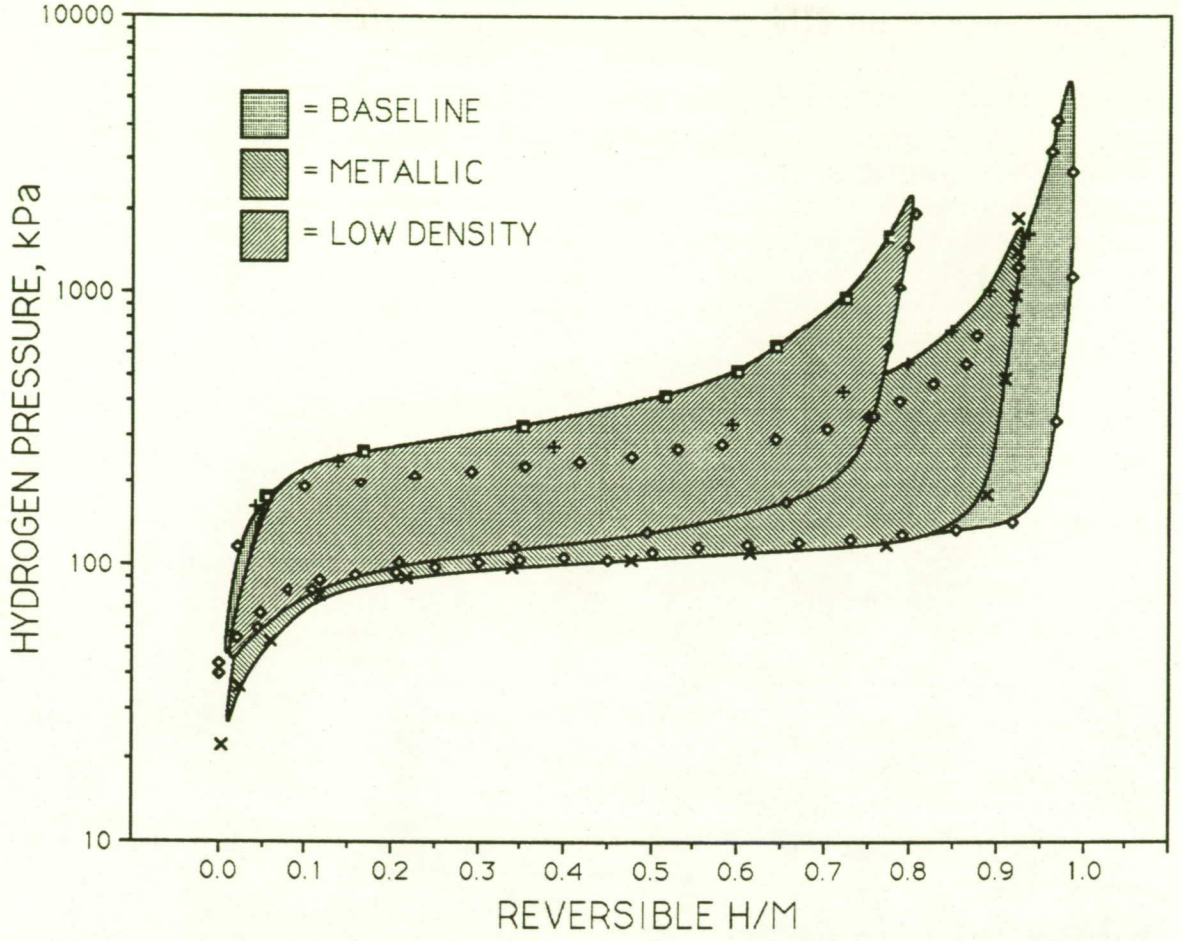

Figure 5-10. Comparison of the 298 K absorption/desorption isotherms of three specimens;

11-cycle baseline (97.5 atom-percent V, 2.0 atom-percent Zr, 0.5 atom-percent C)-dihydride,

6182-cycle metallic particles that resemble the original material comprising a small fraction of the 6182-cycle material,

6182-cycle fluffy black substance comprising a large fraction of the 6182-cycle material.

The RCA results (Section 5.2) show that the loss in reversible hydrogen capacity is due to trapping of hydrogen within the solid phase. RCA measurements are of lower precision than direct Sieverts measurements so the data of Figure 5-10 were used to quantify the amount of trapping. The 11-cycle material had a Reversible H/M of 0.99. Nearly all of the 6182-cycle material was in the low density form with a Reversible H/M of 0.81--i.e., 18% of its hydrogen is trapped within the highly strained monohydride phase $VH_{1.18}$.

5.5 Mechanical Strain Effects on Vanadium Dihydride Isotherms

A highly strained form of $V_{0.995}C_{0.005}$ was prepared by high speed rotary filing of arc-melt buttons. The material was intended for use in a hydrogen compressor built by HCI for Aerojet Electronic Systems Division (AESD), Azusa, CA. Isotherms, generated as a quality control measure, were entirely unacceptable. Figure 5-11 compares hydride isotherms of the filings with those of chunks of the identical material (i.e., remnants from the milling process). The reduced capacity and broadened hysteresis band of the filings are similar to the isotherms of cyclically degraded vanadium alloy dihydrides (e.g., Figure 5-10).

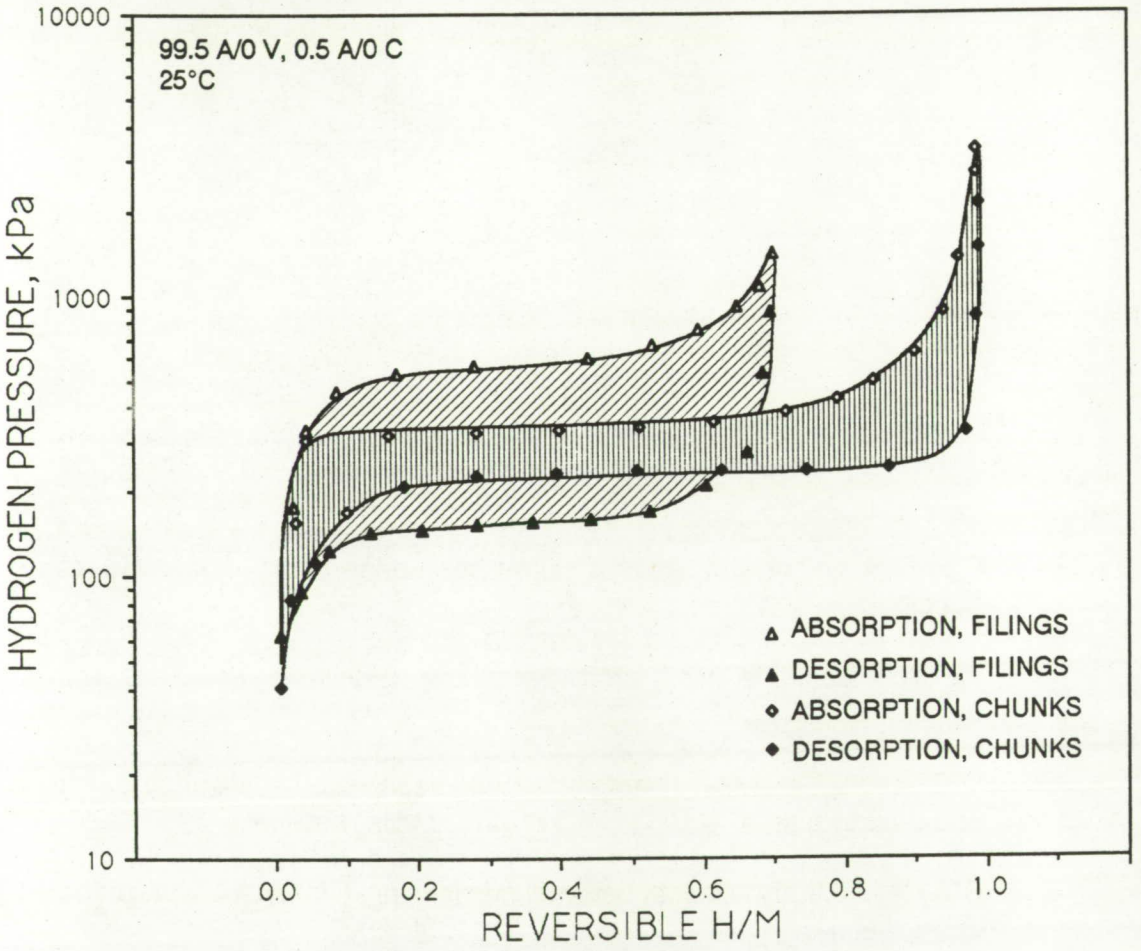

Figure 5-11. Comparison of dihydride isotherms for highly strained filings and as-cast chunks.

HCI's past experience with $V_{0.995}C_{0.005}$ included milling of arc-melt buttons into coarse mill chips, such as those in Figure 5-5. The AESD material consisted of much finer filings. X-ray diffraction patterns by UNR (see Section 5.7) showed that the filings were highly strained relative to filings that were annealed at 1473 K (2192°F) for 24

hours. The annealed fillings also produced a normal dihydride isotherm, virtually the same as the chunks in Figure 5-11.

The implication of this experience in the context of hydride degradation is powerful; strain introduced by mechanical means affects hydride properties in a way that is similar to extensive cycling. Removing the strain by annealing produces normal hydride isotherms. X-ray diffraction of cyclically degraded hydrides shows that strain has accumulated during cycling. Taken together, these observations present a strong argument for a cause/effect relationship between V-hydride degradation and strain.

5.6 Electron Microscopy

Scanning electron microscopy (SEM) was performed by Aerojet Electronic Systems Division (AESD), Azusa, CA in the course of an internally supported hydride research project conducted by Mr. Neil Sherman and Dr. Robert Bowman. HCI sent specimens of the low density dark gray sponge material and the shiny mill chips described in Section 5.4 to AESD. AESD's SEM micrographs are copied here as Figures 5-12 through 5-16. Aside from the fact that the SEM makes the dark gray material look white, there is little change in appearance between the 171x micrograph of Figure 5-12 and a 1x photograph (compare with Figure 5-7). The same can be said as the magnification is increased to 1.13kx in Figure 5-13, zooming in on the particle at the center of Figure 5-12. The texture and fringe detail of the sponge at the center of Figure 5-13 is similar to the larger particle at the upper left of Figure 5-12. Aside from a change in contrast in the micrograph, zooming in further to 5.67kx in Figure 5-14 does not draw out any major changes in appearance. Clarity suffers at 14.7kx in Figure 5-15 but the sponge-like appearance remains. Scale invariant appearance over nearly 4 orders of magnitude is a fascinating property of the vanadium hydride sponges. The fractal viewpoint (e.g., diffusion limited aggregation[25]) may provide an enlightening approach for further studies.

Figure 5-16 is a 200x SEM micrograph of crystalline particles that survived 6182 cycles in the RCA. Particles like these were used to generate the isotherms of Figure 5-8. It is curious that the sponge-like material seems to be growing preferentially from certain sides of the particles. It would be interesting to subject a single crystal of vanadium to cyclic hydriding to see if the sponges develop on a particular crystal plane. The curving striations on the particle surfaces that are relatively free of sponge growth may be slip bands from the hydriding/dehydriding strains. The striations cannot be from the machining process that produced the original mill chips because they terminate at grain boundaries.

[25]P. Meakin and S. Tolman, "Diffusion Limited Aggregation: Recent Developments", *Fractals' Physical Origin and Properties*, ed. A. Zichichi, Plenum Press, N.Y. (1988).

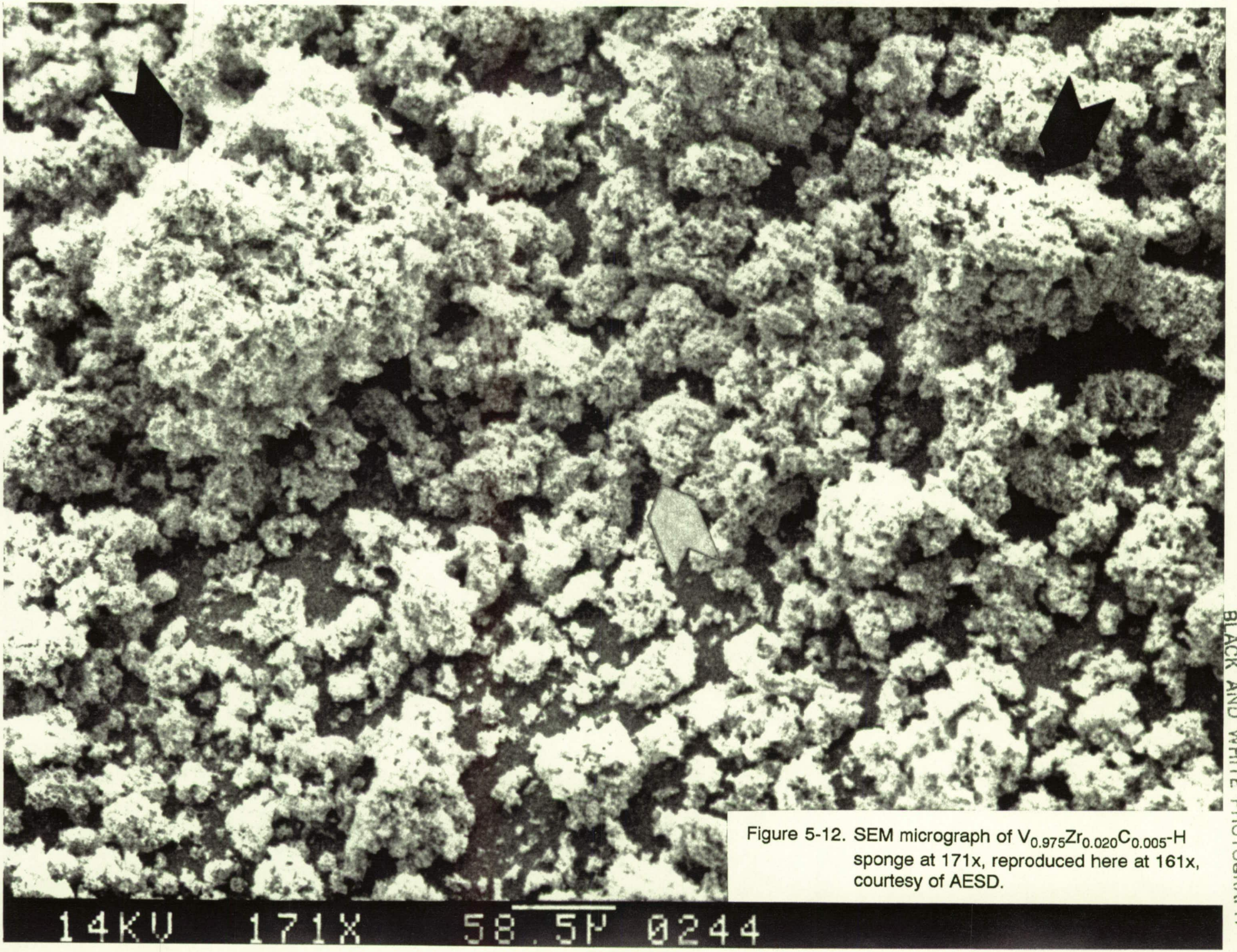

Figure 5-12. SEM micrograph of $V_{0.975}Zr_{0.020}C_{0.005}$-H sponge at 171x, reproduced here at 161x, courtesy of AESD.

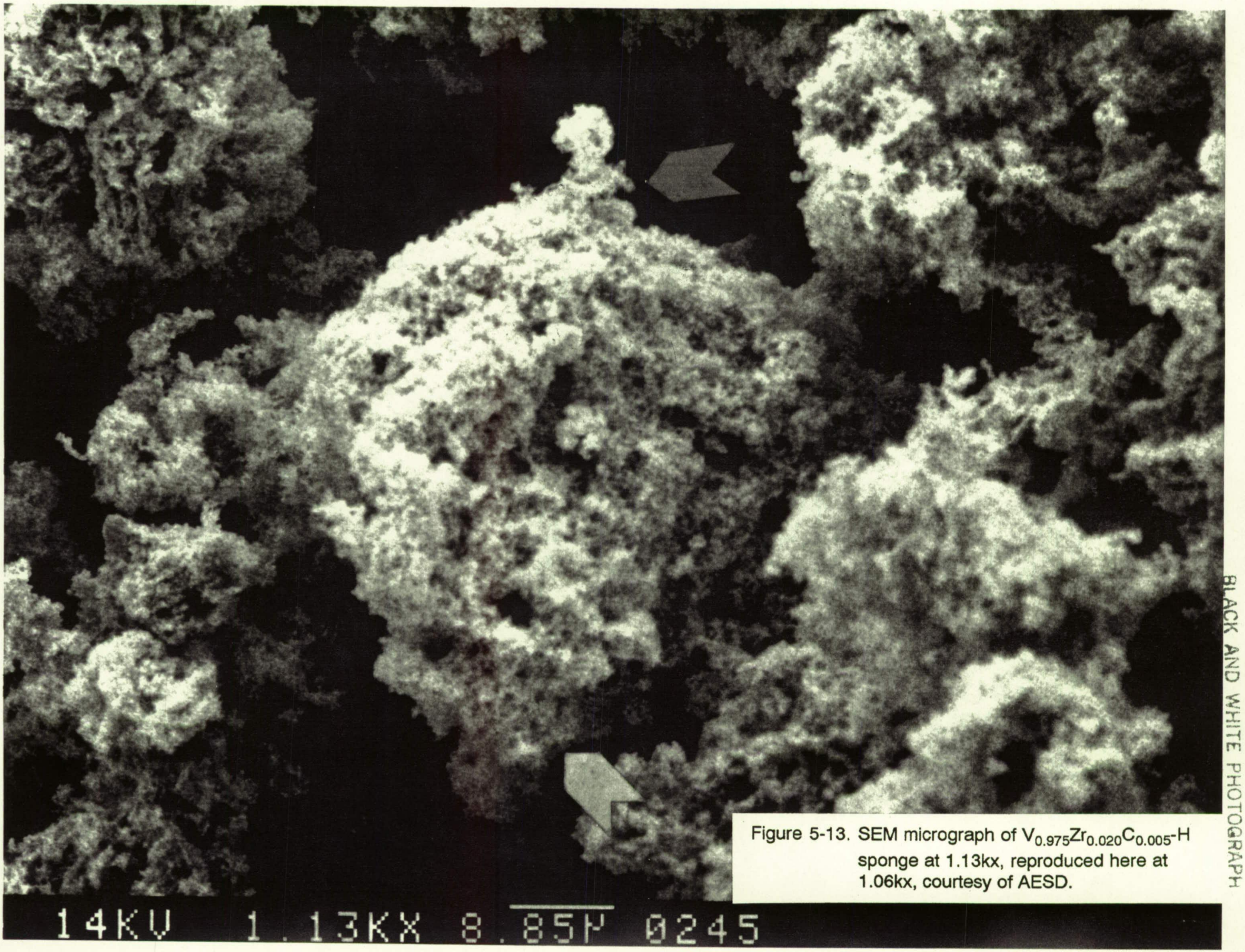

Figure 5-13. SEM micrograph of $V_{0.975}Zr_{0.020}C_{0.005}$-H sponge at 1.13kx, reproduced here at 1.06kx, courtesy of AESD.

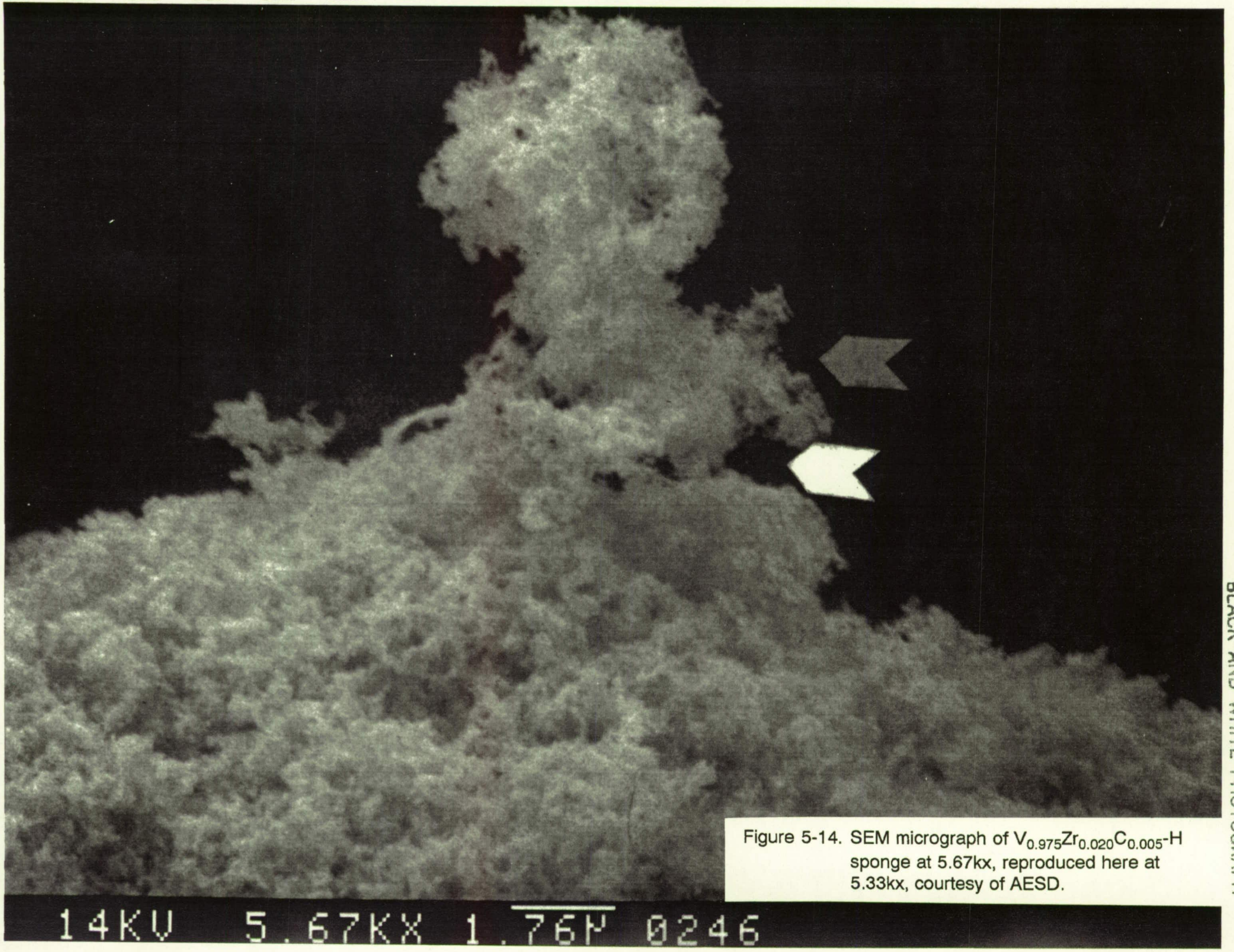

Figure 5-14. SEM micrograph of $V_{0.975}Zr_{0.020}C_{0.005}$-H sponge at 5.67kx, reproduced here at 5.33kx, courtesy of AESD.

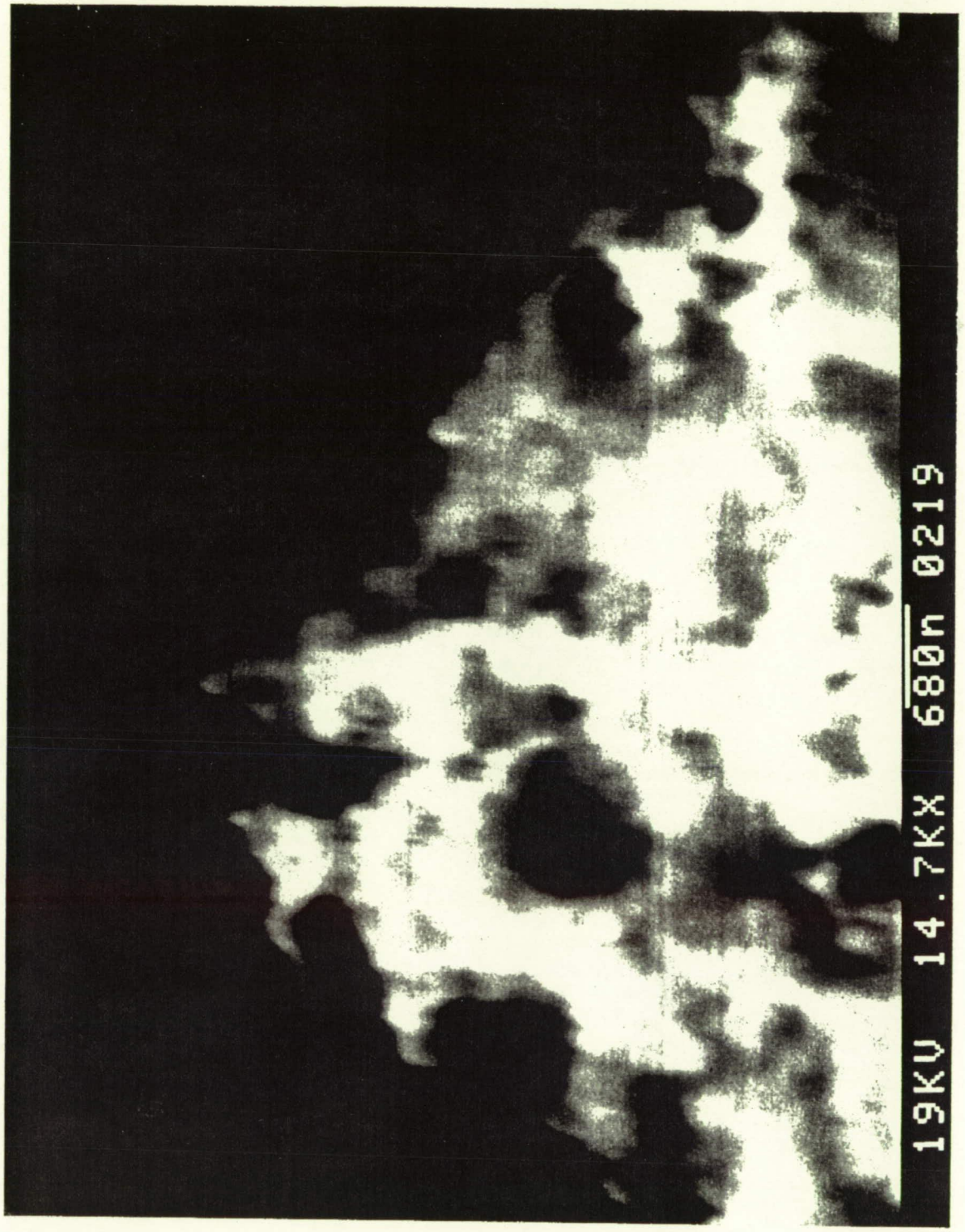

Figure 5-15. SEM micrograph of $V_{0.975}Zr_{0.020}C_{0.005}$-H sponge at 14.7kx, reproduced here at 22.6kx, courtesy of AESD.

Figure 5-16. SEM micrograph of $V_{0.975}Zr_{0.020}C_{0.005}$-H metallic particles at 200x, reproduced here at 188x, courtesy of AESD.

5.7 X-ray Diffraction Patterns of Vanadium Alloys and Hydrides

The lattice parameters measured in this study for vanadium alloys and their hydrides are listed in Tables 5-I, 5-II and 5-III below. X-ray powder diffraction patterns from high purity V (refined by the U.S. Bureau of Mines laboratory at Reno) were used as a baseline standard. The lattice parameter of the high purity V obtained in this study agrees, within limits of error, with the NBS reported value. The lattice of $V_{0.995}C_{0.005}$ was found to be slightly contracted, relative to pure vanadium, in the annealed form. The highly strained filings lattice, however, was similar in size to pure vanadium.

X-ray powder diffraction [XRPD] analyses performed on a 1-cycle hydride sample revealed a major $V_{0.995}C_{0.005}H_2$ phase and minor $V_{0.995}C_{0.005}H_1$ phase. The samples in the hydrided condition are air stable and the X-ray diffraction patterns of the hydrides exposed to air showed no change in the position of the peaks or the amount of the hydride phases. The structures of $V_{0.995}C_{0.005}H_1$ and $V_{0.995}C_{0.005}H_2$ were determined as body centered tetragonal (BCT) and cubic fluorite (CaF_2 type), respectively. The lattice parameters of the $V_{0.995}C_{0.005}H_1$ phase increased by 0.366% in a-direction and decreased by 4.23% in the c-direction, when cycled from 1 to 4000 times. The lattice parameter of the cubic $V_{0.995}C_{0.005}H_2$ phase decreased only by ~0.03% from 1 to 4000 cycles. In general, when hydrogen is introduced in the lattice of body-centered cubic (BCC) vanadium there is a tetragonal distortion to BCT in the c-direction with a contraction in the a-direction relative to the original BCC cell. Removal of hydrogen decreases the d-spacing of the planes (002), (112), (202) etc. normal to the c-direction of this BCT structure.

Microstrain in the lattice of $V_{0.995}C_{0.005}H_1$ was determined by X-ray diffraction line profile analyses for the 1-cycle and 778-cycle materials. The root mean square strain in the $V_{0.995}C_{0.005}H_1$ increased from 1.3×10^{-3} in the 1-cycle sample to 2.5×10^{-3} in the 778-cycle sample. The associated effective domain size also showed an increase from 200Å to 210Å, from 1 to 778 cycles. The trend is that the microstrain in the $V_{0.995}C_{0.005}H_1$ increases after more hydriding/dehydriding cycles. The reverse appears to be true for the $V_{0.995}C_{0.005}H_2$ phase, where the microstrain decreases after prolonged cycling. A striking difference between 778-cycle and 4000-cycle $V_{0.995}C_{0.005}H_1$ phase is that there is selective broadening of the (002) and (220) Bragg peaks in the 4000-cycle sample. This suggests stacking faults in the BCT structure.

Table 5-I. Summary of lattice parameters of BCC vanadium alloys.

SPECIMEN	LATTICE PARAMETER, Å a_o
NBS Standard Vanadium	3.0274
USBM High-Purity Vanadium	3.0279 (±0.0013)
HCl $V_{0.995}C_{0.005}$ - Annealed	3.0256 (±0.0008)
HCl $V_{0.995}C_{0.005}$ - Filings	3.0276 (±0.0003)
HCl $V_{0.975}Zr_{0.020}C_{0.005}$-Annealed	3.03165 (±0.0006)

Table 5-II. Summary of lattice parameters of BCT vanadium monohydrides. Note: hydrogen content affects the lattice parameters of vanadium monohydride. The presence of VH_2 in all of the UNR specimens suggests that the VH phase is saturated (i.e., VH_{-1}). However, it is possible that the specimens were inhomogeneous, containing some unsaturated $VH_{<1}$.

SPECIMEN	LATTICE PARAMETER, Å a_o	c_o
Low Cycle Monohydrides		
NBS Standard $VH_{0.81}$	3.0280	3.400
HCl $V_{0.995}C_{0.005}$ - Mill Chips, 10-Cycle	3.0241 (±0.0019)	3.4360 (±0.0020)
HCl $V_{0.995}C_{0.005}$ - Filings, 10-Cycle	3.0337 (±0.0050)	3.4062 (±0.0056)
HCl $V_{0.975}Zr_{0.020}C_{0.005}$- Mill chips, 10-Cycle	3.0251 (±0.0001)	3.4470 (±0.0001)
High Cycle Monohydrides		
HCl $V_{0.995}C_{0.005}$ - Sintered, 778-cycle	3.0190 (±0.0032)	3.3870 (±0.0013)
HCl $V_{0.995}C_{0.005}$ - Sintered, 4000-cycle	3.0200 (±0.0005)	3.4281 (±0.0013)
HCl $V_{0.975}Zr_{0.020}C_{0.005}$-Mill Chips, 6182-Cycle	3.0276 (±0.0025)	3.3566 (±0.0060)

Table 5-III. Summary of lattice parameters of vanadium dihydride. The compound has the cubic fluorite structure (CaF_2) with V-atoms on an FCC lattice and hydrogen at the tetrahedral fluorine sites.

SPECIMEN	LATTICE PARAMETER, Å a_o
Low Cycle Dihydrides	
NBS Standard $VH_{2.01}$	4.271
HCl $V_{0.995}C_{0.005}$ 10-cycle	4.2685 (±0.0005)
HCl $V_{0.995}C_{0.005}$ Filings 10-cycle	4.2760 (±0.0018)
HCl $V_{0.975}Zr_{0.020}C_{0.005}$- Mill chips, 10-Cycle	4.2780 (±0.0004)
High Cycle Dihydrides	
HCl $V_{0.995}C_{0.005}$ Sintered, 778-cycle	4.2594 (±0.0001)
HCl $V_{0.995}C_{0.005}$ - Sintered, 4000-cycle	4.2681 (0.0027)
HCl $V_{0.975}Zr_{0.0.020}C_{0.005}$- Sponge, 6182-Cycle	-*

* Peaks were apparent but signal was too low to get an accurate lattice parameter.

6.0 DEGRADATION OF $LaNi_5$-HYDRIDE

Degradation in $LaNi_5$-hydride was studied from several different perspectives. In addition to the Rapid Cycle Apparatus (RCA), Thermal Aging (TA) at moderate temperatures was applied and data from earlier Slow Cycle Apparatus (SCA) studies was reviewed. Hydride isotherms and corresponding X-ray data are discussed below.

6.1 RCA Testing of $LaNi_5$-Hydride

The 25°C absorption and desorption isotherms for $LaNi_5$-hydride after 10 break-in cycles in the Sieverts Apparatus are shown in Figure 6-1. The plateaux are slightly high indicating an excess of nickel relative to the target formula[26]. The actual formula is thought to be about $LaNi_{5.1}$. The saturated hydrogen capacity, determined from the initial activation cycle, was found to be 1.1 hydrogen atoms per metal atom (H/M). Dissolved hydrogen content at the left of the plateau is about 0.13 H/M. This is typical of $LaNi_5$-hydride. Dissolved hydrogen will be ignored in the balance of this discussion because absolute calibration is lost during the cycling process. After the initial activation, only the *reversible* hydrogen content can be stated with high precision because cumulative errors during cycling cause loss of absolute calibration, relative to H/M = 0.

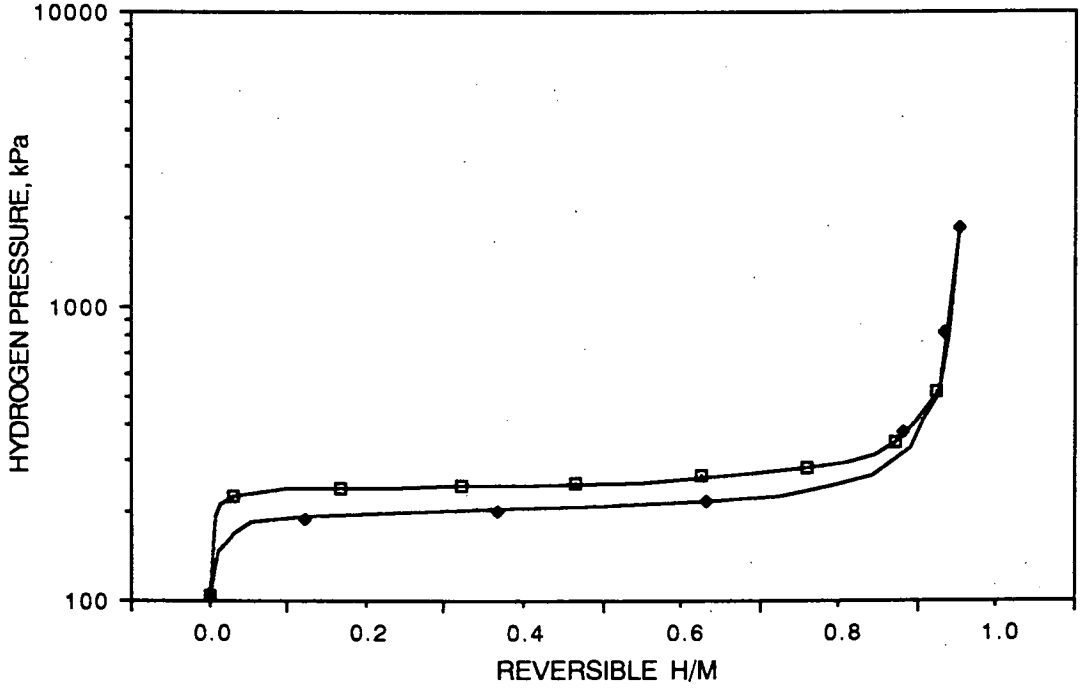

Figure 6-1. $LaNi_5$-hydride absorption (upper) and desorption (lower) isotherms at 25°C after 10 pressure-induced (break-in) cycles.

[26] K. H. J. Buschow and H. H. Van Mal, "Phase Relations and Hydrogen Absorption in the Lanthanum-Nickel System, *Journal of the Less Common Metals*, Vol. 29, pp. 203-210, Elsevier Sequoia S. A., Lausanne, Netherlands, 1972.

A piece from the same arc-melt button was placed into the RCA. The RCA was evacuated, purged and filled with hydrogen in the manner described in Section 3.3. The sample was activated by raising the hydrogen pressure in the RCA to 4130 kPa (600 psia). The pressure was then reduced to the log mean value for the cycle, 560 kPa (81 psia) with the cooling water temperature held at 11°C (52°F).

Cycling began and, after a few adjustments, the maximum and minimum temperatures were set at 15°C (59°F) and 95°C (203°F). The cycle duration was set at 360 s total with 180 s of heating and 180 s of cooling. The maximum and minimum cycle pressures were 634 kPa (92 psia) and 560 kPa (81 psia) respectively.

Contrary to expected results, after 5919 cycles, carried out over a period of 28 days, there were no changes in the max./min. cycle pressures within the 7 kPa (1 psia) resolution of the RCA's transducer. A Sieverts sample was removed from the RCA by encasing the apparatus in a polyethylene glove bag thoroughly purged with hydrogen prior to opening the RCA. Figure 6-2 compares the absorption/desorption isotherms for the 5919 cycle $LaNi_5$ to the 10 cycle data of Figure 6-1. There is much less degradation than expected, based on previous data from HCl and others. Apparently rapid cycling is not as detrimental to the properties of $LaNi_5$-hydride as slower cycling.

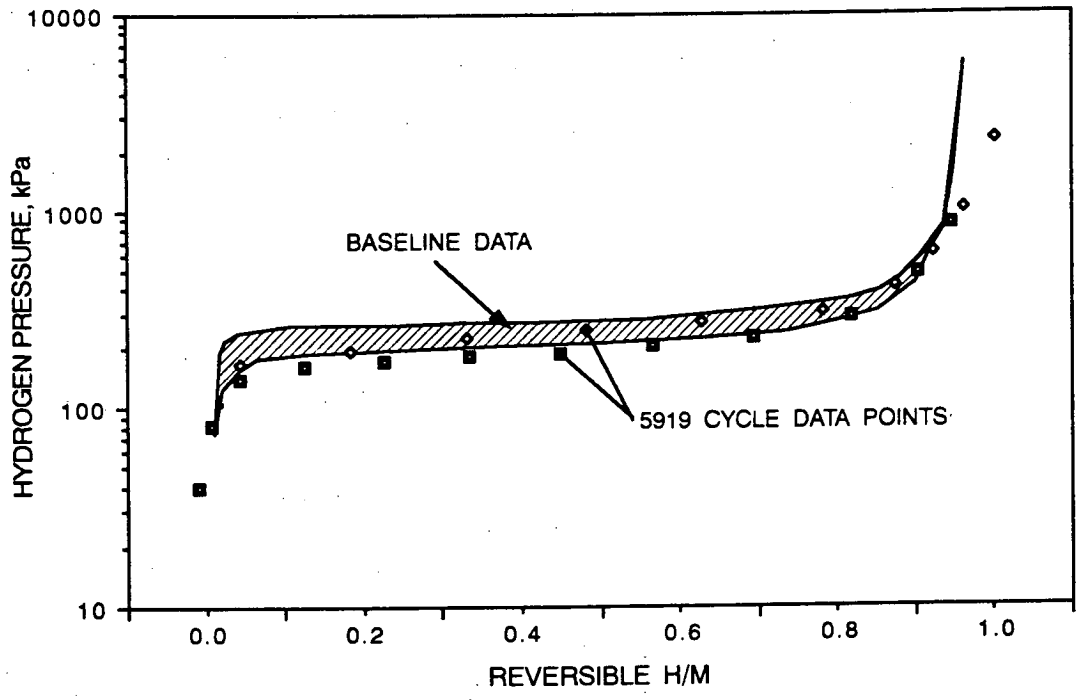

Figure 6-2. $LaNi_5$-hydride 5919 cycle absorption and desorption data (the diamonds and squares respectively) compared to the baseline isotherms (see Figure 6-1).

No X-ray data were taken with this $LaNi_5$-hydride sample. There are many sources of this information in the literature so the sample was reserved for Thermal Aging tests.

6.2 SCA Testing of $LaNi_5$-Hydride

A very similar alloy was tested in the SCA during an earlier NASA project (NAS9-17549) and subsequent IRAD work by HCI/UNR. The cycle consisted of heating to ~125°C (257°F) and cooling to room temperature, ~20°C (68°F). Figure 6-3 shows how the *Reversible*[27] hydrogen capacity and isotherm shape changed over the course of 10000 cycles in the SCA. The damage after 1500 cycles is much more extensive than nearly 6000 cycles in the RCA (see Figure 6-2).

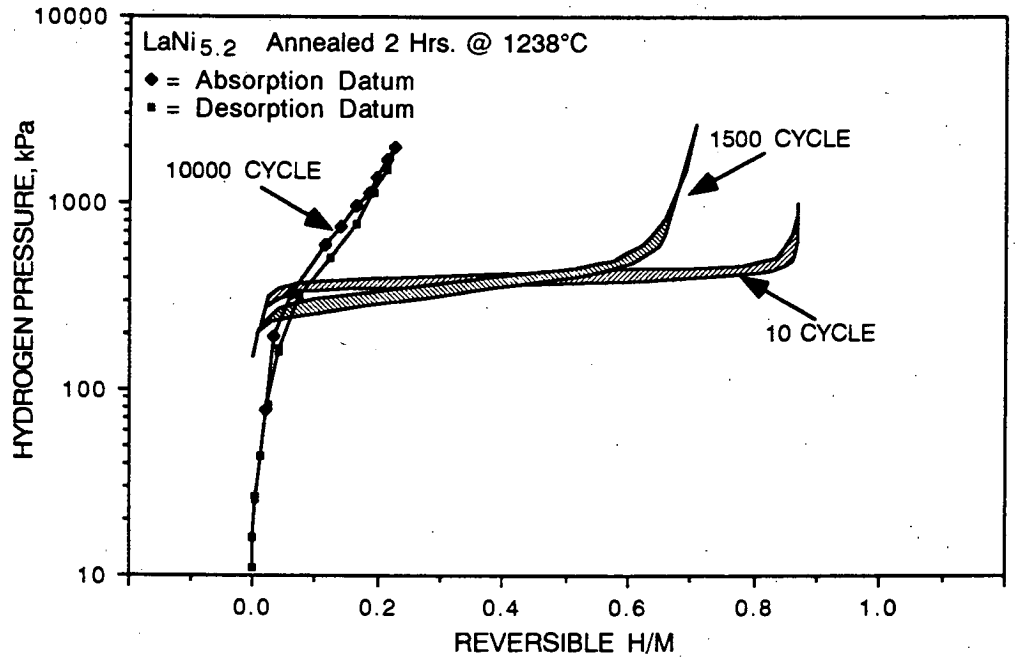

Figure 6-3. 10000 cycle absorption/desorption data for $LaNi_{5.2}$-H compared to 10 cycle and 1500 cycle isotherms. All data were taken at 25°C (77°F).

6.3 Thermal Aging of $LaNi_5$-Hydride

The next step in the investigation of $LaNi_5$-hydride degradation was to conduct Thermal Aging (TA) experiments. The same sample used to generate Figure 6-1 was pressurized to 13.8 MPa (2000 psi) and heated to 180°C (356°F). The high hydrogen pressure maintains the sample in the saturated condition despite the elevated temperature. These conditions were maintained for 260 hours. Figure 6-4 compares the degraded isotherm to the baseline 10-cycle material at 25°C

[27] Absolute calibration is lost during cyclic testing. Figure 6-3 is drawn assuming that H/M = 0 at the minimum pressure of the isotherm.

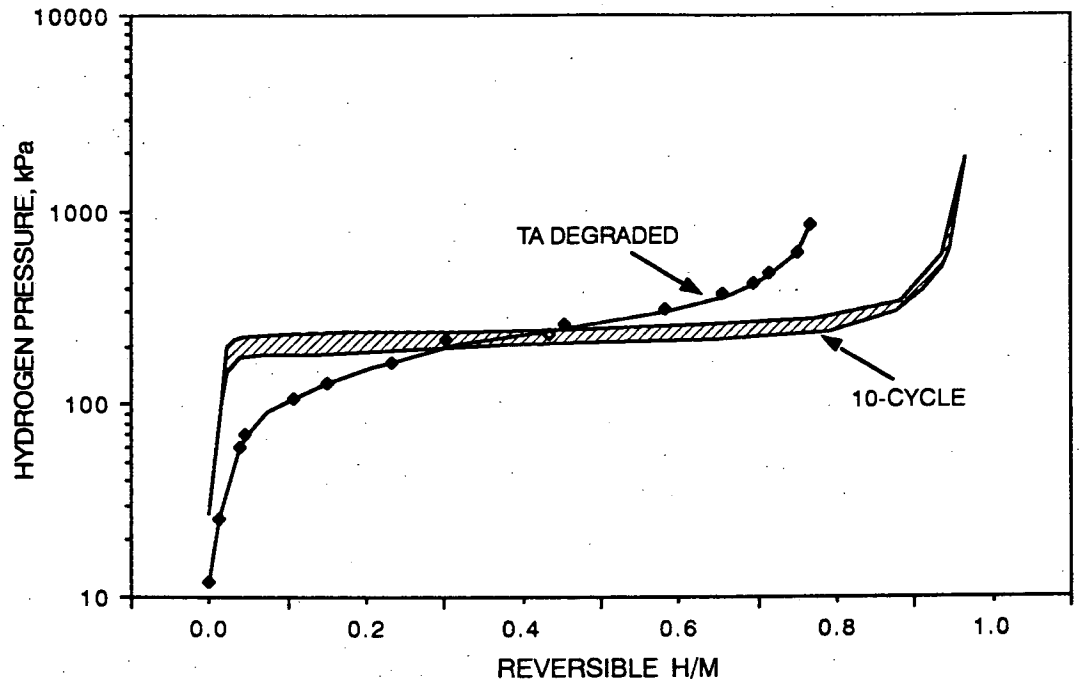

(77°F).

Figure 6-4. $LaNi_5$-hydride absorption and desorption isotherms at 25°C after 260 hours at 180°C in hydrogen at 2000 psia compared to the baseline data (see Figure 6-1).

Comparing Figures 6-3 and 6-4, it is apparent that 1500 SCA cycles or 260 hrs. at 180°C (356°F) produced comparable amounts of degradation. In each case there was ~20% loss in hydrogen capacity and significant isotherm slope developed. An interesting difference is that the TA degraded sample of Figure 6-4 shows a significant reduction in hysteresis, whereas the hysteresis after 1500 cycles in Figure 6-3 was similar to the 10-cycle material.

6.4 X-ray Diffraction Analysis of Degraded $LaNi_5$

X-ray diffraction analysis showed that $LaNi_{5.2}$, before and after initial hydriding, had the hexagonal $CaCu_5$ structure. Lattice parameters, a_o and c_o, and the ratio c_o/a_o for virgin alloy and 10 cycle hydride are listed in Table 6-I. After 10000 cycles, low signal to noise ratio prevented the measurement of the XRPD pattern. The more powerful Rigaku diffractometer clearly showed the peaks of the silicon internal standard so absorption of X-rays by the capillary was ruled out.

There are two possibilities for the loss of the XRPD pattern; 1) the degraded material is amorphous or 2) the degraded material is nanocrystalline. Amorphous materials cannot diffract X-rays because they lack discrete crystal planes, whereas

Table 6-I. Lattice parameters and c_o/a_o ratio for $LaNi_{5.2}$ and its hydride after 10 cycles and 10000 cycles in the SCA.

Material	Cycles	a_o (Å)	c_o (Å)	c_o/a_o
$LaNi_{5.2}$	0	4.9986±0.0058	4.0032±0.0039	0.801
$LaNi_{5.2}$-$H_{\sim 6}$	10	5.1050±0.0169	4.0512±0.0092	0.794
$LaNi_{5.2}$†	10000	4.9672±0.0139	4.0560±0.0085	0.817
$LaNi_{5.2}$-$H_{\sim 1}$	10000	Bragg Peaks not Readable		

†Nickel peaks 2d and 3d were found in the 10000 cycle $LaNi_{5.2}$ sample.

nanocrystalline materials have crystallites that are too small to provide a distinctive XRPD pattern.

Two nickel peaks were found in the 10000 cycle material indicating the formation of precipitates of Ni or a Ni-rich phase. These peaks did not appear in the virgin or 10 cycle material and are therefore thought to be associated with the degradation process. It is not possible, from the X-ray evidence alone, to determine just how much nickel was precipitated. The broadened low intensity peaks suggest that the precipitates are on the order of 150 Å. If a significant quantity of nickel precipitates, the La/Ni ratio of the intermetallic must increase. $LaNi_3$-hydride or La_2Ni_7-hydride may have formed, both of which are known to be amorphous[28]. That would explain the lacking XRPD pattern.

The $LaNi_{5.2}$-hydride capillary was subsequently broken open allowing hydrogen to escape. The dehydrided material regained its original hexagonal structure but considerable microstrain was apparent from the XRPD pattern. Selective peak broadening in the basal plane (002) of the hexagonal structure was apparent. As a working hypothesis, it is suspected that crystal defects, resulting from strain that occurs during absorption/desorption cycles, produce sites that are favorable for hydrogen trapping. The trapped hydrogen is stably bound--not *reversible* in the practical sense[29].

Unfortunately, the thermally aged specimen was damaged during handling so X-ray analysis was not conducted.

[28] J.H. Han and J.H. Lee,"Influence of Oxygen Impurity on the Hydrogenation Properties of $LaNi_5$, $LaNi_{4.7}Al_{0.3}$ and $MmNi_{4.5}Al_{0.5}$ During Long-Term Pressure-Induced Hydriding-Dehydriding Cycling", *Journal of the Less Common Metals*, Vol. 152, pp. 329-338 (1989).

[29] J.F. Lynch and J.J. Reilly, "Behavior of H-$LaNi_5$ Solid Solutions", *Journal of the Less Common Metals*, Vol. 87, pp. 225-236 (1982).

7.0 DEGRADATION OF $La_{0.9}Gd_{0.1}Ni_5$-HYDRIDE

7.1 RCA Testing of $La_{0.9}Gd_{0.1}Ni_5$-Hydride

The 25°C absorption and desorption isotherms for $La_{0.9}Gd_{0.1}Ni_5$-hydride after 10 break-in cycles in the Sieverts apparatus are shown in Figure 7-1. This is the same alloy that was developed earlier as a candidate for use in JSC's Metal Hydride Heat Pump (NAS 9-17549) and rejected for its lack of cyclic stability. A single 25.18 gram piece of alloy was placed into the RCA, pumped and flushed with UHP hydrogen (see Section 3.3) and activated with 600 psia hydrogen. A video camcorder was used to record the activation process (copies of the video tape are on file at HCI and JSC).

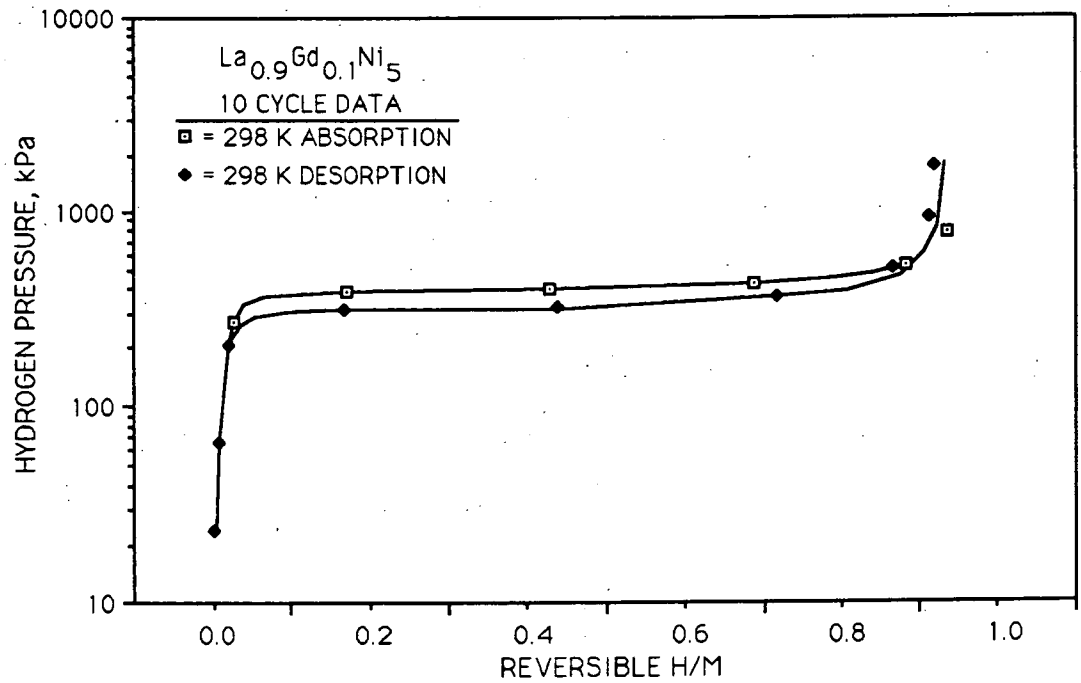

Figure 7-1. Baseline absorption and desorption isotherms for $La_{0.9}Gd_{0.1}Ni_5$-hydride at 298 K (77°F) after 10 pressure-induced cycles.

Pressure-time curves for the absorption and desorption cycles are shown in Figure 7-2. These curves indicate that the absorption and desorption processes are only about 70% complete within the 600 second cycle period applied[30] . The 25.18 gram sample mass is too large to completely absorb/desorb during a reasonably short cycle period in the RCA because the material at the core of the reactor is too far from the heating/cooling surfaces. However it was observed that the material stirs itself due to

[30] It is significant to note that 70% completion of a hydride cycle does not mean that the phase transformation was partial. "70% complete" means that 70% of the $La_{0.9}Gd_{0.1}Ni_5$ crystals in the sample were completely converted to $La_{0.9}Gd_{0.1}Ni_5$-hydride during the cycle. The stirring action of the RCA, illustrated in Figures 7-3a,b,c,d, assures that each 1000 cycles in the RCA results in about 700 complete transformations of the specimen from metal to hydride and back again.

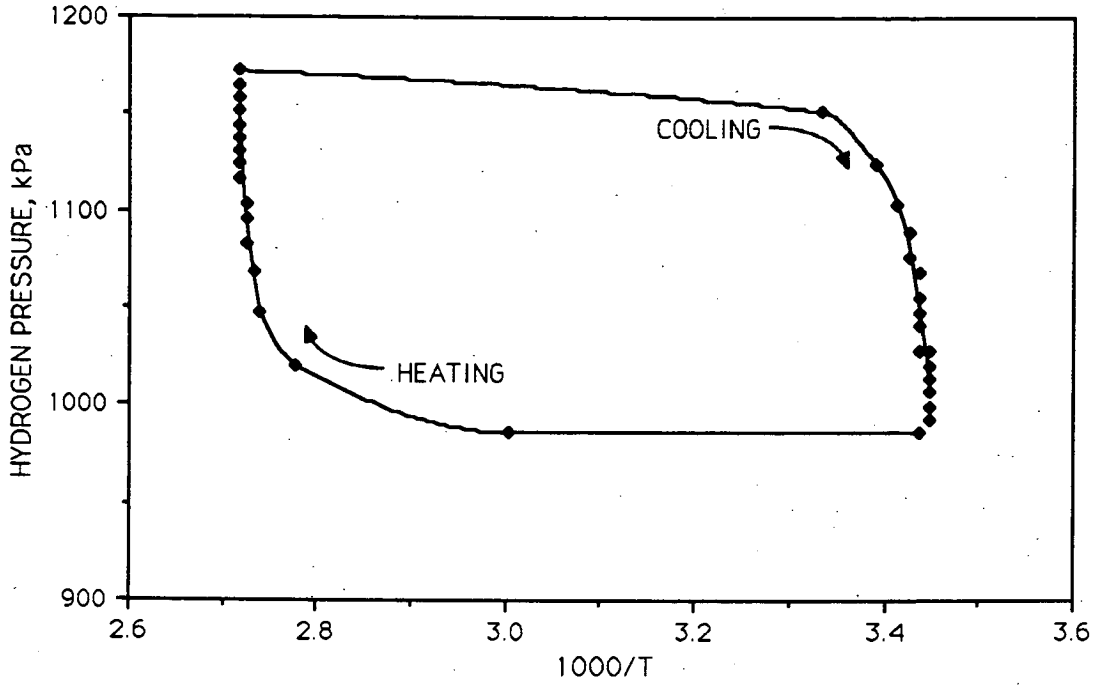

Figure 7-2. Pressure vs. inverse temperature plot of the heating/cooling cycle applied to $La_{0.9}Gd_{0.1}Ni_5$-hydride in the RCA.

the expansion and contraction during the absorption/desorption process.

Figures 7-3a, b, c, d are a series of still photos taken through the viewing port of the RCA over a period of one week. It is apparent that the material is constantly rearranging itself. A closer look shows that a column of powder is growing vertically from the center of the sample. The angle of the light source casts a shadow below any elevated material in the sample. Notice the shadow beneath the column as it grows in Figures 7-3a, b, c. Each succeeding photo shows a longer shadow. Figure 7-3c shows that the column is leaning to the left and Figure 7-3d shows that it has toppled and a new column is growing in its place. The material around the center is also rearranged in each photo. This constant stirring assures that, on the average, all particles acquire a similar cyclic history.

During rapid cycling, the minimum and maximum temperatures were set at 16°C (61°F) and 95°C (203°F) respectively. The cycle duration was set at 600 s total with 300 s of heating and 300 s of cooling. The maximum/minimum cycle pressures and temperatures are plotted in Figure 7-4 below. A small decline in ΔP over the course of the 30 day test period is mainly attributable to a decrease in ΔT. After 6445 actual cycles (4511 accounting for the 70% complete sorption) over a period of 30 days there was no observable degradation within 7 kPa (1 psi) resolution of the 179 kPa (26 psi) swing during the cycle.

Figure 7-3a. Column at center begins to grow vertically, casting a shadow at the lower left side on June 18.

Figure 7-3b. By June 20 the column is taller, casting a longer shadow. The surrounding clods of powder are also rearranged.

Figure 7-3c. The column is taller yet on June 22 and it is beginning to lean toward eight o'clock.

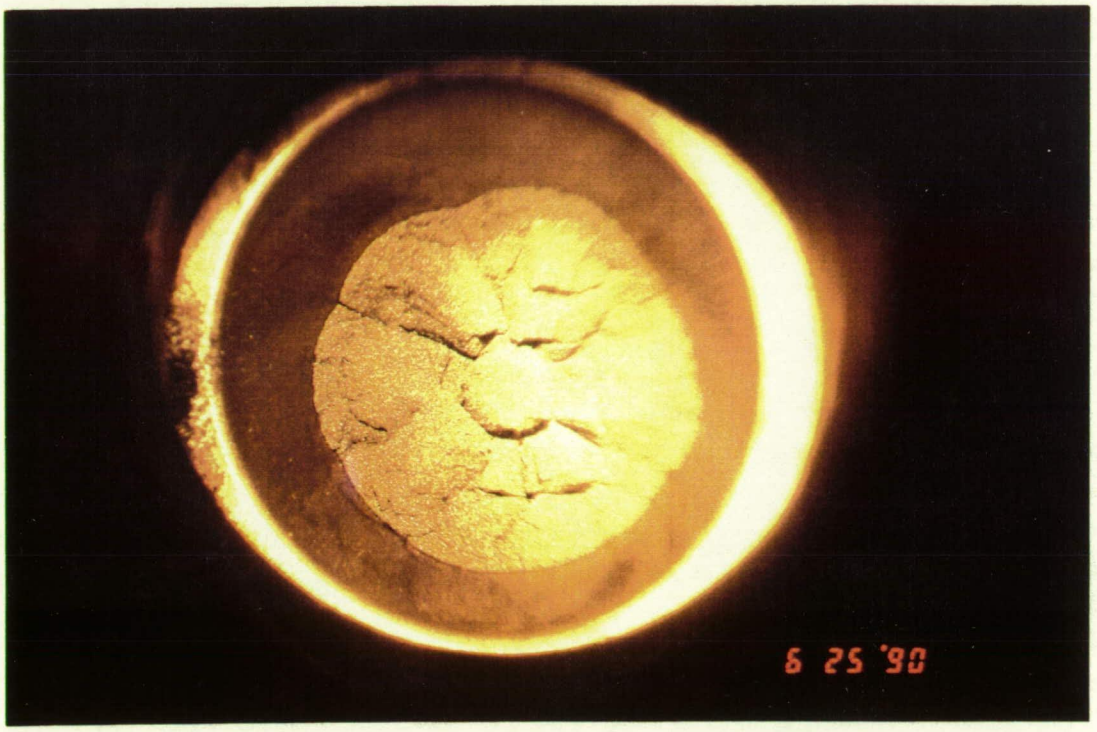

Figure 7-3d. By June 25 the column has toppled at eight o'clock and a new one is growing from the center.

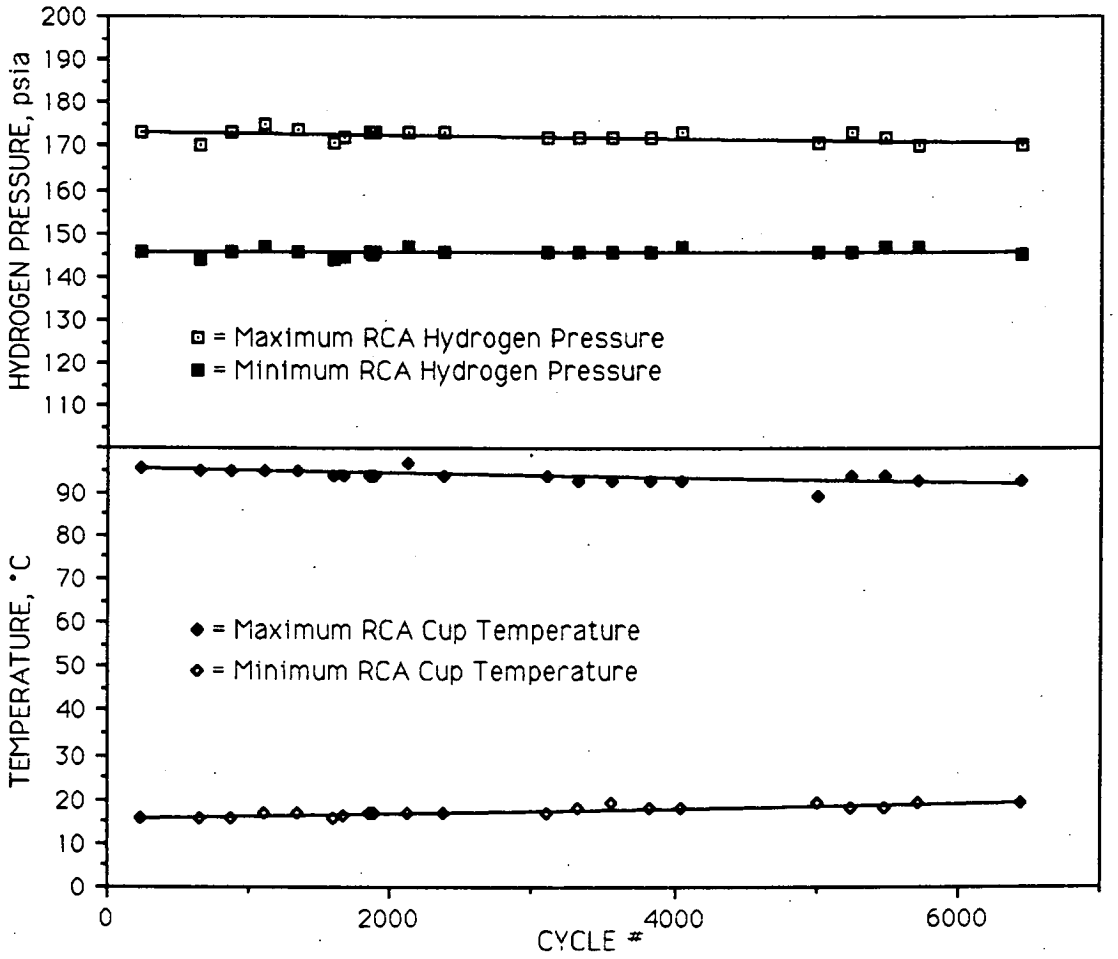

Figure 7-4. A minor change in reversible hydrogen capacity during the first 6445 cycles in the RCA is largely attributable to a small change in ΔT. The hydride remains in good condition.

Sandrock et al contend that it is *time* in the saturated condition rather than number of cycles per se that leads to degradation[31]. HCI's experience with this hydride in the SCA as well as several other studies reported in the literature (see Section 2) confirm that slower cycling degrades many hydrides in fewer than the 4511 complete cycles applied in the RCA. The RCA cycle was therefore slowed down. The 180 s desorption period was retained but the absorption period was extended to 1620 s. The testing continued for an additional 4297 cycles over a period of 94 days. The sample accumulated a total of 10742 cycles which, when scaled down for the 70% complete reaction with stirring, is equivalent to 7519 complete transformations of each crystal in the specimen.

At first glance, Figure 7-5 looks very similar to Figure 7-4. The gradual decrease in cycle ΔP could be attributed to a decrease in ΔT. However, after 7500 cycles, the ΔT

[31] Op. Cit.

levels off and the ΔP continues to fall. A closer look, from 7.5k-10.7k cycles, reveals a steady decrease of reversible hydrogen capacity vs. cycles (or time). The line in Figure 7-6 is a least squares linear fit to the ΔP data over a period of 74 days and 3248 cycles.

The type of loss in reversible capacity is difficult to determine because there is so little damage. It appears that approximately equal amounts of degradation have occurred by hydrogen trapping and by loss in total hydrogen capacity (see Section 3.3 for definitions).

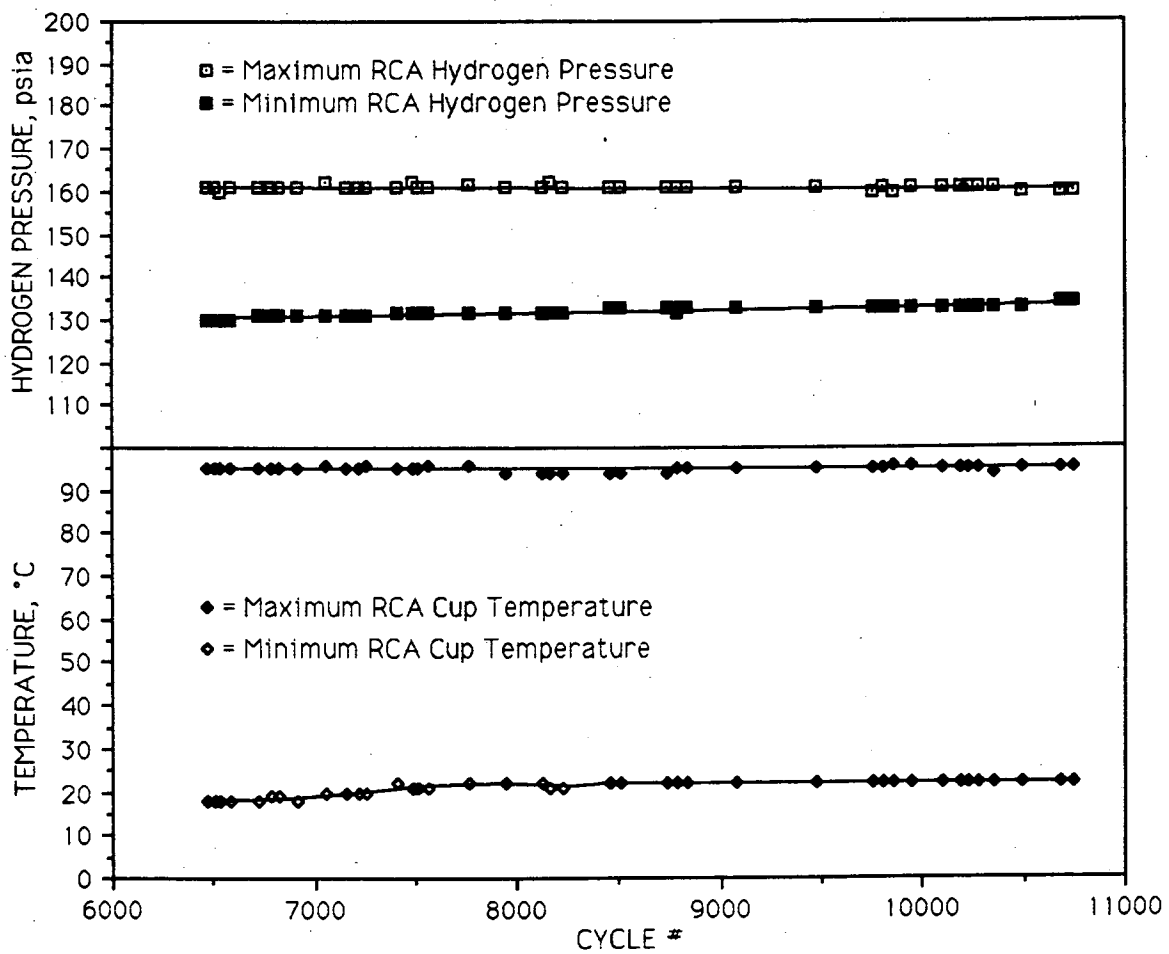

Figure 7-5. A small loss in reversible hydrogen capacity was observed after the cooling period (time in the saturated condition) was increased from 3 to 27 minutes.

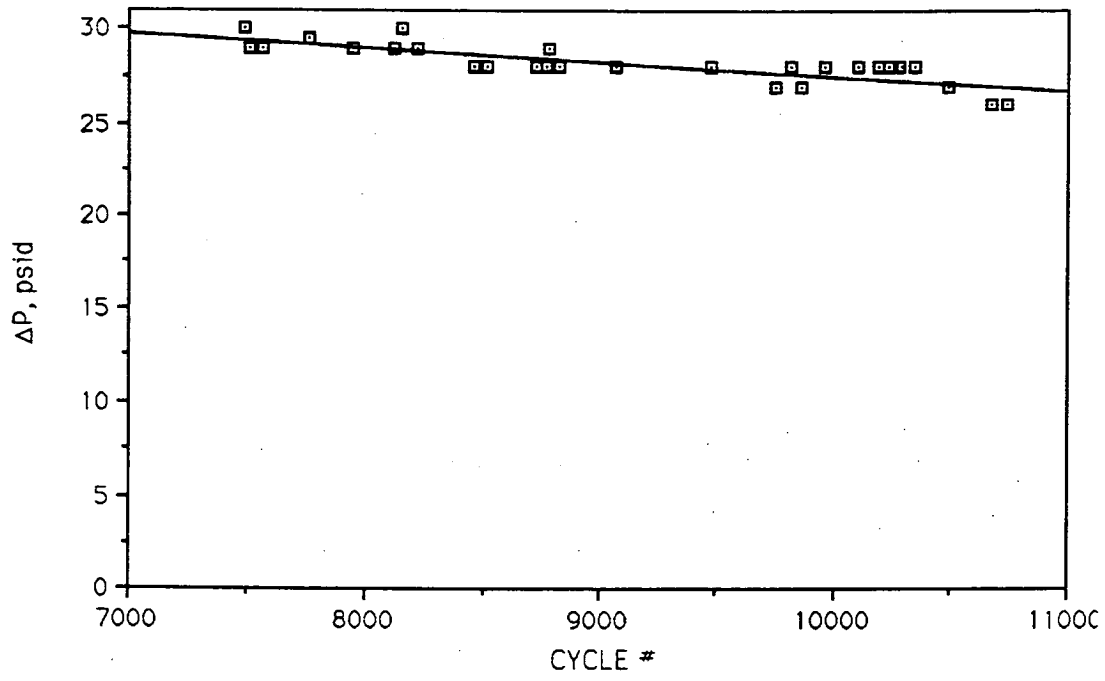

Figure 7-6. A steady decrease in cycle ΔP tracks the loss of reversible hydrogen capacity during the final 3248 cycles (2274 cycles accounting for incomplete reaction and stirring). From 7500 cycles onward, the RCA cycle consisted of 3 minutes of heating and 27 minutes of cooling.

Post RCA isotherms are shown in Figure 7-7. There is an undetermined error (probably an imprecise volume) in the Sieverts data that causes the the isotherms to diverge slightly. It is clear, nonetheless, that the loss in reversible hydrogen capacity (~12%) is considerably less than expected, based upon SCA experience and published studies of cyclic degradation (references in Section 2.0). There is no evidence of the eutectoid separation observed by others, which would have produced a discontinuity in the isotherm's plateau.

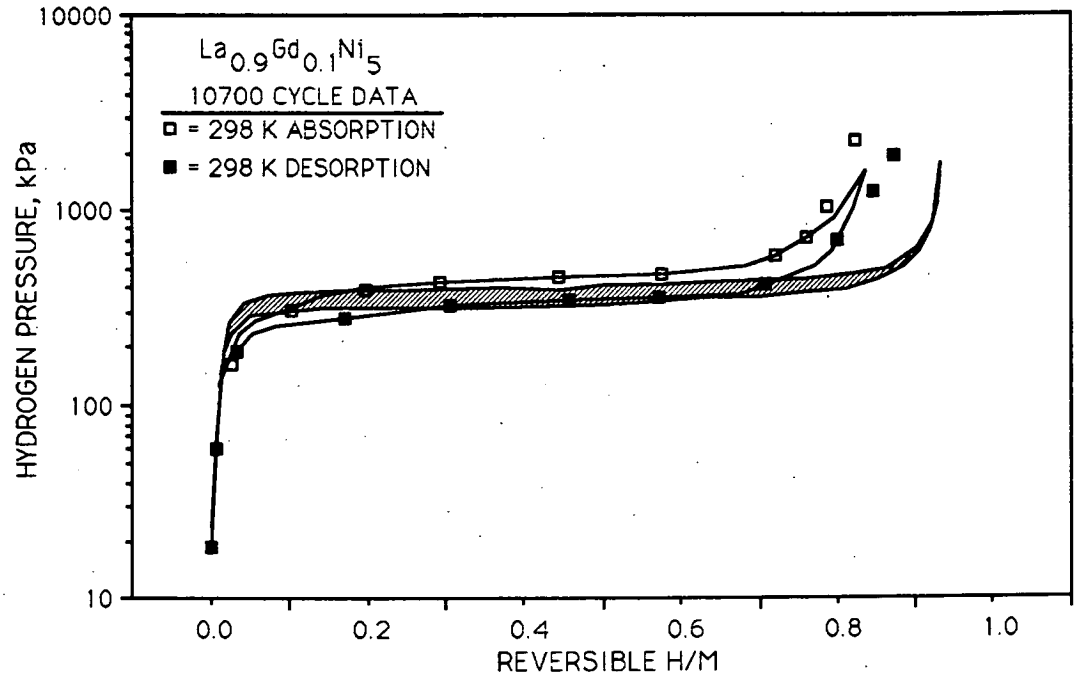

Figure 7-7. Comparison of $La_{0.9}Gd_{0.1}Ni_5$-hydride isotherms after 10 cycles and 10,700 cycles (7519 accounting for incomplete reaction and stirring) in the RCA. *Reversible*[32] H/M was decreased by about 12% during cycling

7.2 SCA Testing of $La_{0.9}Gd_{0.1}Ni_5$-Hydride

The Slow Cycle Apparatus was used to study $La_{0.9}Gd_{0.1}Ni_5$-hydride during an earlier NASA project (NAS9-17549) and subsequent IRAD work by HCI/UNR. The cycle consisted of heating to ~125°C (257°F) and cooling to room temperature, ~20°C (68°F), as described in Section 3.4. Figure 7-8 shows how the hydrogen capacity and isotherm shape changed over the course of 10000 cycles in the SCA. The damage after 1500 cycles is much more extensive than after more than 7500 complete cycles in the RCA (compare Figure 7-8 with Figure 7-7).

An unexpected result of this study was that rapid cycling of AB_5-hydrides does not result in as much degradation over the same period of time as does slower cycling. Cycle periods of 60 minutes on the SCA seriously damaged $LaNi_{5.2}$ and $La_{0.9}Gd_{0.1}Ni_5$ during 1500 cycles in 2 months of testing. However, cycle periods of 6 minutes on the RCA had relatively little effect on these hydrides during 4511 complete cycles in 1 month of testing. Lengthening the RCA's absorption period finally caused some damage (~10% loss of reversible H-capacity) after nearly 11000 cycles during 4 months of testing. However, the damage was not as severe as 1500 cycles in

[32] Absolute calibration is lost during cyclic testing. Figure 7-8 is drawn assuming that H/M = 0 at the minimum pressure of each isotherm. This ignores dissolved and trapped hydrogen that is known to be present but unquantifiable.

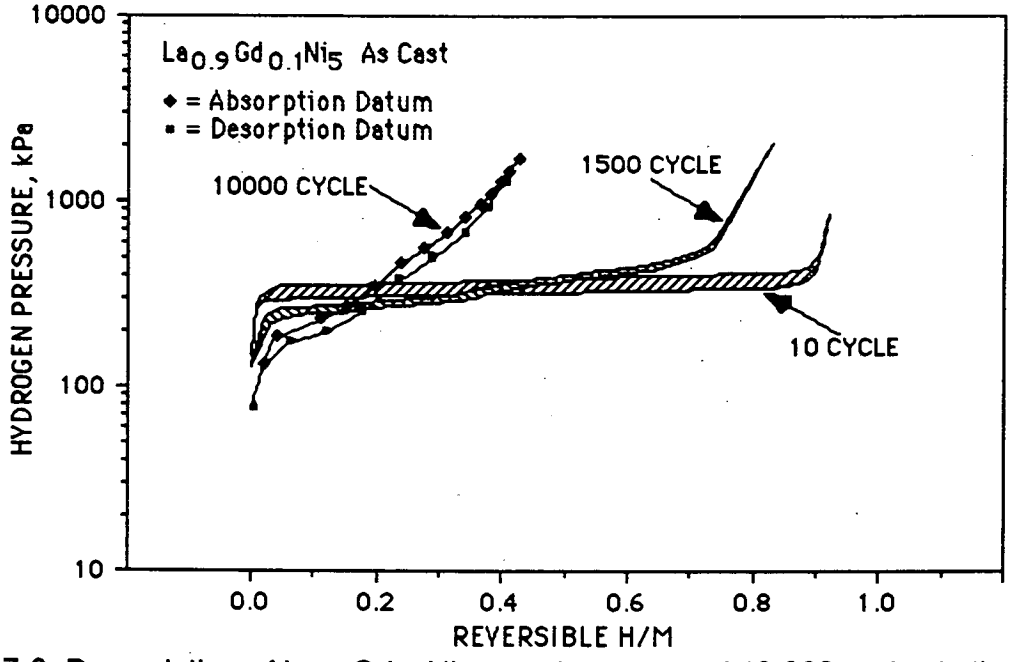

Figure 7-8. Degradation of $La_{0.9}Gd_{0.1}Ni_5$ over the course of 10,000 cycles in the SCA.

the SCA (~20% loss of reversible H-capacity) during 2 months of testing.

The less degraded RCA specimen spent more time in the saturated condition at room temperature than the more degraded 1500 cycle SCA specimen. This contradicts the notion that residence time in the hydrided condition is the primary cause of degradation[33].

The peak temperatures in the RCA were about 30°C lower than the SCA. The literature[34] indicates that baking hydrogen out of AB_5-hydrides at higher temperatures reverses cyclic degradation rather than causing it. Furthermore, holding a hydride at a pressure just below its plateau at elevated temperatures (i.e., the peak temperature conditions of the SCA or RCA) does not degrade it[35]. Therefore, the difference in peak cycle temperatures (125°C in the SCA, 95°C in the RCA) cannot explain the differences in degradation.

Having ruled out *time in the saturated condition* and *peak cycle temperature* as explanations for the minimal degradation observed in the RCA, *difference in sorption rates* comes into question. The mean transformation time of an RCA specimen is about 1 minute. Transformation times in the SCA are on the order of 10 minutes. HCl

[33] G. D. Sandrock et al., "On the Disproportionation of Intermetallic Hydrides", *Zeitschrift für Physikalische Chemie Neue Folge*, R. Oldenbourg Verlag, Munich, West Germany, Vol. 164, pp. 1285-1290 (1989).

[34] R.L. Cohen and K.W. West,"Intrinsic Cycling Degradation in LaNi5 and Annealing Procedures for reforming the material", *Journal of the Less Common Metals*, Vol. 95, pp. 17-23, Elsevier Sequoia S. A., Lausanne, Netherlands, 1983.

[35] Sandrock et al, op. cit.

intends to conduct future IRAD studies of hydride degradation with a Very Slow Cycle Apparatus (VSCA) to learn whether transformation rate is a significant variable in hydride degradation. If greater degradation occurs in fewer cycles during the same period of calender time and the same temperature swing, the rate effect will be confirmed.

There is evidence in Figure 7-8 that the eutectoid decomposition reported by others (discussed in Section 2) has occurred. The slight discontinuity near mid plateau in the 1500-cycle and 10000-cycle isotherms suggests that two distinct phases may be involved in the absorption and desorption processes.

7.3 Thermal Aging of $La_{0.9}Gd_{0.1}Ni_5$-Hydride

Thermal Aging (see Section 3.5) was applied to a specimen of $La_{0.9}Gd_{0.1}Ni_5$. The specimen was activated and pressure-cycled 10 times to normalize the isotherms. Figure 7-9 charts the progress of the TA degradation process. The 11-cycle

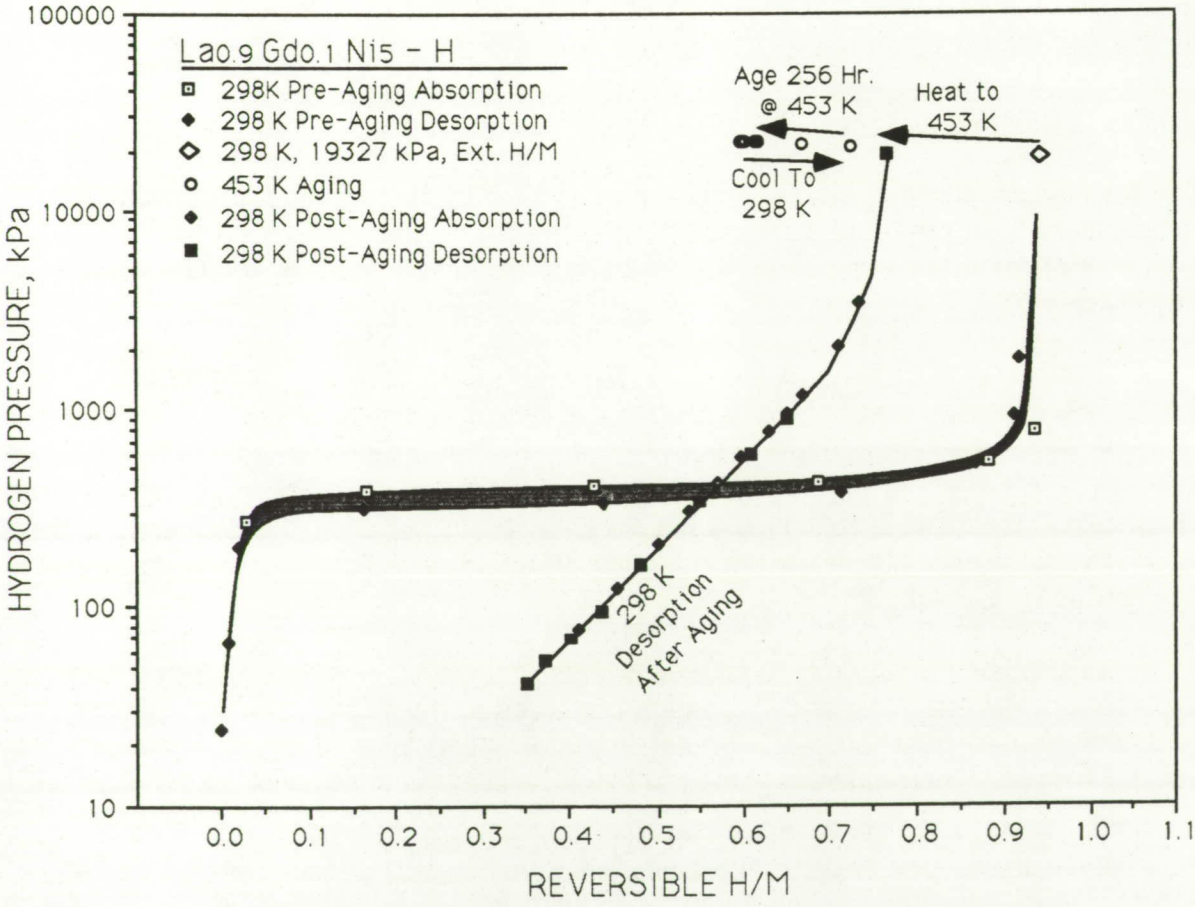

Figure 7-9. Changes in hydrogen capacity and plateau shape caused by aging $La_{0.9}Gd_{0.1}Ni_5$-hydride for 260 hours at 453 K (356°F).

absorption isotherm data at 298 K (77°F) are indicated by ▫ and the desorption data by ◆. The isotherms cross slightly on the right side of the plateau as a result of cumulative experimental errors. The point marked ◇ is located at the applied pressure, 19327 kPa (2803 psia), and a composition extrapolated from the lower pressure hydrogen-hydride solvus.

The arrow to the left from ◇ indicates the pressure and composition changes that occurred as the hydride was heated to 453 K, arriving at the first of a series of points marked ○. The arrow above the series of ○ data shows how pressure and composition changed over the course of the 260 hour test. The pressure rise over time indicates a loss in total hydrogen capacity. The arrow below the ○ data indicates the changes that occurred upon cooling the sample to 298K after the aging process, arriving at the point marked ▪.

Post aging isotherms in absorption and desorption are marked ⬦ and ▪ respectively in Figure 7-9. The degradation is more severe in this material than in pure $LaNi_5$, discussed in Section 6.3. The general shape of the post degradation isotherms looks very similar to Ergenics' data[36]. As with degraded $LaNi_5$-H in Figure 6-4, there is little or no apparent hysteresis and a steep slope developed on the isotherm plateau.

Figure 7-10 provides a closer look at the progress of the degradation during the 260 hour exposure at 453 K with hydrogen pressures in the neighborhood of 19 MPa (2756 psia). The moderate scatter in the data results from small uncertainties in pressure and room temperature amplified by the large amount of gas in the TA apparatus at this high pressure. The trend is nonetheless clear that most of the degradation took place during the first 100 hours.

[36] Sandrock et al, ibid.

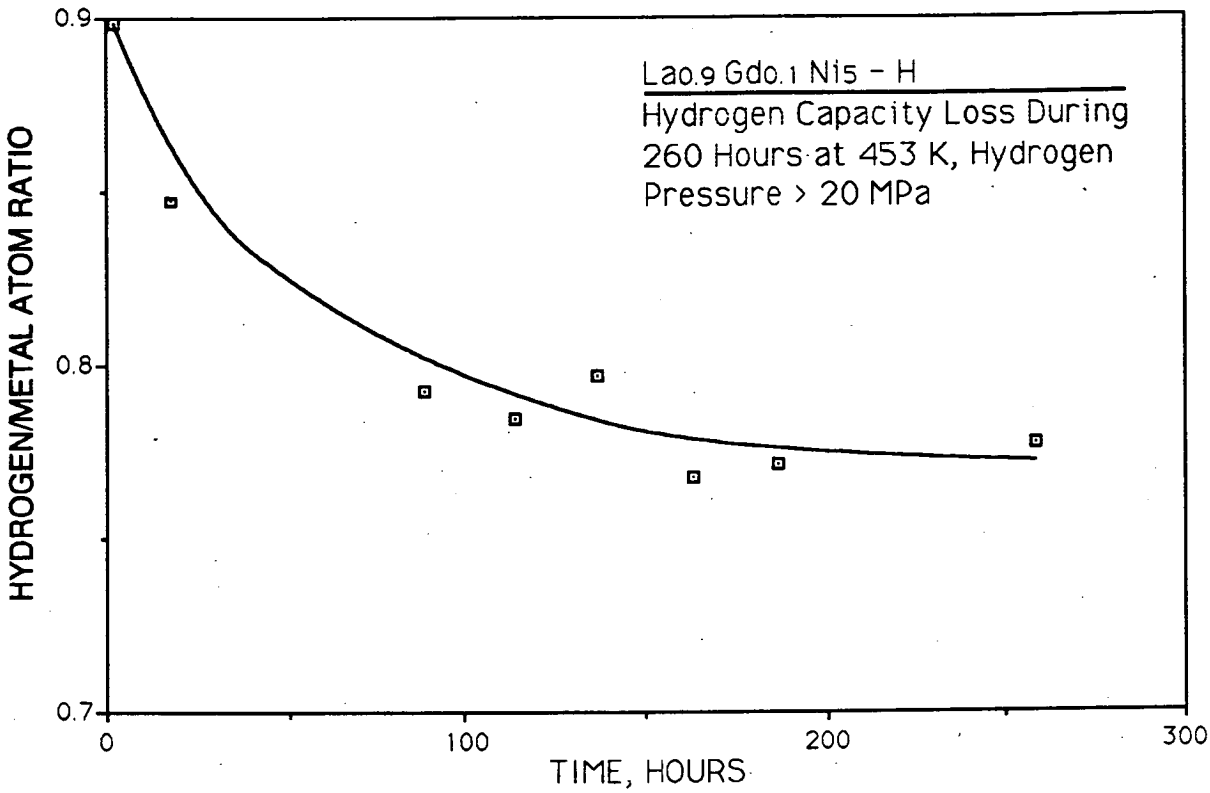

Figure 7-10. Degradation of $La_{0.9}Gd_{0.1}Ni_5$-hydride during thermal aging was most rapid during the first 100 hours.

After completing the post aging isotherms in Figure 7-9, a high temperature bakeout was performed. First, the Sieverts reactor was opened in the hydrogen glove box to extract an X-ray specimen of thermally aged $La_{0.9}Gd_{0.1}Ni_5$-hydride. The reactor was then resealed, removed from the glove box and installed on the Sieverts apparatus. Beginning at 298 K (77°F) and atmospheric pressure (83 kPa or 12.1 psia in Littleton, CO) the sample was heated to higher temperatures and held until outgassing stopped. Figure 7-11 shows the results. The lower temperature data are thought to represent the decomposition of the degraded $La_{0.9}Gd_{0.1}Ni_5$-hydride. The higher temperature data fall fairly along a straight line. However, this data should not be interpreted as a van't Hoff plot because the hydrogen content varies as the specimen outgases.

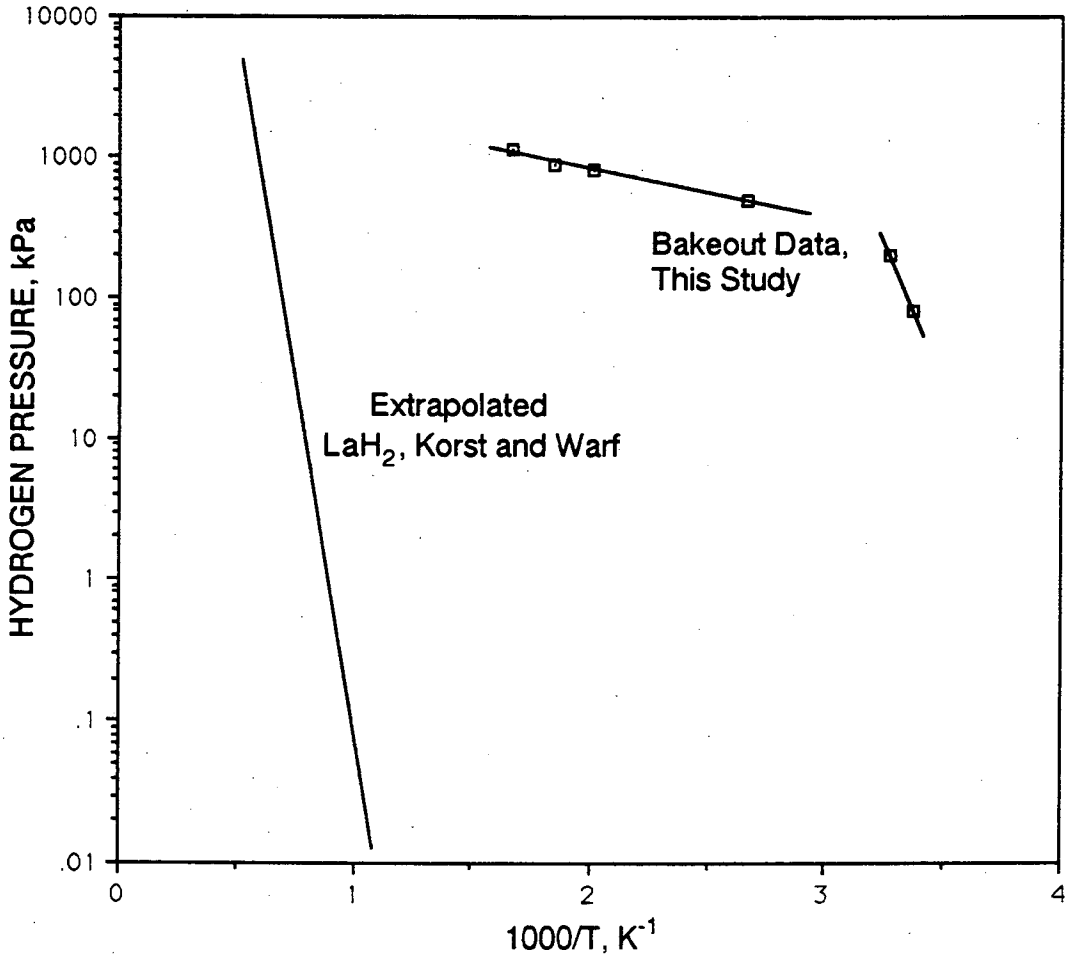

Figure 7-11. Bakeout of degraded $La_{0.9}Gd_{0.1}Ni_5$-hydride shows that the degradation product is not LaH_2.

Figure 7-11 proves conclusively that the decomposition product is not LaH_2. LaH_2 van't Hoff data of Korst and Warf[37] are extrapolated into the range of Figure 7-11 for comparison. The pressure generated by the outgassing of the degradation product is several orders of magnitude greater than the equilibrium pressure of LaH_2 at equal temperatures. The gradual slope of the final bakeout line indicates that the trapped hydrogen is not held within a hydride phase with flat isothermal plateaux and a large heat of formation. If that were the case the line would be steeper--more like the extrapolated LaH_2 data or the initial bakeout line for the degraded AB_5-hydride phase.

[37] W.L. Korst and J.C. Warf, "Rare Earth-Hydrogen Systems. I. Structural Thermodynamic Properties, Inorg. Chem., Vol. 5, No. 10, pp. 1719-1726 (1966).

7.4 X-ray Diffraction Analysis of Degraded $La_{0.9}Gd_{0.1}Ni_5$

X-ray diffraction analysis showed that $La_{0.9}Gd_{0.1}Ni_5$, before and after initial hydriding, had the hexagonal $CaCu_5$ structure. Lattice parameters, a_o and c_o, and the ratio c_o/a_o for virgin alloy and 10 cycle hydride are listed in Table 7-I. Low signal to noise ratios prevented the measurement of the XRPD patterns for the hydrides. The more powerful Rigaku diffractometer clearly showed the peaks of the silicon internal standard so absorption of X-rays by the capillary was ruled out.

Table 7-I. Lattice parameters and c_o/a_o ratio for $La_{0.9}Gd_{0.1}Ni_5$ after 10 cycles and 10000 cycles in the SCA.

Material	Cycles	a_o (Å)	c_o (Å)	c_o/a_o
$La_{0.9}Gd_{0.1}Ni_5$	0	5.0538±0.0012	4.0268±0.0006	0.797
$La_{0.9}Gd_{0.1}Ni_5$	10	5.0039±0.0025	3.9866±0.0097	0.797
$La_{0.9}Gd_{0.1}Ni_5$†	10000	4.9672±0.0139	4.0560±0.0085	0.817

†Nickel peaks 2d and 3d were found in the 10000 cycle $La_{0.9}Gd_{0.1}Ni_5$ sample.

There are two possibilities for the loss of the XRPD pattern; 1) the degraded material is amorphous or 2) the degraded material is nanocrystalline. Amorphous materials cannot diffract X-rays because they lack discrete crystal planes, whereas nanocrystalline materials have domains that are too small to provide a distinctive XRPD pattern.

Two nickel peaks were found in the 10000 cycle material indicating the formation of precipitates of Ni or a Ni-rich phase. These peaks did not appear in the virgin or 10 cycle material and are therefore thought to be associated with the degradation process. It is not possible, from the X-ray evidence alone, to determine just how much nickel was precipitated. The broadened low intensity peaks suggest that the precipitates are on the order of 150 Å. If a significant quantity of nickel precipitates, the (La,Gd)/Ni ratio of the intermetallic must increase. $(La,Gd)Ni_3$-hydride or $(La,Gd)_2Ni_7$-hydride may have formed, both of which are thought to be amorphous[38]. That would explain the lacking XRPD pattern.

The $La_{0.9}Gd_{0.1}Ni_5$ -hydride capillary was subsequently broken open allowing hydrogen to escape. The dehydrided material regained its original hexagonal structure but considerable microstrain was apparent from the XRPD pattern. As a

[38] J.H. Han and J.H. Lee, "Influence of Oxygen Impurity on the Hydrogenation Properties of $LaNi_5$, $LaNi_{4.7}Al_{0.3}$ and $MmNi_{4.5}Al_{0.5}$ During Long-Term Pressure-Induced Hydriding-Dehydriding Cycling", *Journal of the Less Common Metals*, Vol. 152, pp. 329-338 (1989).

working hypothesis, it is suspected that crystal imperfections, resulting from strain that occurs during absorption/desorption cycles, produce sites that are favorable for hydrogen trapping. The trapped hydrogen is stably bound--not *reversible* in the practical sense[39].

[39] J.F. Lynch and J.J. Reilly, "Behavior of H-$LaNi_5$ Solid Solutions", *Journal of the Less Common Metals*, Vol. 87, pp. 225-236 (1982).

8.0 DEGRADATION OF $LaNi_{4.8}Sn_{0.2}$-HYDRIDE

Work with $LaNi_5$ and $La_{0.9}Gd_{0.1}Ni_5$ show that the Rapid Cycle Apparatus (RCA) produces less degradation than the Slow Cycle Apparatus (SCA). Having failed to degrade $LaNi_{4.8}Sn_{0.2}$-hydride in earlier work with the SCA, it was deemed unnecessary to attempt degradation with the RCA. Work with La-Ni-Sn hydrides in the present study consisted of collecting the results of previous SCA and X-ray studies, further X-ray analysis of SCA specimens and thermal aging experiments.

8.1 SCA Testing of $LaNi_{4.8}Sn_{0.2}$-Hydride

The Slow Cycle Apparatus was used to study $LaNi_{4.8}Sn_{0.2}$-hydride during an earlier NASA project (NAS9-17549) and subsequent IRAD work by HCI/UNR. The cycle consisted of heating to ~125°C (257°F) and cooling to room temperature, ~20°C (68°F), as described in Section 3.4. Figure 8-1 shows how the hydrogen capacity and isotherm shape changed over the course of 10000 cycles in the SCA. In contrast to $LaNi_{5.2}$-hydride and $La_{0.9}Gd_{0.1}Ni_5$-hydride (see Figure 1-1), $LaNi_{4.8}Sn_{0.2}$-hydride suffered relatively little degradation. After 10000 cycles, the *reversible* hydrogen

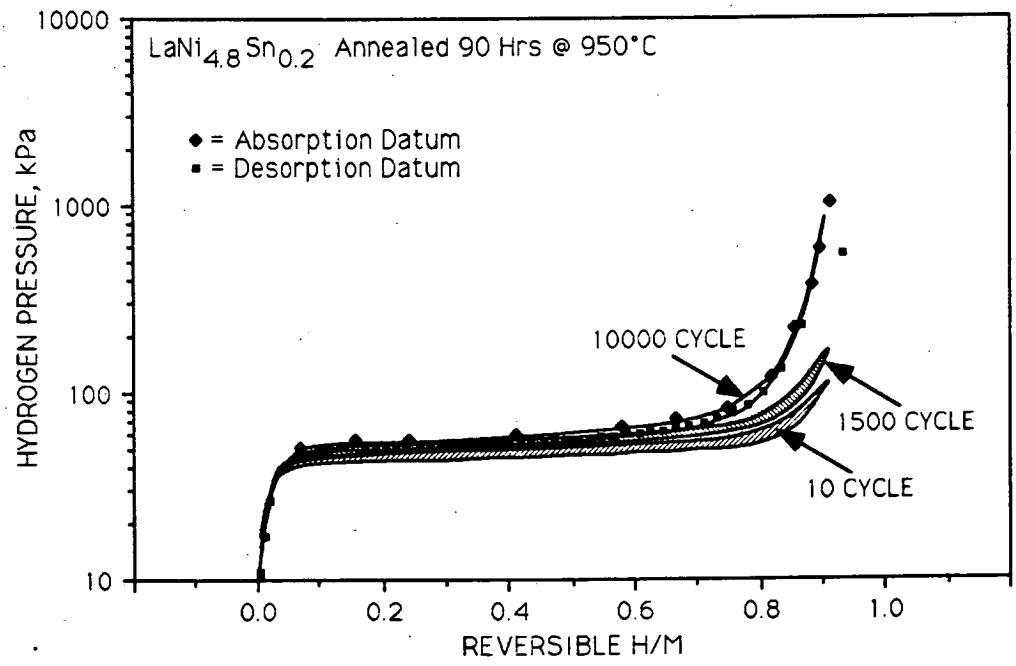

Figure 8-1. Hydrogen pressure vs. composition isotherms for $LaNi_{4.8}Sn_{0.2}$-hydride show relatively little degradation through 10,000 cycles in the SCA.

[1] Absolute calibration is lost during cyclic testing. Figure 8-1 is drawn assuming that H/M = 0 at the minimum pressure of each isotherm. This ignores dissolved and trapped hydrogen that is known to be present but unquantifiable.

capacity at a given absorption pressure (say 100 kPa) is over 90% of the original 10-cycle reversible capacity. The absorption and desorption pressures are increased by a small amount that is acceptable for most practical applications.

The absorption/desorption pressure hysteresis is small in all three sets of isotherms. There is no hint of the eutectoid decomposition discussed in the literature (see Section 2) and suspected in $La_{0.9}Gd_{0.1}Ni_5$ (see Section 7.2). From the perspective of SCA data, $LaNi_{4.8}Sn_{0.2}$-hydride is an excellent choice for long term cyclic stability.

8.2 Thermal Aging of $LaNi_{4.27}Sn_{0.24}$-Hydride

A hydride alloy with the composition $LaNi_{4.27}Sn_{0.24}$ was induction melted by Molycorp, Washington, PA. The unusual stoichiometry ($4.27 + 0.24 \neq 5.00$) results from adding excess lanthanum to improve the properties of the hydride. Another way of expressing the formula is $La_{1.11}Ni_{4.73}Sn_{0.27}$--close to the same Ni/Sn ratio used in the earlier SCA tests. Section 3.5 describes the thermal aging (TA) experiment. The hydrogen pressure in the TA apparatus rose and fell slightly with small variations in room temperature and furnace temperature but at the end of the test, when all components were returned to standard temperature, the change in *total* hydrogen capacity (see Section 3.3 for definition) was zero (±0.3%).

Absorption and desorption isotherms at 298 K (77°F) before and after the TA experiment are shown in Figure 8-2. A slight reduction in absorption and desorption pressures is apparent in the aged isotherms. Isotherm slopes are the same before and after aging. The apparent reduction in reversible H/M is small enough to be within limits of experimental errors. As discussed in the preceding paragraph, there was no loss in *total* hydrogen capacity so any loss in *reversible* hydrogen capacity must be attributed to trapping. The changes in pressures and reversible hydrogen capacity are significantly less than those observed in $LaNi_5$ and $La_{0.9}Gd_{0.1}Ni_5$.

The earlier SCA studies were conducted on $LaNi_{4.8}Sn_{0.2}$, arc-melted at HCI. This TA study was performed on induction-melted $LaNi_{4.27}Sn_{0.24}$ from Molycorp. It is reassuring that the Sn additive consistently improves the degradation resistance of $LaNi_{5-x}Sn_x$-hydrides, regardless of the source of the materials or the method of preparation.

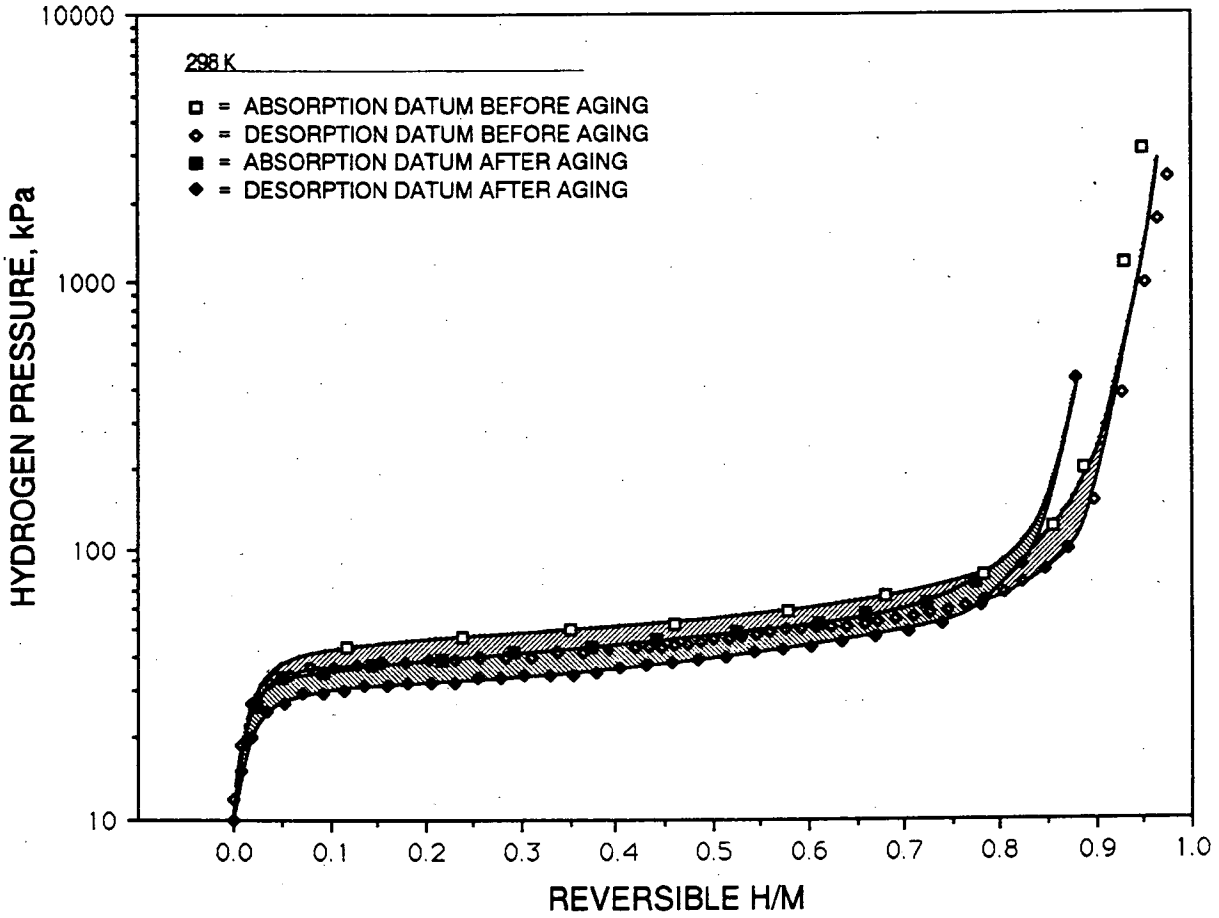

Figure 8-2. Absorption and desorption isotherms before and after 281 hours of TA at 180°C. The small change in plateau width is within experimental uncertainty. The plateau pressures have shifted downward slightly.

8.3 X-ray Diffraction Studies of $LaNi_{4.8}Sn_{0.2}$ and its Hydride

Table 8-I gives the lattice parameters and c/a ratio of $LaNi_{4.8}Sn_{0.2}$ and its hydride before and after 10,000 cycles in the SCA. Both phases have the hexagonal $CaCu_5$-type structure. Unlike $La_{0.9}Gd_{0.1}Ni_5$ (see Section 7.4) the hydride retained its macro crystallinity after 10,000 cycles. The peaks show significantly less broadening than $LaNi_5$ or $La_{0.9}Gd_{0.1}Ni_5$. Variations of lattice parameters before and after cycling are within limits of uncertainty. Minimal hydride degradation in $LaNi_{4.8}Sn_{0.2}$, taken together with reduced peak broadening, supports the hypothesis that crystal disorder and hydride degradation are related. Nickel peaks were not apparent in diffraction patterns of $LaNi_{4.8}Sn_{0.2}$ or of its hydride.

Table 8-I. Lattice parameters and c_o/a_o ratio for $LaNi_{4.8}Sn_{0.2}$ after 10 cycles and 10000 cycles in the SCA.

Material	Cycles	a_o (Å)	c_o (Å)	c_o/a_o
$LaNi_{4.8}Sn_{0.2}$	0	5.0723±0.0038	4.0389±0.0025	0.796
$LaNi_{4.8}Sn_{0.2}$†	10000	5.0751±0.0065	4.0280±0.0125	0.794
$LaNi_{4.8}Sn_{0.2}H_{\sim 6}$	10	5.3785±0.0012	4.2642±0.0036	0.793
$LaNi_{4.8}Sn_{0.2}H_{\sim 6}$	10000	5.3850±0.0139	4.2683±0.0006	0.793

†Evacuated at room temperature

9.0 CONCLUSIONS

9.1 Conclusions Regarding Degradation of AB_5-Type Hydrides

It is apparent from the literature and the results of this study that cyclic degradation of AB_5-type metal hydrides varies widely according to the details of how the specimens are cycled. Some studies report severe degradation in as little as 1500 cycles[1,2] while others report relatively little degradation after 45000 cycles[3] all with nearly identical materials.

The Rapid Cycle Apparatus (RCA) used in the present study produced less degradation in 5000-10000 cycles than HCI's earlier work with a Slow Cycle Apparatus (SCA) produced in 1500 cycles. There is evidence reported in the literature[4] and confirmed by 453 K (356°F) Thermal Aging (TA) during the present study that time spent in the saturated condition causes hydride degradation. But increasing the cooling (saturation) period in the RCA did not dramatically increase the rate of degradation. It appears that TA type degradation is secondary at lower temperatures to another degradation mechanism.

If rapid cycles are less damaging than slow cycles when the saturation time is equal, rate of hydriding/dehydriding may be an important factor. The mean transformation time of an RCA specimen is about 1 minute. Transformation times in the SCA are on the order of 10 minutes. HCI intends to conduct future IRAD studies of hydride degradation with a Very Slow Cycle Apparatus (VSCA) to learn whether transformation rate is a significant variable in hydride degradation. If greater degradation occurs in fewer cycles during the same period of calender time with the same temperature swing, the rate effect will be confirmed.

The peak temperatures in the RCA were about 30°C lower than the SCA. The literature indicates that baking hydrogen out of AB_5-hydrides at higher temperatures reverses cyclic degradation rather than causing it. Furthermore, holding a hydride at a pressure just below its plateau at elevated temperatures (i.e., the peak temperature conditions of the SCA or RCA) does not degrade it. Therefore, the difference in peak cycle temperatures (125°C in the SCA, 95°C in the RCA) cannot explain the

[1] P.D. Goodell, "Stability of Rechargeable Hydriding Alloys During Extended Cycling", *Journal of the Less Common Metals*, Vol. 99, pp. 1-14, Elsevier Sequoia S. A., Lausanne, Netherlands, 1984.

[2] D. Chandra and F.E. Lynch, "Cyclic Stability of Rare Earth Pentanickel Hydrides", Proc. AIME Rare Earth Symposium, ed. R. G. Bautista and M. M. Wong, TMS Publications, p. 83 (1989).

[3] Y. Josephy, E. Bershadsky and M. Ron, "Investigation of $LaNi_5$ upon Prolonged Cycling", Proc. International Symposium on Metal Hydrogen Systems, Banff, Alberta, Canada (1990).

[4] G. D. Sandrock et al. "On the Disproportionation of Intermetallic Hydrides", *Zeitschrift für Physikalische Chemie Neue Folge*, R. Oldenbourg Verlag, Munich, West Germany, Vol. 164, pp. 1285-1290 (1989).

differences in degradation.

TA-type degradation is similar to cyclic degradation in that nickel peaks and line broadening are observed in X-ray diffraction patterns after either form of degradation. Both types of degradation produce sloping pressure vs. composition isotherms with reduced reversible hydrogen capacity. Hydrogen is trapped within the solid with either method of degradation and removal of the trapped hydrogen reverses the degradation. The substitution of tin for nickel in $LaNi_{5-x}Sn_x$ gives excellent resistance to either method of degradation.

There are, however, significant differences in the isotherms generated by cycling vs. thermal aging. Cyclic degradation does not greatly affect absorption/desorption hysteresis band width but thermally degraded hydrides in the present study lost their hysteresis bands altogether. TA degraded $La_{0.9}Gd_{0.1}Ni_5$-hydride isotherms did not show any indication of the mid-plateau inflection that signals the eutectoid decomposition noted in the literature[5, 6, 7, 8] and in previous HCl studies (see Figure 7-8).

All methods of AB_5-hydride degradation applied during this study resulted in line broadening. Peaks in severely degraded hydrides could not be resolved, even with the most powerful X-ray equipment, but a highly strained hexagonal structure reappeared when hydrogen was removed from the degraded materials at room temperature. The degradation-resistant $LaNi_{5-x}Sn_x$-hydride retained relatively narrow peaks through 10,000 cycles.

Figure 9-1 shows how crystal domain particle size in three hydride alloys changed during 10,000 cycles of absorption/desorption in the SCA. The $LaNi_{4.8}Sn_{0.2}$ alloy, which suffered only minimal loss of reversible hydrogen content shows a small reduction in domain particle size. $La_{0.9}Gd_{0.1}Ni_5$ and $LaNi_{5.2}$ were severely degraded and they show significant reduction in domain particle size. Figure 9-2 shows how strain varied in the same set of three alloys during 10,000 cycles of absorption/desorption in the SCA. Once again $LaNi_{4.8}Sn_{0.2}$ shows stability where $La_{0.9}Gd_{0.1}Ni_5$ and $LaNi_{5.2}$ do not.

[5] H. Hayakawa et al, "Time of Flight Neutron Powder Diffraction Study of the $LaNi_5D_3$ Structure", *Journal of the Less Common Metals*, Vol. 143, pp. 315-324, Elsevier Sequoia S. A., Lausanne, Netherlands, 1988.

[6] P.D. Goodell, ibid.

[7] T. Matsumoto and A. Matsushita, "A New Intermediate Hydride in the $LaNi_5$-H_2 System Studied by In Situ X-ray Diffractometry", *Journal of the Less Common Metals*, Vol. 123, pp. 135-144, Elsevier Sequoia S. A., Lausanne, Netherlands, 1986.

[8] A. L. Shilov, M. E. Kost and N.T. Kuznetsov, "The System $LaNi_5$- H_2", *Journal of the Less Common Metals*, Vol. 144, pp. 23-30, Elsevier Sequoia S. A., Lausanne, Netherlands, 1988.

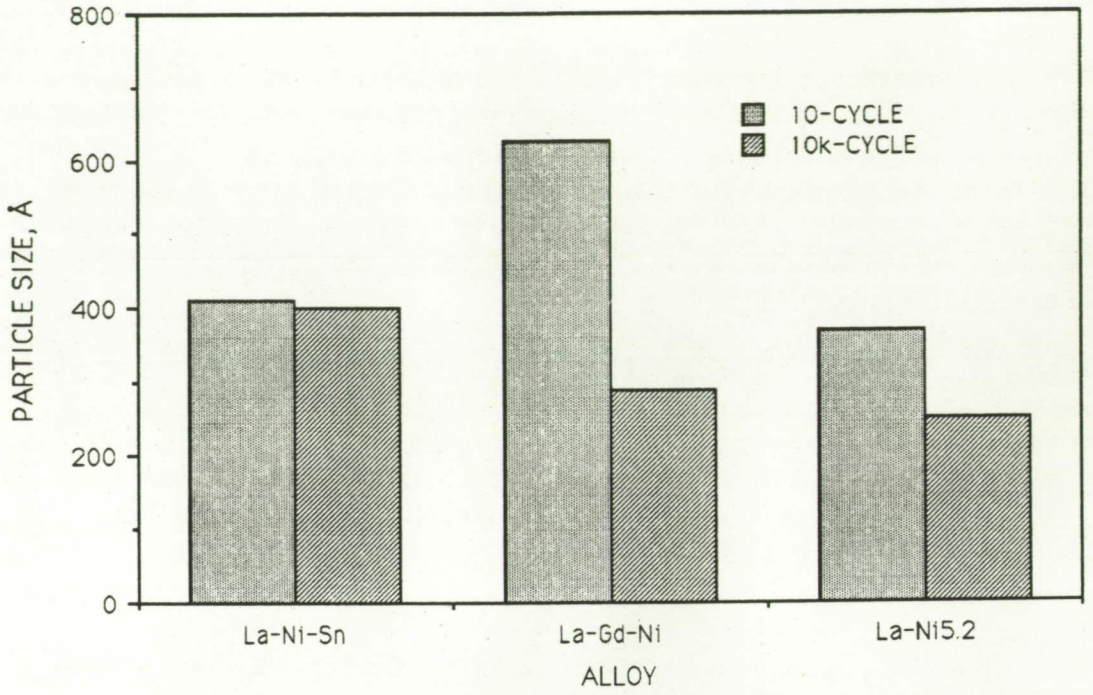

Figure 9-1. Variation of crystal domain particle size between 10 and 10k cycles in the SCA.

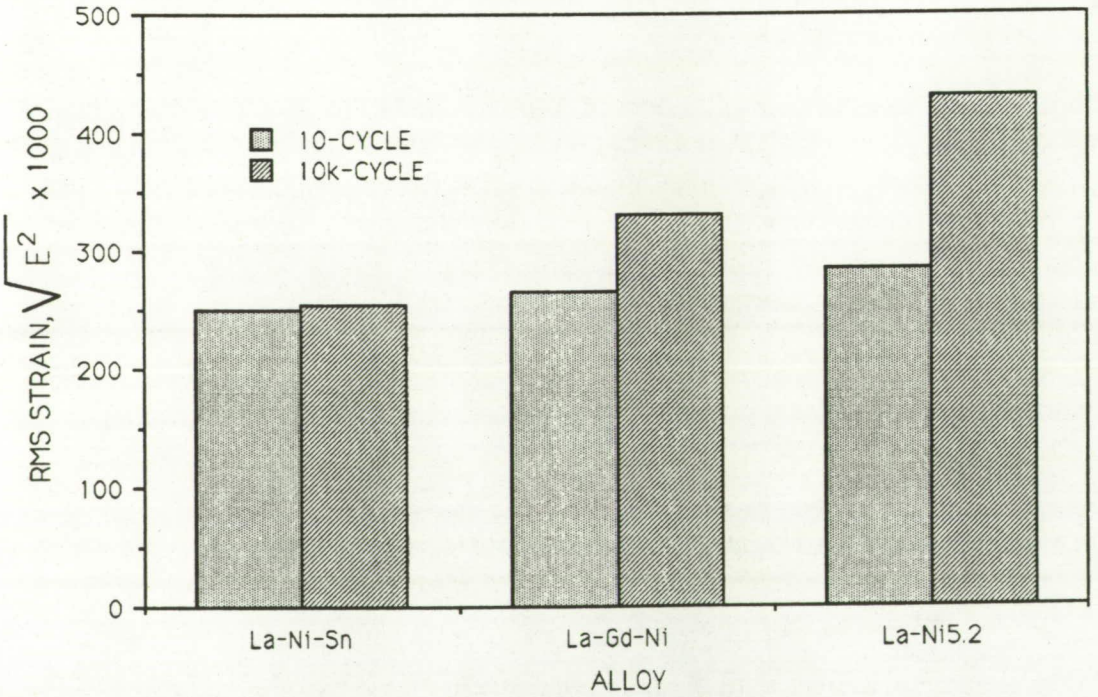

Figure 9-2. Variation of strain in the 001,002 planes of the hexagonal crystals between 10 and 10k cycles in the SCA.

Crystal imperfections accumulate from strain that occurs during absorption/ desorption cycles. The altered atom arrangement surrounding these crystal imperfections may produce sites that are favorable for hydrogen trapping.

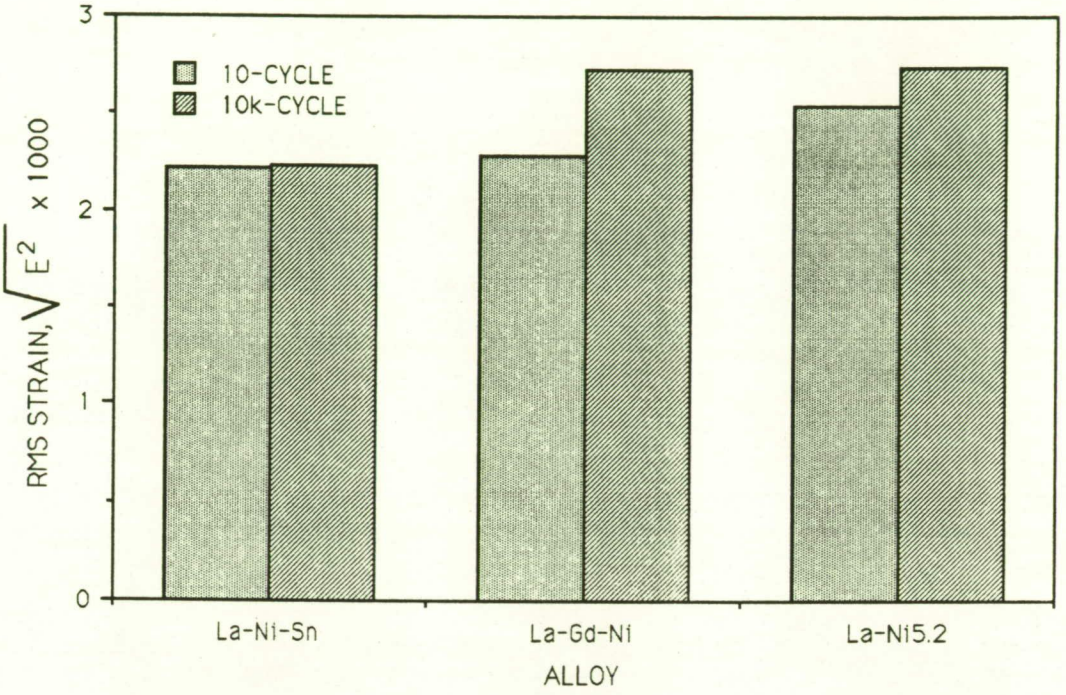

Figure 9-3. Variation of strain in the 101,202 planes of the hexagonal crystals between 10 and 10k cycles in the SCA.

Clearly, hydrogen trapping is one mode of hydride degradation. The mode of trapping however is controversial. One mode suggested in the literature (see Sections 1 and 2) involves the formation of LaH_2. After TA degradation of $La_{0.9}Gd_{0.1}Ni_5$-hydride, a bakeout was conducted to determine the stability of the trapped hydrogen. Figure 7-11 shows that the trapped hydrogen is less stable, by several orders of magnitude, than LaH_2 (GdH_2 is more stable yet). Several other hydrides are known to exist in the La-Ni-H system and many of them are thought to be amorphous.

The controversy over the mode of hydrogen trapping centers around two schools of thought: 1) trapped hydrogen exists in distinct nanocrystals (~100 Å) of stable hydrides or 2) hydrogen is randomly trapped at sites within disordered crystals where local geometric and electronic effects are favorable for binding hydrogen. The controversy cannot be resolved by conventional X-ray studies because nanocrystalline hydride phases do not produce Bragg peaks and none are expected from disordered or amorphous materials. The present study observed nickel peaks in degraded AB_5 materials, confirming magnetic evidence of nickel segregation in the

literature[9]. The clusters of nickel are thought to be on the order of 150Å. A simple mass balance demands that the remainder of the specimen has a greater rare earth/nickel ratio than the stoichiometric AB_5. The question remains whether the excess rare earth is distributed randomly throughout an amorphous degradation product, or organized into nanocrystals with a distinct $A_xB_yH_z$ stoichiometry. As Lee Huston of Ergenics points out[10], the distinction between the two points of view gets hazy at some small scale of nanocrystallinity.

9.2 Conclusions Regarding Degradation of Vanadium Hydrides

Concurrent studies of AB_5 and vanadium hydrides provided an opportunity to apply information from one sub-study to the benefit of the other. Vanadium dihydride degradation provides clear evidence that strain and crystal disorder can cause hydride degradation. Line broadening analysis shows increases in strain in VH with the number of absorption/desorption cycles. The strains are anisotropic.

A specimen of $V_{0.995}C_{0.005}$, milled into very fine shavings, confirmed the importance of strain in degradation of V-based dihydrides. The severely cold-worked specimen showed a large hysteresis band and reduced capacity, similar to a cyclically degraded hydride isotherm. Annealing the shavings reduced the hysteresis and recovered the original hydrogen capacity.

RCA data clearly show that hydrogen becomes trapped within degraded VH. After 6182 cycles in the RCA, VH_2 desorption yields hydrogen gas and a solid product whose composition is approximately $VH_{1.18}$. With pure vanadium, there is no concern, as with the AB_5-hydrides, that the trapping mechanism may involve stable hydride phases with different metal stoichiometry than the original material, e.g., A_2B_7. When the degraded VH_2 phase decomposes on heating in the RCA, it leaves VH with about 18% excess hydrogen trapped within its strained and disordered BCT structure.

A cause-effect relationship between strain accumulation and hydride degradation is inferred by the following observations; metals that are mechanically strained before hydriding yield degraded isotherms that resemble hydride isotherms after large numbers of cycles; annealing of mechanically strained specimens before hydriding results in normal undegraded metal hydride characteristics; cyclically degraded hydrides show X-ray evidence of severe strain; annealing of cyclically degraded hydrides also reverses the damage.

A new form of cyclic degradation, peculiar to vanadium-based hydrides, was observed during this study. Over the course of 6182 absorption/desorption cycles in the RCA, time-lapse photography shows that the original shiny metallic-looking material undergoes a spontaneous physical change. A low density dark gray phase,

[9] L. Schlapbach, "Magnetic Properties of $LaNi_5$ and Their Variation with Hydrogen Absorption and Desorption", J. Phys. F: Metal Phys., Vol. 10 pp. 2477-2490 (1980).

[10] L. Huston, Private communication with F. Lynch, October, 1990.

graphically dubbed "dust bunnies" by HCI test personnel, gradually grows by transforming higher density metallic particles. The material appears to the eye, and to the highest resolutions of electron microscopy, as a fluffy porous sponge-like mass. This growth has strained and eventually fractured the sturdiest of hydride containers.

The low density material does not have a crystalline appearance, but X-ray diffraction patterns show BCT and cubic fluorite--just like the higher density material but with more strain. Hydride isotherms confirm that the normal and low density phases are chemically similar. The density decrease is of a physical nature, i.e., a modified state of aggregation, rather than a chemical change. X-ray line broadening analysis indicates an increased domain size in the low density form of VH_2. There is also an indication in TEM electron diffraction patterns that domain size is larger in the low density phase.

The appearance of the low density material does not change significantly from 1x optical photography to the limits of scanning electron microscopy. The material looks like a sponge, regardless of magnification. Scale invariant appearance over nearly 4 orders of magnitude is a fascinating property of the vanadium hydride sponges. The fractal viewpoint (e.g., diffusion limited aggregation[11]) may provide an enlightening approach for further studies.

Not all of the particles were converted to low density sponges. Micrographs of the surviving high density metallic particles show that the sponge-like material is growing preferentially from certain sides of the particles. It would be interesting to subject a single crystal of vanadium to cyclic hydriding to see if the sponges develop on a particular crystal plane. Unfortunately the method of sponge growth is not presently understood and there is no known method for stopping it. Hydride applications that require more than a few hundred absorption/desorption cycles will have to use other materials because the growth will eventually break the strongest of hydride containers.

9.3 Practical Implications

Metal hydrides are promising engineering materials that may be termed "enabling" in several areas of new technology that are of interest to NASA. The present study gained insight into the nature of hydride degradation via cycling, moderate temperature aging and mechanical strain (machining). A growing base of practical experience and the results of this study confirms that tin substitution in AB_5-type hydrides provides resistance to degradation. Tin-containing alloy manufactured by arc-melting at HCI and induction-melted alloy from another foundry have shown equivalent resistance to degradation. This inspires confidence that high quality hydride alloys are *manufacturable* for future NASA requirements.

[11]P. Meakin and S. Tolman, "Diffusion Limited Aggregation: Recent Developments", *Fractals' Physical Origin and Properties*, ed. A. Zichichi, Plenum Press, N.Y. (1988).

The preparation of vanadium alloy for hydride applications invariably involves milling or hydriding and crushing to render the material into a granular form. Such operations must be performed with consideration for the effects of mechanical strain and cold work on the properties of the hydride. Excessive cold work has an effect on the absorption/desorption pressures and hysteresis band width that is comparable to cyclic degradation.

Vanadium-based hydrides are not suitable for many NASA applications at present, owing to the formation of a low density sponge-like degradation product. Vanadium should only be used in special circumstances where the number of cycles is low and sturdy (heavy) containers can be used to temporarily resist the expansion forces of the sponges. Strict inspection schedules must be observed and the containers must be retired before their inevitable rupture.